

THE DEVELOPMENT OF A SIMULATIVE  
HYBRID MODEL FOR OPTIMISING THE  
PRODUCTION OF A HIGH-CARBON  
FERROMANGANESE FURNACE

*by*

Ashley William Sundström

Thesis submitted in partial fulfilment  
of the requirements for the Degree

*of*

MASTER OF SCIENCE IN ENGINEERING  
(EXTRACTIVE METALLURGICAL ENGINEERING)



in the Department of Process Engineering  
at the University of Stellenbosch

*Supervised by*  
Prof. J.J. Eksteen  
Prof. C. Aldrich

STELLENBOSCH

December 2009

## **DECLARATION**

By submitting this dissertation electronically, I declare that the entirety of the work contained therein is my own, original work, that I am the owner of the copyright thereof (unless to the extent explicitly otherwise stated) and that I have not previously in its entirety or in part submitted it for obtaining any qualification.

December 2009

Copyright © 2009 Stellenbosch University

All rights reserved

## SYNOPSIS

A project was initially commenced for optimising the production output at a specific high-carbon ferromanganese furnace. Since operational difficulties were experienced in this furnace and with a lack of reliable data for the year 2007, it was decided that data from a more stable high-carbon ferromanganese furnace should be analysed instead. Three key performance indicators (KPI's) were selected to give an indication of overall process performance. These were: (1) the total tonnes of high-carbon ferromanganese produced per tonne of feed material, (2) the percentage recovery of manganese to the alloy product, and (3) the alloy:slag ratio. Maximisation of each of these would contribute to the overall improvement of the process.

To achieve the objectives of the project, a hybrid model was developed to characterise the production behaviour of the furnace and to optimise the proposed KPI's. The hybrid model consisted of two modelling branches, viz. equilibrium and dynamic modelling. An equilibrium sub-model was created and the output results were then used as inputs into a dynamic sub-model, which not only considered the effects of thermo-equilibrium interactions, but also the faster-changing electrical dynamics of furnace control. The final modelling step involved genetic optimisation, whereby model variables were manipulated to optimise the proposed KPI's. In other words, operating conditions were established to improve furnace performance.

It was determined that significant improvement in the values of the KPI's may be expected if the optimised setpoints are implemented on-site. The existing setpoints for electrical operation should be maintained while the power expended per tonne of alloy should be altered (by tapping more regularly). Specific adjustments to the proportions of the feed recipe should also be made.

## OORSIG

'n Projek is aanvanklik begin om die produksieproses by 'n spesifieke hoëkoolstof ferromangaanoond te optimiseer. Sedert operasionele probleme ondervind is in die oond en daar 'n tekort is aan vertroubare data vir die jaar 2007, is daar besluit om data van 'n meer stabiele hoëkoolstof ferromangaanoond te analiseer. Drie sleutelverrigtingsaanwysers (SVA's) is geselekteer om die algehele prosesverrigting aan te dui. Hulle is: (1) Die totale tonnemaat hoëkoolstof ferromangaan geproduseer per tonnemaat van voermateriaal, (2) die persentasie herwinning van mangaan tot die allooiproduk, en (3) die allooï:slak verhouding. Die verhoging van elk van die bogenoemde sal bydra tot die algehele bevordering van die proses.

Om die doelwitte van die projek na te kom, is 'n Kombinasie-model ontwikkel om die produksie gedrag van die oond te karakteriseer en om die voorgestelde SVA's te optimiseer. Die Kombinasie-model het bestaan uit twee modelleringsvertakings, nl. termodinamiese ewewig en dinamiese modellering. 'n Termodinamiese ewewig sub-model is geskep en die uitset resultate is gevolglik gebruik as invoerdata na 'n dinamiese sub-model, wat nie slegs die uitwerking van termo-ewewiginteraksies in ag neem nie, maar ook die vinnigveranderende elektriese dinamika van die oond. Die finale modelleringstap het genetiese optimisering behels, waarby model veranderlikes gemanipuleer is om die voorgestelde SVA's te optimiseer. Met ander woorde, operasionele kondisies is vasgestel om oond produksie te bevorder.

Dit is bepaal dat kenmerkende verbetering in die waardes van die SVA's verwag kan word as die ge-optimeerde setpunte toegepas is op die oond. Die oorspronklike setpunte vir elektriese beheer hoort gehandhaaf te word terwyl die krag verbruik per ton allooï verander moet word (deur om meer gereeld te tap). Spesifieke verstellings op die proporsies van die voerresep moet ook gemaak word.

## FOREWORD

The investigation presented in this thesis entails the development of a troubleshooting and/or optimisation simulation for a high-dimensional and complex processing system. The project was initiated for the purpose of improving the production capacity of a high-carbon ferromanganese furnace of industrial proportions.

Attention was paid to the application of relevant engineering – and modelling principles in order to satisfy the criteria of the project creatively. The project objective was to propose setpoint values for certain manipulable process variables to achieve overall process improvement.

The work contained in this thesis not only discusses the development of a hybrid model or the results of an optimisation simulation, but also provides the reader with an improved understanding of pyrometallurgical processing in submerged-arc furnaces. The proposed model does not need to be used exclusively for the production of high-carbon ferromanganese, but can be recalibrated for any multivariate thermochemical process which is dynamically controlled. The modelling method is therefore especially useful for highly complex and ill-defined chemical or metallurgical systems.

## VOORWOORD

Die ondersoek wat in hierdie tesis voorgestel word bring mee die ontwikkeling van 'n probleemoplossende en/of optimiserende simulatie vir 'n hoë-dimensionele en komplekse proses-sisteem. Die projek is geïnisieer met die doel om die produksie kapasiteit van 'n hoëkoolstof ferromangaanoond van industriële skaal te verbeter.

Aandag is bestee aan die toepassing van relevante ingenieurs – en modellerende beginsels om op 'n kreatiewe wyse aan die kriteria van die projek te voldoen. Die doel van die projek was om setpunt-lesings van sekere manipuleerbare prosesveranderlikes vas te stel om algehele prosesbevordering te behaal.

Die werk wat in hierdie tesis saamgevat word bespreek nie slegs die ontwikkeling van 'n kombinasie-model of die uitslae van 'n optimaliseringsoefening nie, maar bied ook aan die leser 'n beter begrip van pirometallurgiese prosessering in dompelboogoonde. Die voorgestelde model hoef nie slegs aan die produksie van hoëkoolstof ferromangaan toegepas te word nie, maar kan herkalibreer word vir enige multiveranderlike termochemiese proses wat dinamies beheer word. Die model is om hierdie rede bruikbaar vir hoëkomplekse en ongedefinieerde chemiese of metallurgiese sisteme.

*Iné, my understanding wife,  
thank you for your love and patience*

# ACKNOWLEDGEMENTS

A special thanks to the following organisations and people:

- Professor Jacques Eksteen, for being a true academic role model and mentor. My sincere appreciation to him for kick-starting my career and for initiating the work of this project.
- Professor Chris Aldrich, for his supervisory input, open-minded support and advice, until completion of the project.
- Professor André Burger, for active moral support and friendship.
- Greg Georgalli, for constructive advice.
- Juliana Steyl, for managing journal orders.
- The financial assistance of the National Research Foundation (NRF) towards this research is hereby acknowledged. Opinions expressed and conclusions arrived at, are those of the author and are not necessarily to be attributed to the NRF.
- CSense Systems (Pty) Ltd, for the use of their unique software product and support.
- Ferdus le Roux, for project authorisation.
- Shobini Singh, for technical mediation.
- Manganese Division employees, for plant data:  
Fanie Landman, System Integration Engineer  
Nakedi Mashangoane, Production Engineer  
Emannual Dube, Production Superintendent  
Daleen Smith, Chemist  
Frik Blaauw, Laboratory Superintendent  
Hannes Schoeman, Laboratory Technician  
Riaan Esterhuizen, Materials and Logistics Superintendent  
Piet van Schalkwyk, Materials Manager  
Corrie van Eyssen, Final Products Superintendent
- Parents and grandparents, for their love, prayers and continual support.
- My helper Iné, for her unconditional love, encouragement and prayers.

All thanks to my saviour Jesus Christ, the son of the living God. All things are made possible according to his good and perfect plan.



# CONTENTS

## CHAPTER 1

<b>INTRODUCTION .....</b>	<b>1</b>
1.1 Project scope.....	1
1.2 Defining a model structure .....	4
1.3 Project objective .....	5

## CHAPTER 2

<b>BACKGROUND AND PROCESS OVERVIEW .....</b>	<b>6</b>
2.1 The importance of ferromanganese .....	6
2.2 Process description .....	7
2.2.1 Raw materials handling .....	7
2.2.2 Furnace operation.....	8
2.2.3 Handling of final products and sampling.....	10

## CHAPTER 3

<b>LITERATURE OVERVIEW OF FURNACE BEHAVIOUR .....</b>	<b>11</b>
3.1 Furnace electrical configuration .....	11
3.2 Reaction chemistry .....	19
3.3 Energy requirements.....	21
3.4 Phase analysis.....	22
3.5 Physical properties.....	26
3.5.1 Resistivity / conductivity.....	26
3.5.2 Density .....	29
3.5.3 Viscosity.....	31
3.6 Slag-metal equilibrium and mineralogical interactions .....	32

## CHAPTER 4

<b>MODELLING METHODOLOGY .....</b>	<b>36</b>
4.1 Furnace modelling and simulation.....	36
4.2 Techniques for simulating furnace behaviour.....	39
4.2.1 Thermochemical simulations with FactSage .....	39
4.2.1.1 Modelling of Furnace 1 (investigation discontinued).....	40
4.2.1.2 Modelling of Furnace 2 (subject of investigation) .....	42
4.2.2 Neural network modelling.....	43
4.3 Modelling methodology quantified .....	49
4.3.1 Summary of assumptions .....	49
4.3.2 The proposed hybrid model.....	51
4.3.2.1 Thermodynamic modelling .....	53
4.3.2.2 Dynamic modelling.....	55

4.3.2.3 Optimisation with genetic algorithms .....	55
4.3.3 Modelling overview .....	58
<b>CHAPTER 5</b>	
<b>RESULTS AND DISCUSSION .....</b>	<b>60</b>
5.1 Thermodynamic process model .....	60
5.1.1 Material flow assumptions .....	60
5.1.2 Temperature calibration .....	62
5.1.3 Thermodynamic neural network model.....	66
5.1.4 Sensitivity of feed materials on FactSage-modelled outputs .....	67
5.2 Energy considerations.....	70
5.2.1 Energy balance and power requirements .....	70
5.2.2 Electrical control .....	72
5.3 Dynamic process model.....	73
5.3.1 Results of dynamic modelling .....	73
5.3.2 Optimisation of the dynamic model .....	78
<b>CHAPTER 6</b>	
<b>CONCLUSIONS.....</b>	<b>90</b>
<b>CHAPTER 7</b>	
<b>RECOMMENDATIONS.....</b>	<b>92</b>
<b>REFERENCES .....</b>	<b>94</b>
<b>APPENDICES.....</b>	<b>98</b>
Appendix A <i>FactSage configuration and factorial design</i> .....	98
A.1 <i>Furnace 1</i> .....	98
A.2 <i>Furnace 2</i> .....	102
Appendix B <i>Neural network model development</i> .....	105
Appendix C <i>Development of a slag density equation</i> .....	109
Appendix D <i>Furnace mass capacity and burden residence time</i> .....	115
Appendix E <i>Development of a slag viscosity model</i> .....	117
Appendix F <i>Feed materials to Furnace 2</i> .....	122
Appendix G <i>Neural network modelling and optimisation with CSense</i> .....	129
G.1 <i>Thermodynamic modelling</i> .....	129
G.2 <i>Dynamic modelling</i> .....	137
G.3 <i>Optimisation and comparison</i> .....	141

## CHAPTER 1

# INTRODUCTION

### 1.1 Project scope

High-carbon ferromanganese (HCFeMn) is one of the alloy products from three specific furnaces of a ferro-alloys company in Gauteng, South Africa. Each of these circular, three phase, submerged-arc furnaces are capable of an annual production capacity of about 150 000 tonnes of metal. A major problem concerning these furnaces is the uncertainty relating to the practice of optimal furnace control as described in more detail in Chapter 2. Under-utilised process data can therefore be investigated for its usefulness in the identification of patterns in furnace behaviour that could be used in a corrective control strategy.

The hypothesis statement of this thesis is that a hybrid model may be developed (from under-utilised process data) and be used as a diagnostic tool to indicate the principal variable setpoints that would lead to improved furnace performance.

The dynamics of molten materials inside metallurgical furnaces are normally difficult to predict, especially for feed mixtures of multiple materials with complex microstructures. Attempts to understand the complexities of furnace dynamics has led to the proposal of various oversimplified solutions by previous investigators. Such solutions are referred to as 'black-box' models, because only input and output material data are considered. Consequently, only moderate success had been achieved when historical plant data were trained with neural networks to predict future results (Eksteen and Reuter, 2006; Reuter and Yang, 2000). On the other hand, models which make predictions based on reaction kinetics only or on thermodynamic models only, may shed light on the nature of molten ferroalloy systems, but may fail to predict the medium and long-term behavioural patterns owing to a number of possible variables that are not considered for such models:

- Residence time of burden throughput
- Imperfect mixing
- Temperature gradients
- Variations in the feed mineralogy
- Incomplete reaction cycles
- Gas blowouts

As a result of the many disturbances, a hybrid model was proposed for predicting and identifying variables that influence furnace performance. The hybrid model incorporated both thermodynamic and dynamic process data, as can be seen in Figure 1. The functions performed and variables used are indicated below the high level blocks displayed in Figure 1. Development of this model is further explained in the paragraphs following the diagram.

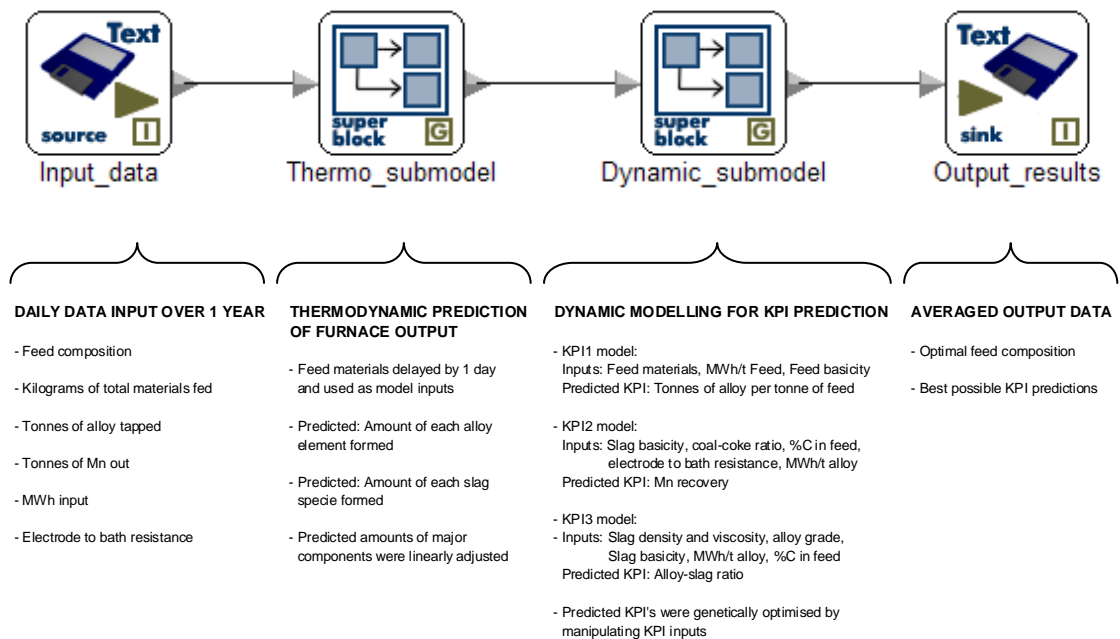


**Figure 1 Conceptual high level layout of the proposed hybrid model**  
**(Block diagram illustrated by permission of CSense Systems (Pty) Ltd)**

First, a sub-model was developed and calibrated to characterise the relationships between a blend of known furnace feed materials and the resulting equilibrium outputs of metal and slag. This step was referred to as the thermodynamic step of the investigation and was necessary for predicting the equilibrium amounts and compositions of the molten materials exiting the furnace, even for varying/alternate blends of the same feed materials. The thermodynamic sub-model was further comprised of two sub-models, each trained to predict the individual outputs of the slag and alloy products for any combination of feed materials.

Secondly, another sub-model was developed to combine some of the results of the thermodynamic sub-model with the dynamic influences of controllable electrical variables to predict optimum setpoints for so called 'key performance indicators' or KPI's. This step was referred to as the dynamic modelling step of the investigation. A performance indicator can be defined as a specific target variable or ratio that can be monitored and optimised to establish good process performance. The dynamic sub-model was comprised of three sub-models, each trained to predict outputs for three different performance indicators. The performance indicators thought to characterise the behaviour of the furnace were (1) the tonnes of alloy tapped per tonne of feed, (2) the percentage of Mn recovered from the feed blend, and (3) the alloy-slag ratio of the molten product materials. The prediction window for both thermodynamic and dynamic models followed after all feed inputs were shifted forward in time by one day, i.e. the average residence time of material throughput. This was done to minimise the uncertainties associated with the effects of burden residence on product output.

The final modelling step involved the application of a genetic optimisation algorithm which would adjust to optimum levels the variables that would improve the selected KPI outputs. Model development and optimisation are further discussed in Chapter 4.

With this combined modelling approach, furnace performance can be predicted and optimised through the implementation of optimised variable setpoints. This modelling method could fit into the control structure of furnace operation in a supervisory capacity in order to complement the normal operation of the furnace (Reuter and Yang, 2000).

## 1.2 Defining a model structure

The flowchart in Figure 2 indicates some of the important developmental steps that are required for an effective furnace model (Eksteen and Reuter, 2006).

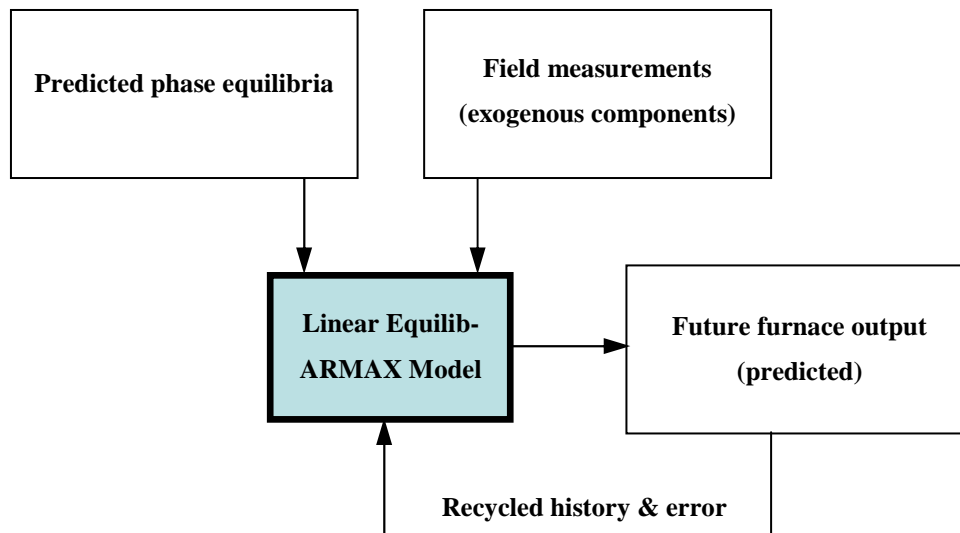


**Figure 2** ‘A flowsheet to develop Equilib-ARMAX models’ as from Eksteen and Reuter (2006)

What is important to note from Figure 2 is that two main data sources are combined to form a complete model. These are (1) predicted equilibrium data and (2) empirical plant data. These data sources are then used to predict furnace output ahead of time. Although this methodology may appear to be conceptually similar to the proposed model in section 1.1, the main difference between these is that no future predictions were calculated for output data in the proposed model, but rather an adjustment of controllable furnace variables was performed to positively affect metal production by the inclusion of an additional step of genetic programming. Also, a neural network model was used instead of a linear ARMAX model (auto regressive moving average model with exogenous variables) to maintain a single model type throughout the entire hybrid model that can easily be trained and configured to effectively predict output data for unseen linear or nonlinear input data.

### **1.3 Project objective**

In essence, the overall model would use electrical furnace data and reconciled metallurgical analyses of furnace products to predict the values of specific performance indicators that would reflect process performance. Model results would be analysed to show the effects of the different variables on the applicable performance indicators. Setpoints would subsequently be optimised for each model variable, enabling plant operators to take corrective action to achieve improved furnace operation.

## CHAPTER 2

# BACKGROUND AND PROCESS OVERVIEW

### 2.1 The importance of ferromanganese

In general, high-carbon ferromanganese is produced from manganiferrous ores in which a Mn : Fe ratio of about 7.5 : 1 is required for a 78% manganese concentration in the ferromanganese product. It finds use as an alloying additive to cast iron, steel and non-ferrous metals.

The primary component of high-carbon ferromanganese is manganese. Its chemical properties are similar to that of iron and chromium and it is physically very hard and brittle. Manganese is primarily extracted from the earth in an oxide form which is most stable when it exists in its divalent state at standard conditions, i.e. Mn(II). This oxide naturally dissociates at high temperatures into oxide forms which have higher manganese valencies, e.g. Mn(III), Mn(VII) and Mn(IV).

The primary reason why manganese is used as an alloying component is that it reacts readily with oxygen, sulphur and phosphorus and it therefore deoxidises and desulphurises the metal in which it is alloyed. Manganese in South Africa is primarily sourced from the Kalahari fields in the Northern Cape Province. The Mamatwan and Wessels mines are two major providers of ore from the Kalahari fields. Open cast operations are employed at the Mamatwan mine, whilst a room and pillar mining system is used to mine the deeper ore body at the Wessels mine. At both of these mines, ore is crushed, beneficiated, sintered and finally distributed to smelting plants where ferromanganese of the correct grade and size fraction is produced.



## **2.2 Process description**

The operations in the production of high-carbon ferromanganese are divided into three distinct sections: raw materials handling, furnace operation and final products handling. Each is briefly discussed in the sections that follow.

### **2.2.1 Raw materials handling**

Raw materials are delivered to a high-carbon ferromanganese production plant by train, truck, or container. The feed materials required for producing high-carbon ferromanganese in this study are ferromanganese ores, coal and coke reductants, and silica flux.

Manganese ore and sinter is obtained from open cast manganese mines in the Northern Cape (South Africa). The minerals contained in one of these ores, Mamatwan ore, are mainly hausmannite, jacobsonite and cryptomelane. The main gangue components of these ores are calcite, dolomite, hematite and various carbonates (Kleyenstüber, 1982). Some of the ores are sintered or pre-reduced to lower the oxidation state of the various manganese oxide minerals and to concentrate the total manganese content to about 50%. Iron ore from the Northern Cape, with a specific minimum iron content of around 60%, is also used intermittently for enriching the iron content of the ferromanganese. The consumption of ore materials in the furnace investigated is indicated in Appendix F.

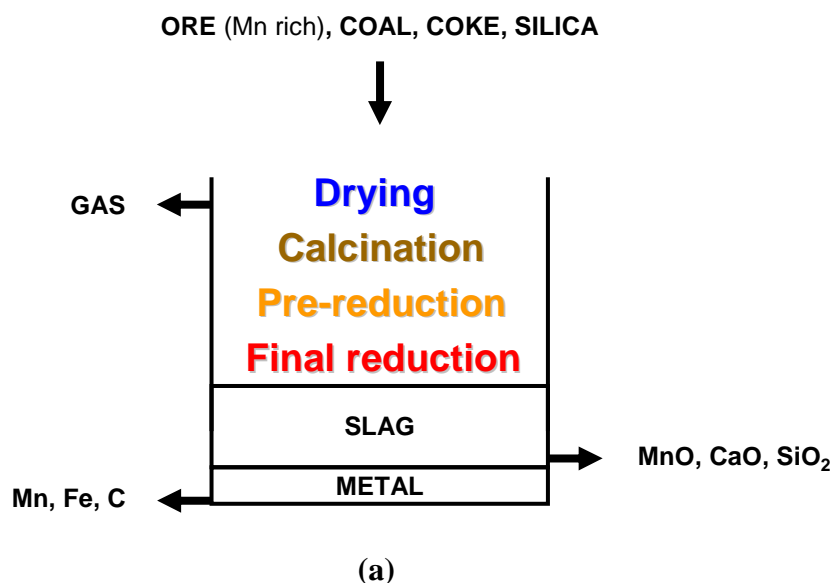
Bituminous coal and coke are typically used for the reduction of manganese ore to metal. The amount of fixed carbon in the coal used for processing had a maximum limit of about 50%. Coke with a higher fixed carbon grade of around 80 to 90% is imported from China to speed the reduction reaction in the furnace.

A fluxing agent is added to the furnace to control the slag basicity and viscosity. The amount of silica in the quartz used is close to 100%.

In the pre-processing operations of the high-carbon ferromanganese process, raw materials are typically offloaded in piles in a stockyard with a stacker. Each material is stacked according to its type and particle size. Materials are then reclaimed onto a conveyor system and sent to storage silos from which the underflow is mixed according to a predetermined mass balance and transferred to the furnace for processing. All coals are screened before being directed to the silos. This limits the amount of fines to be charged to the furnace.

### 2.2.2 Furnace operation

A high-carbon ferromanganese furnace is typically gravity-fed from feeding bunkers that are situated above the level of the furnace. Energy is transferred to the ore from three carbon-based electrodes that are lowered into the furnace with hydraulic clamps. The rate at which electrodes are lowered depends on the required depth of operation and rate of electrode consumption. Figure 3 illustrates the basic layout of a submerged-arc furnace used for producing high-carbon ferromanganese. The furnace is called a submerged-arc furnace, because energy is supplied via electrodes that are submerged under the material burden.



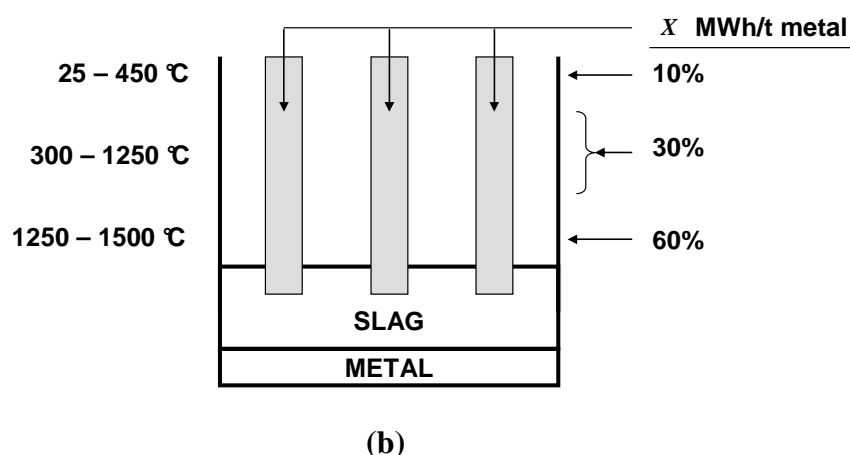


**Figure 3 (a) Material flows and reaction zones in a high-carbon ferromanganese furnace**

**(b) Energy input dispersion (theoretical) and temperature profile of burden**

Saleable high-carbon ferromanganese metal and discard slag are the liquid products produced from the furnace. The metal is only tapped after a certain amount of energy has been supplied to the burden. This supposedly allows enough time for good reduction of the ore and for adequate settling of metal through the slag layer. A maximum power input to the furnace for a specific feed blend is achieved through varying the electrode tip positions to obtain desired setpoint values for electrical resistance and electrical current. Three-phase current is supplied to the electrodes from three transformers (one for each electrode), each delivering a secondary current in the order of about 100 kA.

In the furnace production of high-carbon ferromanganese, off-gas is also produced as a by-product in the reaction zones of the furnace. A gas plant is therefore operational for scrubbing and drying the off-gas. Cleansed gas can then be used in energy recovery operations or for power generation. Sludge captured from the gas plant is transferred to waste slimes dams.

Furnace discard slag is tapped into large ladles and transported to a slag dumping site or to a secondary metals recovery plant. Tapped ferromanganese metal is poured into

slabs which are broken into pieces by large excavation trucks and transported to a products handling section of the plant. Samples are spooned from molten slag and metal as they are tapped from the furnace and these are then passed to the sampling laboratory for analysis.

### **2.2.3 Handling of final products and sampling**

Solidified ferromanganese is typically crushed and screened into saleable size fractions. A screening house screens the product into the correct size fractions and these are conveyed to storage silos or stockpiles for quality control and dispatch.

Materials from each of the three major plant sections are sampled for the purpose of quality control. All furnace-product samples are typically analysed by XRF (x-ray fluorescence) spectrometry. This analytical technique is reliable for identifying the concentration of bulk phases within a sample and has an average accuracy of approximately 99.5 percent. Wet chemical analysis and titration techniques may also be performed on raw material samples to determine very accurately the concentrations of pure constituents such as carbon, sulphur, manganese and iron.

## CHAPTER 3

### LITERATURE OVERVIEW OF FURNACE BEHAVIOUR

The following sections point out some important aspects of furnace operation and – dynamics. The relevance of each topic to the research work is also discussed where necessary.

#### 3.1 Furnace electrical configuration

High voltage and low current are converted to low voltage and high current in each of three single phase transformers that is connected between two electrodes. The large conductors that transfer current to the electrodes are referred to as busbars. All the furnace busbars are connected to the three electrodes in a triangular, or delta, configuration. Only small amounts of current flow directly between the electrodes through the solid burden in the upper region of the furnace, because of the high resistance of the solid materials. Most of the current therefore flows between the electrodes and molten metal by means of star conduction, with the molten metal being the star point. The total electrical connection is referred to as a delta-star connection.

The electrical resistance of current-flow from one electrode is increased if the distance between the electrode tip and the metal bath is increased. Reactance of AC circuits is caused by interference of magnetic flux around current-carrying conductors (magnetic inductance). Changes in magnetic flux patterns induce voltage along conductors which leads the current by 90°. Reactance is therefore dependent on the geometry of the furnace, the diameter of the electrodes, the magnetic properties of the raw materials charged and the stability of the feed current. As all of these variables only change slightly during operation, or do not change at all, the reactance of a furnace remains relatively constant.

For large submerged-arc furnaces, the large ratio between reactance and resistance will result in low energy absorption in the furnace burden. This ratio generally increases with the size of the furnace, because of greater electromagnetic interference (or reactance) in larger furnaces owing to greater current flows and greater flux densities. The relationship between reactance and resistance is well understood electrically. This is not the case in an electrical furnace, where certain control and operation problems cause reactance and resistance imbalances that cannot be explained. Some of these problems are:

- Uneven refractory erosion – causes reactance imbalances
- Uneven power distribution through the load during tapping – geometric changes brought about by tapping and uneven distribution of the burden
- One electrode riding higher than the other two due to electrode interaction – causes resistance and power imbalances
- Electrode movement causes phase current to become less sensitive to lower resistance levels, according to the equation:

$$I = \frac{V}{\sqrt{R^2 + X^2}} \text{ for a single phase} \quad (1)$$

$I$  = Current,  $V$  = Voltage,  $X$  = Reactance

Electrodes would therefore have to be moved further to keep the current constant when normal changes of the resistance of a phase results. Conversely, small variations of current may cause large changes in resistance (and power). Other unwanted effects are kneeding of the burden and a greater risk of electrode breakage. Compression of the burden by kneeding may put strain on the electrodes and may also limit free material movement to under the electrodes. These effects occur when a furnace is current controlled at a specific electrode current. Furnaces are generally not current controlled but are resistance controlled with all three electrodes at the same electrode-to-bath resistance value, to minimise electrode movement and to negate the interaction effects of current

control. Operation will therefore be more balanced. More is explained about resistance control in the paragraphs that follow. Barker and Stewart (1980)

The current input to a submerged-arc furnace is controlled at specific setpoints by adjusting the height of each electrode. Moving an electrode up decreases the current and moving it down increases the current. This happens because resistance to current flow increases between the electrode tip and the conductive burden when the electrode is raised and vice versa. Gray (1980)

It was confirmed with measured electrical data from a specific high-carbon ferromanganese furnace that the power factor decreases as the ratio between reactance and resistance increases, for non-zero values of reactance and resistance. This can be seen in Figure 4. The furnace power factor is a measure of the amount of power supplied for resistive heating in the furnace burden. This is explained in more detail later on. A greater measure of reactance impacts the sensitivity of electrode motion negatively. The total MVA power measurement of a furnace decreases as reactance increases and the result is a lower power factor.

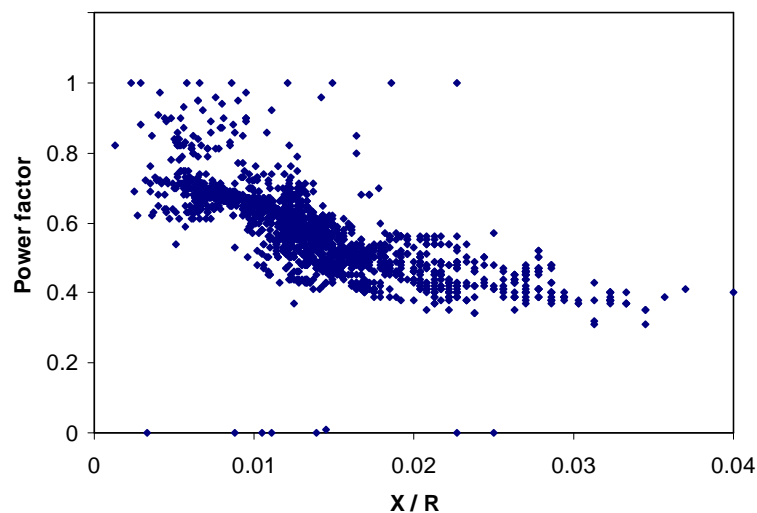


**Figure 4** Power absorption in a furnace burden decreases as the reactance ( $X$ ) increases relative to resistance ( $R$ )

The depth of electrode immersion and the resistive/conductive properties of the raw materials charged are primary variables affecting the electrode-to-bath resistance within a furnace. Other variables are however also influential on the resistance measurement such as the geometry of the furnace and the diameter of the electrodes. Since electrode immersion is related to the geometry of the furnace, some researchers have combined the depth of electrode immersion with the other geometric parameters (electrode diameters and furnace geometry) and have formed a ‘geometric factor’,  $f_g$  [1/cm]. The electrode-to-bath resistance,  $R$ , is therefore proportional to the geometric factor and burden conductivity,  $\sigma$  [1/mohm.cm], as follows (Jiao and Themelis, 1991):

$$R \propto \frac{f_g}{\sigma} \quad [\text{mohm}] \quad (2)$$

In normal furnace operation, reactance measurements do not vary much as they are more dependent on the geometry and size of the furnace and electrical connections. Electrode-to-bath resistance measurements are however widely variable and are strongly dependent on the resistivity of the burden and the positioning of the electrodes.

A furnace should be resistance controlled to minimise electrode movement and thereby significantly reduce the occurrence of the problems associated with current control. An optimum electrode resistance should be maintained by moving the electrode up (away from the low-lying conductive metal bath) to increase the resistance (electrode-to-bath resistance) or down to decrease the resistance. Electrode movement has to be manipulated in order to control the resistance for the reason that the electrodes are continually consumed in the reduction of the oxide materials. In a furnace which is current controlled, electrodes are continually moved to establish constant electrode currents through each electrode. This kind of control is not ideal, because various problems may occur such as those listed above Equation (1).



Heat loss from the surface of the bed of raw materials can be minimised by running the furnace at a low electrode-to-bath resistance. The measured resistance should however not be made too low (or the electrodes should not be immersed too close to the conductive metal bath), because higher current will flow at lower resistances, causing excessive current densities that could overheat and vapourise a high proportion of the product alloy and would inhibit burden movement to underneath the electrodes. Also, too many unwanted metal oxides may be reduced, causing the product to be contaminated. Any one or combination of these may be limiting factors for a burden with a given specific resistivity. Optimum and consistent electrode penetration will therefore promote high current densities below the electrodes and optimal heat transfer from the hot gas to the burden. This then boosts the rate of reduction of the metal oxides in the feed materials and may also improve the grade of the product.

The amount of power supplied per tonne of alloy, i.e. the MWh/t value, can be minimised through the practice of regular tapping. No heat is therefore wasted in keeping the molten mass at a high temperature. The characteristic curves for the furnace under investigation are shown in Figure 5 and are useful for pinpointing electrical performance based on the resistance and tap position setpoints.

On this diagram, curves of constant electrode-to-bath resistance are displayed as the upward sloping curves. Also displayed are curves for each transformer tap position. Manipulation of the resistances (by moving the electrodes) and of the transformer tap positions (voltage levels), will induce change in the electrode current (along the x-axis) and in the total MW power supply (y-axis) to the burden. Tap voltage is a term used to define the secondary voltage level obtained for a specific transformer tap position. Each transformer will have several tap positions, each delivering a different secondary voltage output, as indicated in Figure 6.

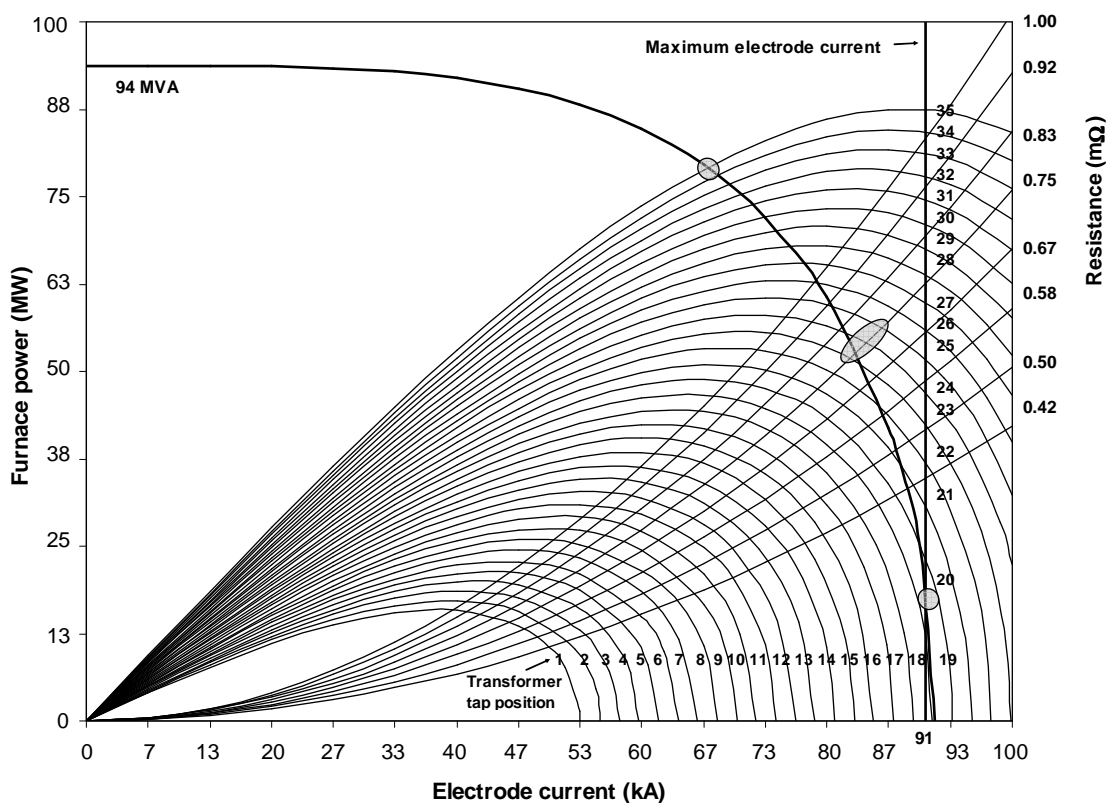


**Figure 5 Electrical characteristic curves for Furnace 2**  
**(Data scaled as per confidentiality agreement)**

Tap positions can be adjusted or controlled in combination with the electrode positions to achieve specific levels of power absorption within a furnace. A higher tap number represents a higher secondary voltage. Higher power absorption will therefore occur at high tap numbers for a fixed resistance. Electrode current may be increased by increasing the tap voltage or by decreasing the resistance, as is consistent with Ohm’s law,  $V=IR$ .

To maintain a given resistance from low to high MW load, each tap voltage increase will cause an increase in electrode current. A maximum current level of 91 kA is indicated as a vertical line in Figure 5. An increase beyond this measurement may cause short-circuiting between the electrodes and the molten alloy, and severe power loss will occur.

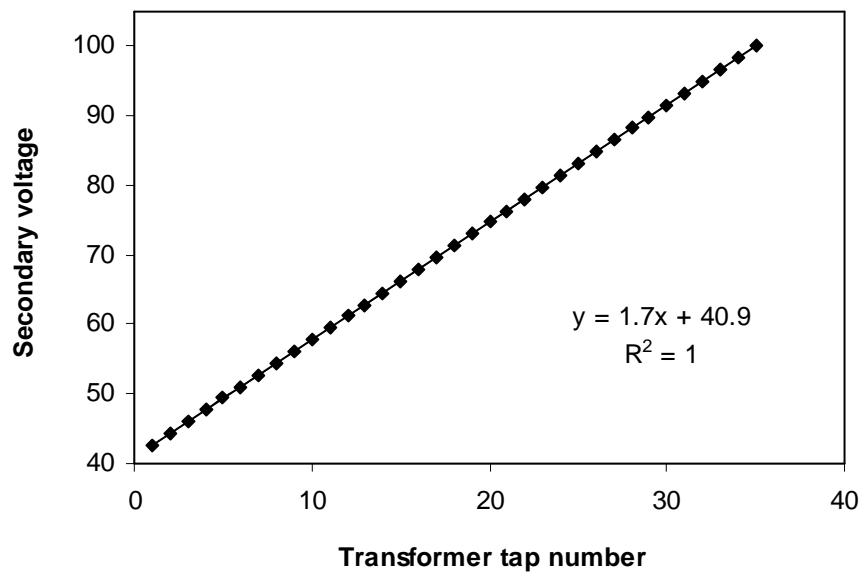


**Figure 6 Secondary voltage output for different tap position in a submerged-arc furnace  
(Data scaled as per confidentiality agreement)**

Large furnaces will have significant reactance levels, owing to interference between strong magnetic flux patterns that are induced by current flow. Maximum electrical efficiency can be obtained by controlling the electrode resistance as close as possible to the electrode reactance measurement for a given tap voltage.

Optimal electrical efficiency can be obtained when electrode resistance levels are controlled as close as possible to the furnace reactance for a given tap voltage. The

optimal power factor will therefore be:  $PF = \cos \theta = \sqrt{\frac{R^2}{R^2 + X^2}} = \sqrt{1/2} = 0.707$ . In

certain metallurgical systems, experience has shown that maximum electrical efficacy is achieved when the electrode resistance is operated slightly below the electrode reactance, for a given tap voltage.

Some metallurgical systems operate at an electrode resistance setpoint that is well below the furnace reactance (for the furnace under investigation, reactance is seen to remain fairly constant at about 1.1 mohm and resistance varies around 0.75 mohm).

This practice may be necessary to prevent excessive heat loss from the surface of the burden when electrodes ride too high at high resistance levels, or to promote optimum oxide reduction rates lower in the furnace where electrodes are immersed deep enough (closer to the conductive metal bath) to bring about higher reaction temperatures. A furnace therefore has to operate at a defined resistance so that the best compromise is achieved between operating variables such as MWh/ton, electrode immersion, consumption rates, alloy tapping ability, alloy production and gas yield. Operating at too low a resistance setpoint, however, tends to reduce the power factor to levels that make electrode control difficult. For example, “when the power factor is less than 0.5, the movement of any one electrode will induce a greater current change in another electrode than to the current in itself. Clearly this has major consequences for electrode control based on current.” Barker *et al.* (1991)

For resistance-based electrode control, interaction problems with electrode movement are not so much the problem, but rather insensitivity to current flow. This means that even if each electrode is controlled at the same resistance (as for the furnace under investigation), greater current imbalances may be experienced at lower power factors and therefore uneven heating of the burden. Barker *et al.* (1991) indicated that electrode control problems get progressively worse as the power factor decreases, and not only for power factors less than 0.5. The severe control problems experienced at different power factors are listed below:

- PF < 0.5 - Perpetual operating problems and system instability
- PF = 0.6 - Operating problems likely to contribute to major production loss
- PF = 0.7 - Operating problems significant, system stability impaired
- PF = 0.8 - Problems noticeable
- PF = 0.9 - Few problems observed

With reference to Figure 5, maximum power absorption is achieved by operating the furnace at maximum design capacity, i.e. along the 94 MVA curve, or even slightly beyond, provided that this practice does not result in escalated maintenance costs caused by excessive wear of the furnace shell. The optimum level of power absorption

is achieved when the furnace is operated as close as possible to the maximum current level to provide sufficient heating, but at the highest resistance value possible to maintain sufficient power absorption and an acceptable power factor. The best compromise between high and low resistance setpoints therefore needs to be established to maximise production and to minimise the energy requirement per tonne of product.

The two grey circles in Figure 5 denote the upper and lower operating extremes for electrical furnace control, while the grey ellipse denotes the average operating region over the last year of production. It seemed that resistance setpoints of about 0.75 mohm and tap positions ranging from 22 to 24 were the most frequently used to achieve maximum power absorption.

### 3.2 Reaction chemistry

Rankin and Van Deventer (1980) investigated a reaction mechanism for the reduction of manganous oxide by graphite. They found that the most probable mechanism for reducing MnO to Mn is by the dissolution of MnO in slag, followed by its reduction from the slag by solid carbon or carbon-saturated alloy.

The rate of gasification of carbon, according to the Boudouard reaction, is the rate controlling step for the reduction of MnO (Rankin and Van Deventer, 1980):



The overall reaction can be written as:



According to Grimsley *et al.* (1977), Reactions (1) and (2) are more appropriate to consider for higher oxides of manganese, e.g.  $Mn_3O_4$  and  $Mn_2O_3$ , as the reaction mechanism between a solid and a gas would be much more rapid and probable at temperatures less than 700 °C than what is possible between the reagents of reaction (3). Reaction (3) becomes the dominating reaction at temperatures exceeding 700 °C, not only for the reduction of MnO but for all the oxides of Mn. Manganese oxides at temperatures greater than 700 °C may be reduced either by dissolved carbon (metal carbides such as  $Fe_3C$ ) or by solid carbon, but not by gaseous CO. Reaction (1) would not be probable for pure MnO, because the standard free energy change for this reaction is positive between 25 °C and 2000 °C. “The rate and degree of reduction were found to increase with additions of carbon and with increasing temperature up to 1300 °C, when they reached their maximum”. This occurrence would most likely continue for temperatures exceeding 1300 °C. Grimsley *et al.* (1977)

The thermodynamic probabilities and experimental results discussed above correspond with the experimental findings of Koursaris and See (1979). They proposed three stages of reduction to explain the mechanism of formation of Fe-Mn-C alloy. Mamatwan ore was reacted with South African coal and coke in the investigation. The first stage appeared to be a pre-reduction stage wherein higher manganese oxides ( $Mn_3O_4$ ) and hematite ( $Fe_2O_3$ ) are reduced by carbon monoxide gas to manganous oxide (MnO) and metallic iron (Fe), respectively. A primary slag forms which is rich in CaO and  $SiO_2$ . “The second stage involves the dissolution of manganous oxide into the slag and reduction at the surface of ore particles by carbon dissolved in the metallic beads. During the third stage, reduction occurs mainly by solid carbon in contact with the molten slag. Some reduction may occur from the slag in contact with the layer of alloy” at the slag-alloy interface (Koursaris and See, 1979).

In the work of Rankin and Van Deventer (1980) it was found that the rate of reduction of MnO increased as the MnO-to-C ratio decreased. This agrees with the findings of Grimsley *et al.* (1977).

### 3.3 Energy requirements

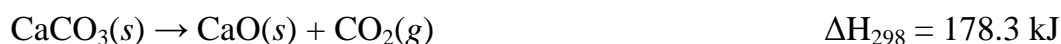
Production of high-carbon ferromanganese can be maximised in two ways by manipulating the power input to the furnace. The first is to minimise the MWh per tonne of alloy tapped as much as possible by tapping more frequently. If the MWh/t value is too high, then energy is lost in maintaining high burden temperatures for too long. If the power input is too low, then the necessary reduction reactions may not be completed in time. The second prerequisite is to maximise the power absorbed (at constant MWh/t) in the furnace within the electrical constraints of operation. More information on maximising the power input to a furnace is discussed in section 3.1. De Waal *et al.* (1992)

The main reactions that would either contribute significant amounts of energy to or from the system, according to Olsen *et al.* (2007), are listed below:

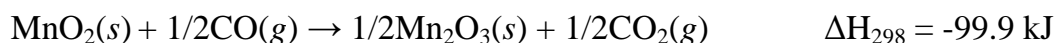
- Moisture drying and vapour reactions (25 - 500 °C)



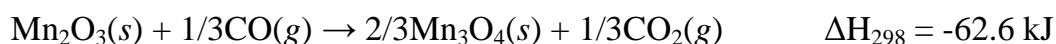
- Calcination/decomposition of carbonates (300 – 900 °C)



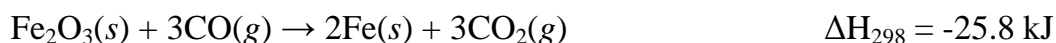
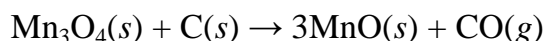
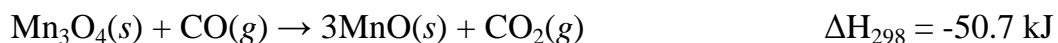
- Low temperature gas pre-reduction (25 – 400 °C)



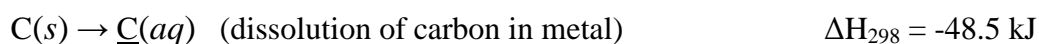
- Medium temperature gas pre-reduction (400 – 800 °C)



- Boudouard pre-reduction and iron oxide reduction (800 – 1250 °C)



- Final melt reduction/smelting (1250 – 1500 °C)



The mixing enthalpy of the latter reaction of carbon dissolution in metal is assumed to be analogous to the energy of formation of  $\text{Mn}_3\text{C}$ , according to the reaction  $3\text{Mn}(l) + \text{C}(s) \rightarrow \text{Mn}_3\text{C}(aq)$ . Olsen *et al.* (2007)

### 3.4 Phase analysis

It has been suggested by Urquhart (1980) that it is practically necessary for the liquidus temperature of the slag to be about 100 °C greater than the liquidus temperature of the alloy. This is necessary to facilitate tapping. If this condition is seen as a minimum temperature constraint, then it would be logical to run the process at the highest temperature possible. This is however impossible, since manganese volatilisation increases as temperature increases. The reduction of silicon from slag to alloy also increases as temperature increases. For these reasons it is necessary to run the process at the lowest possible temperature without crystallising solids from the molten phases. The temperature should nonetheless be high enough to melt all the feed materials and to promote favourable commencement of the reduction reactions. The liquidus conditions of the Mn-Fe-C alloy system and the MnO-SiO<sub>2</sub>-CaO-Al<sub>2</sub>O<sub>3</sub>-MgO slag system were further investigated with reference to the phase diagrams in Figure 7 and Figure 8 below. Note that Figure 8 only appears on the page following Figure 7.



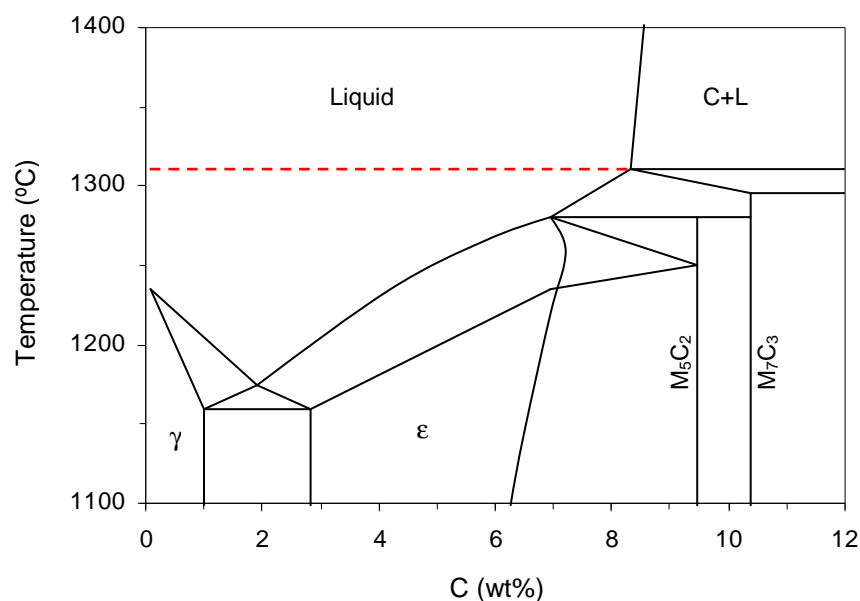
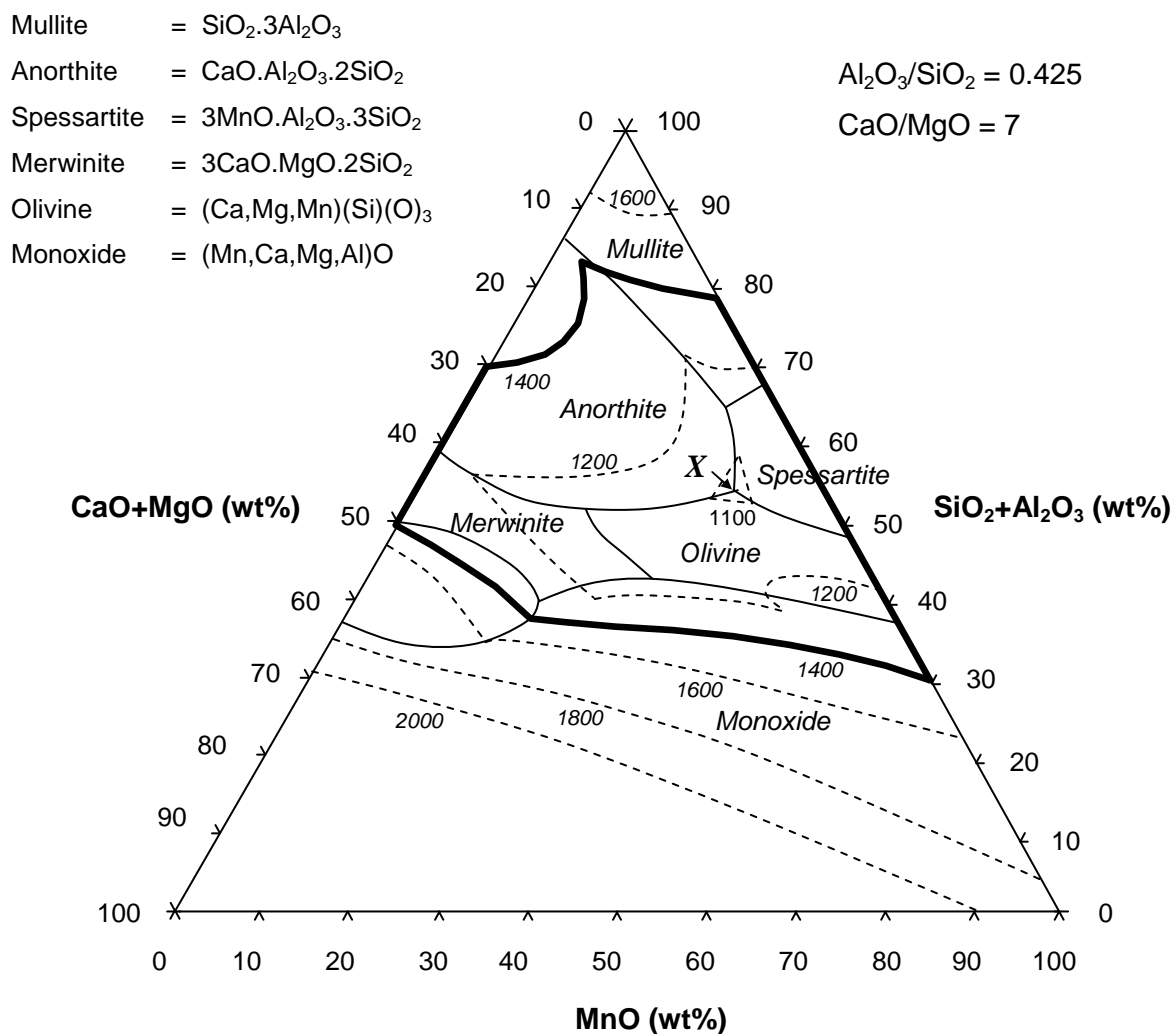


Figure 7 ‘Calculated vertical section of the Mn-Fe-C system for Mn/Fe = 6’ as from Olsen *et al.* (2007)

The usual Mn grade for high-carbon ferromanganese is 78% and the carbon content should not be more than 7%. This therefore constrains the Mn/Fe ratio to about 6, as in Figure 7, for a saleable product. The curves immediately below the dotted red line in Figure 7 are the liquidus curves for the alloy system. Solids will start crystallising from molten alloy if the process temperature drops below these liquidus curves. The curve above and to the right of the dotted red line is the solubility line for carbon in the alloy. If the carbon content of the alloy increases above 7% at an alloy temperature of about 1300 °C, then undissolved (solid) carbon would probably become visible in the alloy product. The presence of solid carbon may weaken the alloy crystal structure by making it brittle. A homogenous alloy product, with a maximum carbon content of 7% is therefore desired so that the alloy will be completely in the liquid state at 1300 °C. The maximum liquidus temperature that may occur across the allowable carbon concentration range is just above 1300 °C, i.e. the temperature inline with the dotted red line. Alloy temperatures should therefore always be slightly above this minimum temperature so that the alloy can be tapped.

If the suggestion by Urquhart (1980) is followed, suggesting that the slag temperature should be about 100 °C greater than the liquidus temperature of the alloy to facilitate

tapping, then the minimum slag temperature should be above 1400 °C. Slag temperatures should not be greater than 1500 °C to minimise fume loss (Urquhart, 1980). The ideal operating slag and alloy temperature range would then be between 1300 °C and 1500 °C to ensure that the slag and alloy phases are entirely liquid and are homogenous.



**Figure 8** ‘Calculated phase and liquidus relations for the MnO-SiO<sub>2</sub>-CaO-Al<sub>2</sub>O<sub>3</sub>-MgO (Al<sub>2</sub>O<sub>3</sub>/SiO<sub>2</sub> = 0.425) (CaO/MgO = 7) system’ as from Olsen *et al.* (2007)

Useful operability criteria can be deduced from the ternary system in Figure 8 at the minimum allowable slag temperature (1400 °C). The system shown in the figure is representative of a typical high-carbon ferromanganese slag system. A concentration region in the ternary triangle is demarcated inside the bold-marked region that borders

along the 1400 °C liquidus contour. Any slag at 1400 °C with a composition within this demarcated region will be a homogenous liquid with a viscosity that is dependent on the liquidus temperatures within the demarcated zone. If the composition of a slag at 1400 °C moves outside the demarcated region, then the crystallisation of solid phases would be likely and highly undesirable, as this would adversely affect the ability to tap the slag. The composition of the slag that will allow it to be most fluid (with the lowest viscosity) would be in the region of the ternary point with the lowest liquidus temperature ( $\pm 1080$  °C), where the three phases Anorthite, Spessartite and Olivine are in equilibrium (point X). A slag with a composition closer to the boundaries of the demarcated region will become more viscous, because the slag liquidus temperatures approach the actual slag temperature as the composition moves closer to the boundary lines of the demarcated region. A slag that is too viscous will be difficult to tap. It would be safe to ensure that the temperature difference between the liquidus surface and the actual slag temperature is at least 50 °C for a slag with a given composition. Therefore, for an actual slag temperature of 1450 °C, a slag composition should not move beyond the 1400 °C liquidus region demarcated in Figure 8.

The optimum slag composition will not necessarily be at point X in Figure 8, because the electrical conductivity of such a slag may cause the slag to heat insufficiently. “The optimum slag composition is one that is the best compromise between low liquidus temperature, low viscosity and low electrical conductivity resulting from the minimum of flux additions therefore giving a minimum slag-to-metal ratio” (Urquhart, 1980). A specific slag should tolerate inevitable compositional variations without marked changes in physicochemical properties (Warren *et al.*, 1975). An acceptable slag composition can be chosen by ensuring that liquidus and property isotherms are well spaced over the composition range of a specific slag.

It has been indicated by Warren *et al.* (1975) that highly basic slags usually have low MnO concentrations and high liquidus temperatures, which is analogous to slags with high MnO activity coefficients (tending to behave ideally). For such slags, the processing temperature will need to be increased to keep the slag fluid enough. High

liquidus temperatures for highly basic slags can be observed in the bottom-left corner in Figure 8. Large losses of Mn may also result through increased volatilization at increased furnace temperatures. The slag composition should ideally be in a position where the basicity level is more acidic than basic with the point of operation being closer to the upper point in the ternary diagram, but without adversely affecting the density and viscosity properties of the slag. Operation within the demarcated region will be ideal.

### **3.5 Physical properties**

#### **3.5.1 Resistivity / conductivity**

Resistivity of a material is the measure of the ability of the material to resist the conduction of current. Electrical conductivity is the inverse of electrical resistivity and is sometimes used instead of resistivity as a measure of the ability for a material to conduct current. Electrical resistivity is an important physical property of a furnace burden, particularly of slag, as it affects directly the power that can be supplied to the process. Urquhart (1980)

In the experimental work of Koursaris and See (1980), it was found that the resistivity of Mamatwan manganese ore and Delmas coal decreases appreciably with an increase in temperature from room temperature to 1400 °C. The resistivity of coke remains almost constant between this temperature range, and the higher resistivity of coal approaches that of coke at 1300 °C. The resistivity of a mixture of coke and manganese ore was found to be very similar to that of ore on its own. A mixture of the same ore and coal, however, had resistivity levels that were closer to that of coal on its own. See Figure 9 for the approximate resistivity values of these ore and reductant mixtures in the areas of the furnace where the burden is partially fused or solid. Koursaris and See (1980)

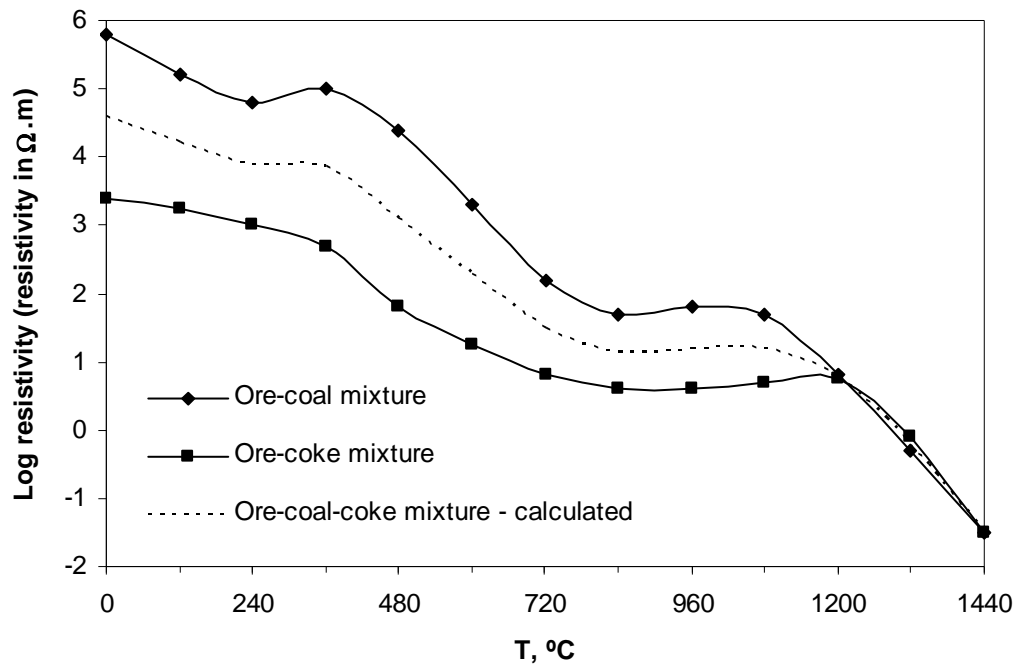


**Figure 9** Approximate resistivities of mixtures of Mamatwan ore and coal, Mamatwan ore and coke, and an assumed mixture of ore, coal and coke (as from the experimental work of Koursaris and See, 1980)

Since the feed materials to the furnace under investigation contain a mixture of manganese ore with coke and coal, it would be reasonable to assume that the resistivity curve lies in-between those for ore-coke and ore-coal mixtures. This is illustrated with the dashed line in Figure 9. For each of these mixtures, above 1200 °C, the resistivity curves decrease steeply and are approximately linear for manganese ore mixed with coal or coke. In practice, however, furnace resistance tends to increase when coal is substituted for coke above this temperature. The high resistivity values at low temperatures indicate that there will not be much electrical conduction in the upper regions of a furnace.

The average amount of coke and coal combined in the ore-coke-coal mixture of Figure 9 was approximately 20 wt%, which is almost identical to the average concentration of the corresponding materials for one of the furnaces investigated. It is

therefore reasonable to assume that the linear relationship between furnace resistivity ( $r$ ) and temperature ( $T$ ) in Figure 9, above 1200 °C, is applicable to the particular furnace:

$$\log(r) = -0.0095T + 12.204 \quad \text{for } T > 1200 \text{ °C, and } T \text{ in °C} \quad (4)$$

The work of Koursaris and See (1980) showed that the resistivities of reducing agents are influenced primarily by the degree of heat pre-treatment and not by its original composition and rank. For instance, the resistivity of coke is lower than that of coal at temperatures less than 1300 °C, because volatiles are driven off in the coking process to significantly reduce the resistivity of coke to approximately an order of magnitude less than that of coal. The resistivity of pure Mamatwan ore decreases steeply when heated at lower temperatures (above 350 °C), since semi-conduction is improved as the higher oxides of manganese are reduced and as dolomite and calcite in the ore are decomposed.

It was found that the resistivity or conductivity was relatively insensitive to different particles sizes of ore and coke in the 3 to 13 mm range. Variations in the packing arrangement of the bed are probably more influential on resistivity than for differences in particle size of the ore and reductants.

Urquhart (1980) observed that the electrical conductivity (inverse of resistivity) of the slag formed during reduction was of the same order of magnitude as that of the reductant used, at temperatures exceeding 1300 °C. Since electrical conductivities of pure ores, pure reductants and ore-reductant mixtures are very similar at high temperatures, it would be a good assumption, this far, to assume that equation (4) is applicable for determining the resistivity of liquid slag formed during the production of high-carbon ferromanganese.

### 3.5.2 Density

Density data is useful in mass and heat transfer calculations. The settling rate of alloy droplets through slag can be calculated, and temperature or concentration gradients cause density variations that bring about natural convection within a molten burden. Knowledge of density data also allows for calculation of material residence times within a furnace.

The value estimated for the density of molten ferromanganese (78% Mn) from two high-carbon ferromanganese furnaces was  $6.65 \text{ t/m}^3$ , according to Dyason and See (1978). This value was calculated by interpolating between the densities of pure Mn and Fe at  $20 \text{ }^\circ\text{C}$  and by assuming that the density decreased for a temperature increase of 20 to  $1600 \text{ }^\circ\text{C}$  as for pure Fe.

For high-carbon ferromanganese slags, a linear density equation was developed to predict the densities of most high-carbon ferromanganese slags, within an error margin of  $\pm 7\%$  (see Appendix C):

$$\rho = 4.423 - 0.052(\text{wt}\% \text{Al}_2\text{O}_3) + 0.018(\text{wt}\% \text{FeO}) - 0.013(\text{wt}\% \text{SiO}_2) + 0.012(\text{wt}\% \text{MnO}) - 0.016(\text{wt}\% \text{MgO}) - 0.011(\text{wt}\% \text{CaO}) - 0.0007(T, ^\circ\text{C}) \text{ [g/cm}^3\text{]} \quad (5)$$

Volumetric changes have been observed by Koursaris and See (1980) during the heating of ore and reductant materials. Where Mamatwan ore material was heated, significant expansion occurred to a temperature of about  $1000 \text{ }^\circ\text{C}$ , after which the ore volume decreased substantially, owing to the cracking open of the thermally stressed particles followed by the decomposition of carbonates, thermal reduction and melting at the higher temperatures. The volumetric change and the rate of volumetric change for coke-ore and coal-ore mixtures were less than for pure ore at temperatures exceeding  $1000 \text{ }^\circ\text{C}$ . Coke and coal reductants are therefore thermally more stable than manganese ore. At temperatures greater than  $1200 \text{ }^\circ\text{C}$ , the decrease in volume of coke-ore is about 10 % less than for coal-ore. This is because coke is thermally and physically more stable than coal, the latter being weaker physically owing to its

layered structure. Coal also contracts significantly as volatile matter evolves as the temperature increases. The rates of contraction of coke-ore and coal-ore mixtures were however very similar.

Since the composition of the coal in the charge was approximately twice as plentiful as the coke in the same charge for one of the furnaces investigated, it would be reasonable to assume a linear decrease in the charge volume with temperature for the ore-coal mixture as in the work of Koursaris and See (1980):

$$\% \text{ volumetric change} = -0.04T + 142 \quad \text{for } T > 1100 \text{ }^\circ\text{C, and } T \text{ in } ^\circ\text{C} \quad (6)$$

A volumetric decrease in the charge materials to the furnace under investigation would certainly be an important consideration when estimating the approximate furnace capacity. One way of considering the volumetric changes of the mixture of ore and reductant material is to adjust the densities of the ore and reductant feed materials according to Equation (6), using the average temperature of the pre-reduction zone in the furnace. This temperature is approximately 600 °C according to Olsen *et al.* (2007) and equates to a volumetric decrease of over 100%. Therefore the density of the solid burden effectively doubles, increasing the residence time of the furnace to about 0.9 days from about 0.5 days. This calculation can be seen in Appendix D.

It would be reasonable to assume a constant temperature profile in the slag layer of large submerged resistance heat furnaces, since buoyancy forces were found to be the dominant force causing fluid flow and turbulent mixing in the work of Choudhary and Szekely (1981). If the molten materials in the system are at equilibrium, then it would be apt to assume that the temperature of the molten alloy will also be at the same temperature as that of the slag and that this temperature will be approximately uniform owing to the alloy layer being in direct contact with the buoyancy-agitated slag layer. With this in mind, a constant estimated temperature of 1320 °C can be used as an input variable to the slag density and slag viscosity prediction models.



### 3.5.3 Viscosity

The viscosity of molten matter is a measure of the ability of the material to flow. It is important to consider the viscosity of melts within furnace systems for various reasons. Slag viscosity controls the rate of reactant and product movement through the reaction zone, and this in turn affects reduction rates of slag components. It is important for slag viscosity to be as low as possible in order for the slag to be tappable and to promote easy slag and metal separation. Slag viscosity should also be low enough to increase the rate of bulk diffusion so that the rate of reduction of MnO from slag is high. Urquhart (1980) and Woollacott *et al.* (1975)

Linear models for viscosity prediction of slags are inaccurate, since component concentrations are related to viscosity nonlinearly. As a result, Arrhenius-type models are generally used to classify slag viscosity  $\eta$ , e.g.

$$\eta = A \cdot T \cdot \exp\left(\frac{B}{T}\right) \quad [\text{poise or Pa.s}] \quad (7)$$

where  $A$  and  $B$  are regression parameters that are dependent on slag chemistry, and  $T$  is the slag temperature in degrees Kelvin. Increasing the temperature results in a lower slag viscosity. This is brought about by a greater degree of depolymerisation in the slag as temperature increases. Under experimental conditions, viscosity measurements are usually extremely sensitive to compositional and temperature change. Large experimental uncertainties can therefore be expected and this makes the prediction of accurate viscosity values very difficult.

Two viscosity models, the Urbain model and the Riboud model, use variations of equation (7) to predict slag viscosity. Their effectiveness of predicting the viscosities of high-carbon ferromanganese slags were evaluated in Appendix E. Urbain's model proved to be unsuitable, giving viscosity values that were excessively high. Riboud's model was subsequently modified by including a viscosity constant to appropriately suppress the viscosity of the system. Riboud's model seemed to be inaccurate for predicting viscosity values less than 1 poise (or for SiO<sub>2</sub> concentrations less than 40 wt%), but is useful when

used within the maximum and minimum composition range of the three major components, enabling viscosity values to be greater than 1 poise:

MnO : 10 to 60 wt%

SiO<sub>2</sub> : 40 to 60 wt%

CaO : 0 to 50 wt%

It was not expected that the low concentrations of MgO, FeO and Al<sub>2</sub>O<sub>3</sub> in high-carbon ferromanganese slags would appreciably affect the viscosity of the system. Therefore, the viscosity output of the modified Riboud model for the six-component system MnO-SiO<sub>2</sub>-CaO-MgO-FeO-Al<sub>2</sub>O<sub>3</sub> was calibrated with measured viscosities from an existing system containing only the three main components of high-carbon ferromanganese slag, namely CaO, MnO and SiO<sub>2</sub>. Riboud *et al.* (1981)

It was expected that the modified model of Riboud had a possible error margin of  $\pm 30\%$  for viscosity values that were predicted above 1 poise. It was also determined that it would be best to use a linear equation relating viscosity to SiO<sub>2</sub> concentration when the modified model of Riboud predicts viscosity values less than 1 poise. See Appendix E.

### 3.6 Slag-metal equilibrium and mineralogical interactions

Barcza (1979) determined experimentally that the Mn distribution ratio of the slag and alloy,  $\frac{(MnO)}{Mn}$ , was minimised for ferromanganese slags with a  $\frac{CaO}{MgO}$  ratio not less than

3 and with a basicity ratio  $\left(\frac{CaO + MgO}{SiO_2}\right)$  of about 1.33. The  $\frac{(MnO)}{Mn}$  ratio was used as

a measure of the degree of Mn recovered to the alloy. The lower this distribution ratio, the greater is the proportion of Mn in the alloy. This method proposed by Barcza is one way of classifying furnace performance. It seems that Mn recovery and the distribution of Mn between slag and alloy are measures by which performance can be evaluated.

In Urquhart (1980), physical properties were reviewed for high-carbon ferromanganese slags in terms of the slag basicity. Typical slags with basicities between 1.5 and 2.1 were

investigated at temperatures of around 1400 °C. A basicity ratio is the ratio of basic oxides to acidic oxides,  $B = \frac{MnO + MgO + CaO}{SiO_2}$ . A basic oxide generally has a low cationic attraction for oxygen, whereas an acidic oxide has a stronger attraction. For this reason, metal oxides with large cationic radii such as those from the alkali and alkali-earth metals tend to de-ionise completely into cations and oxygen anions, donating free oxygens to oxygen accepting acidic oxides. It is common knowledge in slag chemistry that SiO<sub>2</sub> is a polymerisation oxide. Oxide molecules such as SiO<sub>2</sub>, P<sub>2</sub>O<sub>5</sub>, B<sub>2</sub>O<sub>3</sub>, have a strong affinity for oxygen and are referred to as acidic oxides. When the concentrations of the acidic oxides increase, they ionise and form long (polymerized) chains that tend to make the slag more viscous and less conductive. Basic oxides such as MnO, CaO and MgO generally have the opposite effect and are called depolymerisation oxides. An excess amount of oxygen anions will break the oxygen bonds within a polymerised chain and form loose-standing, or non-bridging oxide molecules. Depolymerisation of a slag will therefore generally have the effect of decreasing the viscosity and increasing the electrical conductivity of a slag.

The change of slag properties (viscosity, electrical conductivity and liquidus temperature) with increasing component concentrations of typical ferromanganese slags are summarised in Table 1.

**Table 1 The effect of increasing the concentration of each oxide in high-carbon ferromanganese slag on selected slag properties, for slags with typical molar basicities between 1.5 and 2.1.**

Component	Liquidus temp	Viscosity	Elec conductivity
<b>MnO</b>	decrease *	decrease	increase
<b>SiO<sub>2</sub></b>	Decrease	increase	decrease
<b>CaO</b>	Increase	slight increase	slight increase
<b>MgO</b>	Decrease	decrease	increase
<b>Al<sub>2</sub>O<sub>3</sub></b>	Increase	min at 15% Al <sub>2</sub> O <sub>3</sub> #	max at 6-10% Al <sub>2</sub> O <sub>3</sub>

\* this is not the case for very basic slags with high concentrations of MnO. The result that the liquidus temperature decreases with increasing MnO concentration is supported by the experimental work of Warren *et al.* (1975).

# for basic slags

Slag viscosities for typical high-carbon ferromanganese slags containing 5-20% MnO showed variations of viscosity of 1.58-0.69 Pa.s at 1400 °C. Electrical conductivity varied between 6.6-22.7 S/m at 1400 °C. Smaller variations in electrical conductivity and viscosity occur for more basic slags containing 10-35% MnO at 1400 °C. In this instance, viscosity varied between 0.24-0.41 Pa.s and electrical conductivity varied between 27-50 S/m. “Due to the nature of slags a compromise is necessary between low viscosity and low electrical conductivity” (Urquhart, 1980). According to the viscosity model developed in Appendix E, it was found that viscosity measurement predictions for high-carbon ferromanganese slags with viscosity values greater than 0.1 Pa.s are highly variable and may be in error by up to 30%. Viscosity values predicted below 0.1 Pa.s may be even more variable. Note that 1 Pa.s = 10 poise.

For a manganese ore suited for electric furnace operation, the following property levels of the product slag would be favourable:

- Low slag to metal ratio to minimise the energy required to keep the slag in a molten state
- Intermediate viscosity and intermediate electrical conductivity to establish a good compromise between the lowest viscosity and conductivity levels possible

The conclusions arrived at in the experimental work of Channon and See (1977) explained the mineralogical effects of fluxing agents, CaO and MgO, on manganese recovery of medium carbon ferromanganese. It was found that manganese recovery decreased if the CaO:MgO ratio of the fluxing agents was decreased or if CaO was replaced by MgO in the flux used. It was also found that an increase in the slag basicity ratio  $\frac{CaO + MgO}{SiO_2}$  (from 1 to 2.2) increased the amount of manganese to the

alloy and decreased the amount of silicon in the alloy. Both effects are desirable. These findings may not provide adequate support for the effects of CaO and MgO additions in high-carbon ferromanganese production, because lime or dolomitic additions are usually not required in the production of high-carbon ferromanganese. The medium carbon ferromanganese process is also different in that the

ferromanganese product is produced by silicothermic reduction and not by carbothermic reduction.

Equilibrium interactions between carbon-saturated Mn-Fe-Si melts and CaO-MnO-SiO<sub>2</sub> slags with and without Al<sub>2</sub>O<sub>3</sub> were investigated in the work of Turkdogan and Hancock (1958). Their conclusions are summarised in Table 2.

**Table 2** Effect of compositional variations of CaO-MnO-SiO<sub>2</sub> slags on alloy-slag distribution ratios

VARIABLES MANIPULATED			CHANGE IN ALLOY-SLAG EQUILIBRIUM	
Iron Fe	Basicity CaO / SiO <sub>2</sub>	Alumina Al <sub>2</sub> O <sub>3</sub>	Si distribution ratio (SiO <sub>2</sub> ) / [Si]	Mn distribution ratio (MnO <sub>2</sub> ) / [Mn]
constant	increase	-	Increases	decreases
decrease	constant	-	Increases	decreases
-	-	decrease	Increases	increases
-	increase	constant, 20%	increases slightly	-
-	increase	constant, 0%	Increases	-
Fe-based	-	constant	higher than MnO-based	higher than MnO-based
Fe-based	constant	increase	Increases	decreases

## CHAPTER 4

# MODELLING METHODOLOGY

### 4.1 Furnace modelling and simulation

In general, models and simulations for metallurgical systems are difficult to develop and employ for a number of reasons. A few of these are: (1) High-dimensionality of the system, (2) poor material and stream characterisation, (3) dynamic nature of operation and (4) multiphase interactions. Improving computing technology allows for the development of complex models, which would not perform well for poorly defined processing variables. It is therefore necessary to develop models that are as simple as possible.

Some of the metallurgical factors that directly influence the performance of submerged-arc furnaces, according to Reuter and Yang (2000), are:

- Burden resistivity and porosity
- Electrode penetration or position in the bath
- Recipe, type and particle size of the burden materials (ore, reductant and flux)
- Degree of burden pre-treatment, e.g. prereduction of ore
- Characteristics of material flow within the furnace

These factors need to be included in an empirical model that would estimate values for a specific performance indicator that can be controlled and optimised. Several of these models may be created for the optimisation of some of the main performance indicators. A performance indicator can be defined as a specific target variable or ratio that can be monitored and optimised to establish good process performance. The production capacity of a process, e.g. tonnes of metal tapped per tonne of ore feed, might be considered as a performance indicator. Two examples of predictive models,

for the prediction of the  $MWh/t$  and  $Si$ -recovery performance indicators in FeSi and Si production, from Reuter and Yang (2000) are given below:

- $MWh/t = f\left(\frac{C}{SiO_2}, m\Omega, FeSi - grade, etc.\right)$
- $Si - recovery = f\left(MWh/t, \frac{C}{SiO_2}, m\Omega, FeSi - grade, etc.\right)$

Some of the semi-empirical variables used in the models above may be predicted ahead of time so that the models may be used as a forward-predictive model. Forward-predictive models are useful for controlling dynamic processes; corrective actions can be made ahead of time to maintain optimised levels of specific performance indicators. Each of the two performance indicators above are affected by various variables that are metallurgical or electrical in nature. Metallurgical variables relate to component concentrations in phase systems, e.g. Mn concentration in the metal, basicity of the slag, etc. Electrical variables are controllable furnace variables such as power input, furnace resistance, furnace power factor, etc. Variables may be selected and eliminated according to their contribution to a specific performance indicator. Variables that strongly affect a performance indicator will remain in the model and the remainder will be eliminated. Variable interactions may also affect a performance indicator significantly, especially in multivariate systems. The contributions of variables and their interactions are determinable by means of variance analysis or significance testing.

Molten phases in a submerged-arc furnace have so-called ‘metallurgical memory’. This is because some of the molten materials remain behind after tapping and may reside in the system for a number of taps. Since submerged-arc furnaces have long residence times (about one day for the furnace under investigation) as a result of a high degree of mixing and large furnace volumes, dynamic predictive models can be developed that predict one or two taps ahead. This is illustrated by the metallurgical-type forward-predictive model from Reuter and Yang (2000):

$$\%Mn_{time=t} = f(\%MnO, \%Al_2O_3, \%FeO, Basicity, \%Mn)_{time=t-1}$$

In this instance, the Mn concentration is predicted one tap ahead of the independent component concentrations from a previous tap. Predicted data can be compared with actual future data to determine whether the model is accurate. Similar, but more extensive predictive models were to be developed in the work of this project.

The following performance indicators were to be optimised for the production of high-carbon ferromanganese in the furnace investigated:

- Optimal tonnes of hot metal produced per tonne of ore fed (the coal to coke ratio was to be determined and had to be considered as a variable; variation in the slag-metal ratio was to be investigated; and the effect of the different feed materials on metal production was to be analysed)
- Highest gas production rate with the focus on the main combustibles, CO and H<sub>2</sub>
- Highest power factor to be maintained with constant MW input

It was decided that the starting point of investigation was to ascertain if actual metallurgical data was closely comparable with modelled results from a thermochemical neural network. Results from such a model could then in some way be used in a separate neural network, together with certain electrical variables, to predict furnace performance. This overall model might be modified to take on the form of a predictive model that would use actual furnace data (electrical and metallurgical) to predict ahead in time the actual specific metallurgical performance of the furnace. The variables in such a predictive model may subsequently be manipulated to bring about an improvement in specific performance indicators. Optimised manipulable variables may finally be presented as a set of setpoints that would be easy to implement on-site. In this way, both dynamic and thermodynamic modelling steps are used for characterising furnace behaviour.



## **4.2 Techniques for simulating furnace behaviour**

The contents of this section of the thesis are developmental to the choice of the final modelling structure as depicted in section 4.3. Development of the two fundamental modelling techniques employed, viz. thermochemical simulation (using FactSage) and neural network modelling, are discussed. The extent of discussion for the latter technique is not exhaustive, but only encompasses the replacement of the FactSage modelling step with neural networks. This step is referred to as thermodynamic modelling. The neural networks following this step, for the prediction of key performance indicators, are not discussed here, because the neural network modelling technique remains fundamentally similar.

### **4.2.1 Thermochemical simulations with FactSage**

Thermochemical modelling was performed with FactSage, a reliable application for calculation of phase equilibria in multiphase and multicomponent systems that are non-ideal. ([www.esm-software.com/factsage](http://www.esm-software.com/factsage))

Initially, data from Furnace 1 were used for carrying out the objectives of this project. A thermodynamic model was initially generated for the data from this system and eventually an overall dynamic model was to be employed. Owing to unforeseen circumstances, the project-drivers at the company that produces the ferromanganese decided that data from a more reliable source, viz. Furnace 2, should be analysed instead of continuing with model development for Furnace 1. The reason for this shift was that the operation of Furnace 2 was more consistent and stable than Furnace 1. Also, a larger data set could be obtained for developing a model that would be more flexible in processing variation in data over a longer period of time. Both Furnaces 1 and 2 produce the same product from similar feed materials. Despite the similarities, the thermodynamic model already developed for Furnace 1 could not be reused for Furnace 2, since there were additional feed materials used in Furnace 2 and because the average flowrate limits of the corresponding feed materials to Furnace 2 were out of range of the flowrate limits used in the development of the thermodynamic model

for Furnace 1. A new, yet fundamentally similar model consequently had to be developed for Furnace 2.

An explanation is provided below in sections 4.2.1.1 and 4.2.1.2, explaining the development of the thermodynamic models created for Furnaces 1 and 2, respectively. Even though the investigation of Furnace 1 data was discontinued, the explanation provided in section 4.2.1.1 provides detail that reinforces an understanding of the simpler model that was redeveloped for Furnace 2 data in section 4.2.1.2. The steps for preparing the data for use in FactSage are discussed separately for Furnaces 1 and 2 in Appendices A.1 and A.2, respectively. A summary of the configuration of the FactSage application is also included in Appendix A.1.

#### **4.2.1.1 Modelling of Furnace 1 (investigation discontinued)**

A full  $3^8$  factorial of all high, normal and low level combinations of each of the feed materials and of the probable temperature range (1300, 1450 and 1550 °C) was designed to cover all the possible combinations of the feed rate of each material to Furnace 1. The base number of 3 is the three levels of material feed rates, i.e. high, normal and low. The power number of 8 represents the number of input variables considered, i.e. furnace temperature, Ore 1, Ore 2, Ore 3, coal, coke, silica and Fe ore. A factorial design of  $3^8$  therefore consists of 6561 runs to account for all possible combinations of the levels of each variable. High – and low level feed rates of each material were obtained by searching for the maximum and minimum feed rates of each material over the period of time for which data were available (2 months). Normal level feed rates were obtained by analysing a feed rate histogram for each material and selecting the feed rate that occurred most frequently. Development of the factorial design is included in Appendix A.1.

Solution species, *SlagA* (*l*), *CaSiO4* (*l*) and *Amonoxide* (*s*), were selected in FactSage to cover most of the output species of slag that would result, and *SGTE-Liquid* was selected for the alloy outputs. Further details on the configuration of FactSage are given in Appendix A.1. Although actual furnace temperatures were not measured,

high, medium and low levels of 1550, 1450 and 1300 °C were selected that relate to the temperature ranges observed in the literature (Grimsley *et al.*, 1977; Koursaris and See, 1980; Olsen *et al.*, 2007; Urquhart, 1980).

It was found that the average amount of actual product materials tapped from Furnace 1, as determined by a materials balance, was comparable with the equilibrium results from FactSage. The results of this comparison are shown in Figure 10. Output results of the complete set of 3<sup>8</sup> factorial runs from FactSage were averaged to give an average composition of the predicted furnace products at an average equilibrium temperature of about 1430 °C.

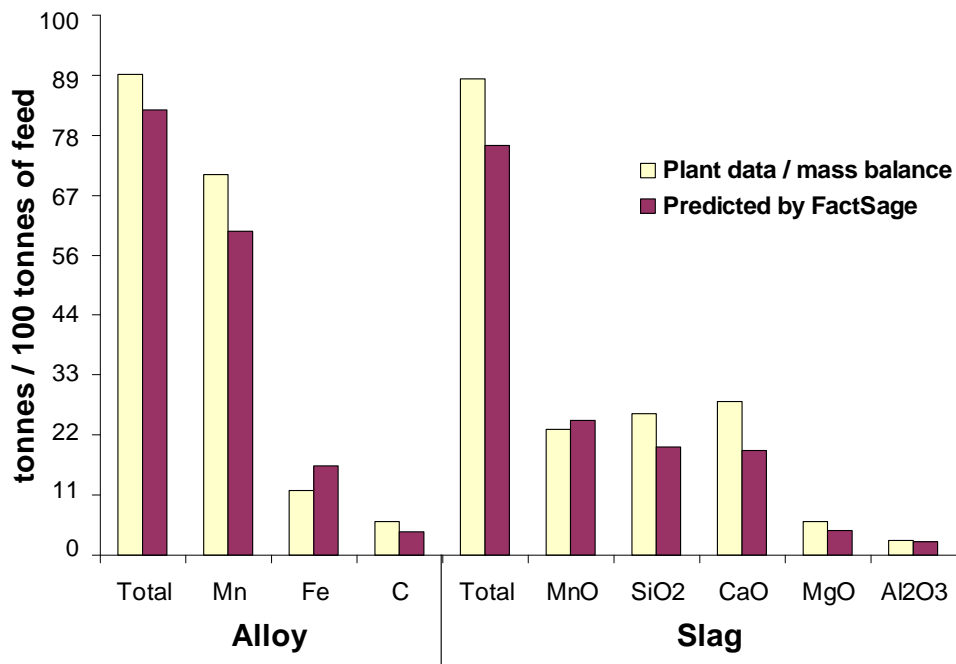


**Figure 10 Tonnes of condensed products tapped per 100 tonnes of feed material  
(Data scaled as per confidentiality agreement)**

Bias shifts of the product tonnages in this figure was thought to be the result of higher gas flow prediction by FactSage. The most probable reason for this is that the average temperature used in the FactSage design was supposedly higher than the actual furnace temperature. The effect is a shift in the equilibrium of the gas-melt system

towards higher amounts of gas relative to the amount of melt. The general trend of the results in the figure is however followed, indicating that the actual furnace melt was near to the equilibrium composition that was predicted. Results from FactSage proved that the output from a high-carbon ferromanganese furnace can be predicted relatively well, for the condensed phases at least. A similar modelling approach was repeated for data from Furnace 2 in the following section.

#### **4.2.1.2 Modelling of Furnace 2 (subject of investigation)**

Unlike the 3 level factorial design that was employed for the data of Furnace 1, a 2 level factorial design was used instead for Furnace 2 for two reasons. First, the data from Furnace 2 had a high dimensionality (13 feed materials) which would require  $3^{13}$  FactSage simulations if three levels (low, medium and high) of each of the 13 variables were used, i.e. one simulation for each of 1594323 factorial runs! Descriptions of the different raw materials and their associated feed profiles are provided in Appendix F. Furnace 1 only had 8 factors to consider and the total number of factorial runs was therefore not as great. The second reason was that a 2 level factorial design was simpler to employ and required only two levels (low and high) for each variable considered. Furnace 2 therefore only required  $2^{13}$  FactSage simulations to classify the equilibrium output for all possible combinations of the different feed materials. The low level of each of the feed materials was set to zero and the high for each material was set to the maximum daily input over the 1-year sampling period. The reason for setting the low level to zero for each variable was to account for material flows that had been stopped for a period of time. Although a 2 level factorial design will produce results that are less accurate than for a 3 level design or for more 'economic' designs (e.g. a fractional factorial design or a central composite design with two levels), its use was found to deliver results that were representative of the actual furnace output. The  $2^{13}$  factorial design employed was subsequently used to train a neural network model that was able to predict quickly the equilibrium output of the furnace for any combination of feed materials, within the limits of the feed rates to the furnace over the period of investigation.

It was decided to ignore the furnace equilibrium temperature as an input factor in the factorial design for Furnace 2 to simplify the model, and to eliminate factors with uncertain values. It was however necessary to specify a temperature in FactSage that was representative of the equilibrium temperature inside the furnace/reaction unit. Even though the equilibrium temperature of the furnace was unknown, it could be estimated by re-iterating the FactSage simulation with a different temperature value for each iteration. The final temperature selection would be based on the alloy and slag output results that would compare most closely with the actual output of alloy and slag from the furnace. The result of this iterative method for temperature calibration and comparisons of the final FactSage results with the actual products tapped from the furnace are given in section 5.1.2.

In the latter paragraph, the iterative method of temperature calibration was only performed for the daily material input into FactSage (scaled to 100 grams) for a total number of 365 factorial runs (one run for each day across the period for which raw material data was supplied). Feed materials were delayed by 1 day against the output results to account for furnace residence time. The best temperature found after repeating the simulation for a number of different temperatures was then specified for simulating the complete set of  $2^{13}$  factorial runs in FactSage to account for all possible feed combinations to the furnace. These output results were then used to train a replacement neural network model to rapidly predict the equilibrium output of the furnace for any combination of the given feed materials.

#### **4.2.2 Neural network modelling**

In the work of King and Nyman (1996), a multilayer perceptron was trained to predict and model the chaotic dynamics of an electric arc in an electric furnace. By means of various statistical techniques, the investigators found that the electrical voltage and current dynamics were chaotic and so they employed the use of two neural nets, one to predict the dynamics of the system and the other for process control. The latter neural net would adjust the furnace current, one time-step ahead, to obtain a desired voltage output. The investigation proved to be successful.

A similar approach was used in this project to predict the dynamics in the melt of a ferromanganese furnace. Not only were the electrical variables considered, but also the raw materials fed and the constituents of the furnace burden. Instead of creating a model that would be used exclusively as a process controller, a few simple setpoints would be drawn from the optimised model for experimental implementation.

Clarification of the modelling approach is given below, using Furnace 1 as an example. The neural networking functions in Matlab were used in this case for illustrative purposes and for its algorithmic transparency. See Appendix B. For the neural modelling of Furnace 2, CSense was selected for its robustness and ease of use. In the CSense software, visual platforms and sub-platforms are provided so that data may be grouped and processed by various predefined functions and models. The advantage here is that a single CSense program may be compiled to execute a number of neural (or nonlinear) models at the same time. A complex solution is therefore simplified. See Appendix G. With CSense, trained model parameters cannot be extracted beyond the application, but this can be compensated for by constructing a neural network in Matlab and then extracting the parameters if required.

Two types of models were used in the research. For the first, a multilayer perceptron with three layers was selected to simulate the role of FactSage in predicting the equilibrium elemental composition of the alloy. The hidden layer used a tan-sigmoid transfer function and the output layer a pure linear transfer function. The number of nodes for the input layer was initially ten, equivalent to the number of input components (not material streams). Each input node was comprised of the total number of a specific mineral species, e.g.  $\text{SiO}_2$ , for all the material streams entering the furnace. The output layer had three nodes, one for each of the major alloy components (manganese, iron and carbon). Insignificant numbers of other possible alloy species, e.g.  $\text{Mn}_3\text{C}$ , were observed from the FactSage output and these were ignored from the neural model. Six nodes were selected for the hidden layer. Another neural network with the same configuration, but with six output nodes, was created to

predict the equilibrium composition of the slag. Two models of the same type were therefore created, one for alloy prediction and the other for slag prediction.

Vector normalisation was performed on the input data to obtain an input vector with a zero mean and a variance of unity (these implementations were reversed after model completion). Subsequent application of a principal component analysis (PCA) halved the dimension of the dataset that entered both neural networks, i.e. only five of the ten input nodes contributed significantly to the output predictions and were uncorrelated with each other. The specific nodal inputs that were disregarded were unknown, because the input data matrix had to be randomized before PCA to ensure that the training, testing and validation data sets were representative of the entire data set. Total variance was therefore explained by five principal components (PC's). The Levenberg-Marquardt algorithm was used for training and the weights and bias weights were left at their initial default settings prior to training. This explanation of model normalisation was only specific to data from Furnace 1.

A schematic depicting the model structure used for alloy prediction from Furnace 1 is illustrated in Figure 11. The model structure for the prediction of slag composition is the same, but has seven nodes (each for individual slag components) in the output layer.

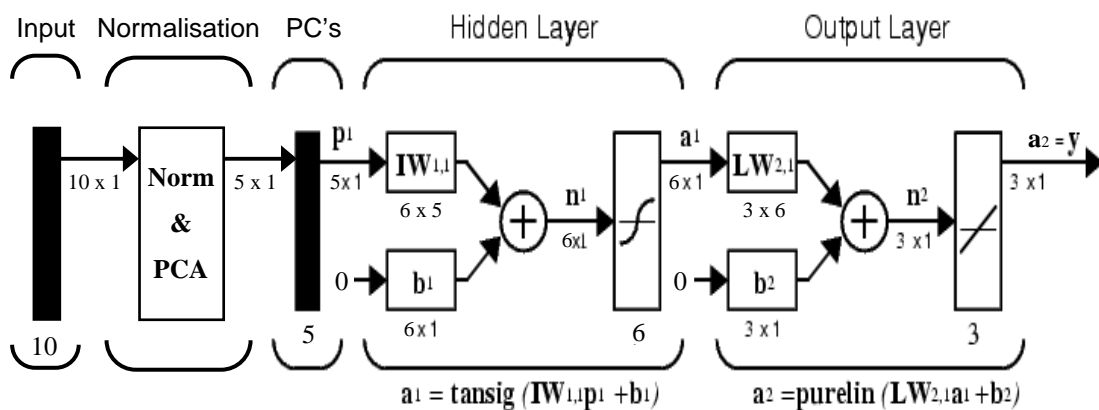


Figure 11 Vector normalisation and multilayer perceptron for alloy prediction from Furnace 1

The second model type, similar to the first (refer two paragraphs back), was a multilayer perceptron with four layers. It was also used in the thermodynamic prediction of alloy and slag constituents, but its use was further extended for the dynamic modelling of specific performance indicators as will be discussed in section 4.3. The two hidden layers of this model type and the output layer used sigmoid bipolar transfer functions. Statistical normalisations on the model inputs were also applied and an RMS (root mean square) calculation was used to determine the training error for adjustment of the weights and bias weights after every iteration. Further details about this model type are undisclosed for proprietary reasons.

Both the model types discussed above proved to be suitable for the purposes of this project. More details are explained in Appendices B and G. The quality of the linear fit of the alloy-prediction model from Figure 11 is shown alongside in Figure 12 for each of the alloy outputs (%C, %Fe, %Mn) from Furnace 1.

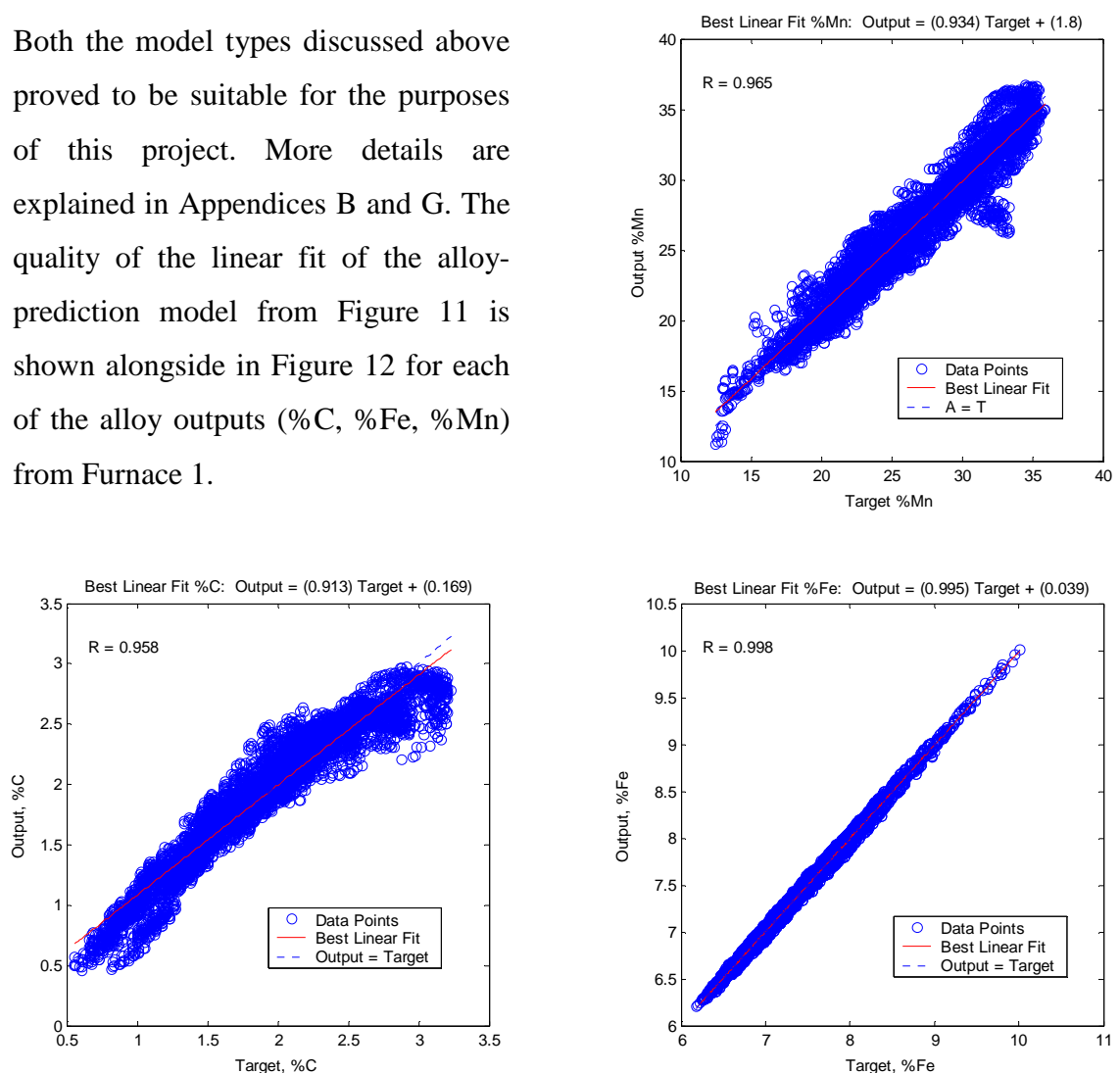
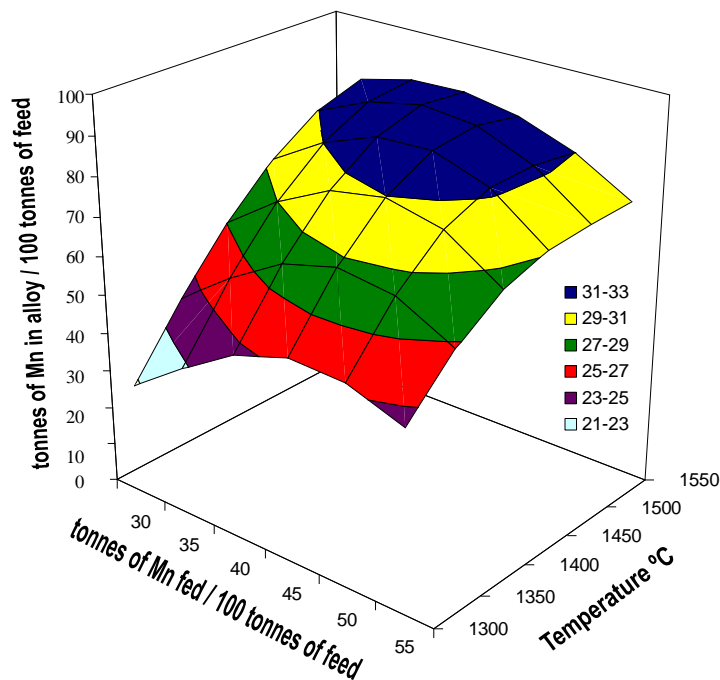


Figure 12 Linear quality of the fit of predicted versus target compositions for alloy production



From this figure it can be observed that the elemental composition of the alloy was predicted with a minimum correlation coefficient of  $R = 0.96$ . Replacement of the functionality of FactSage with a neural network for alloy prediction was therefore a reasonable option.

The thermodynamic output of the alloy and slag neural network models may be used to create response surfaces that would be useful for observing regions of optimal performance. Response surfaces were not used for investigating regions of good thermodynamic performance in this project. Instead, the x-y plots in section 5.3.1 were used to rate performance. The response surface for alloy production from Furnace 1 is shown below for illustrative purposes only.



**Figure 13 Variables influencing the amount of Mn in equilibrium with the alloy  
(Data scaled as per confidentiality agreement)**

The diagram above shows the influence of temperature and the amount of input manganese on the amount of manganese in equilibrium with the alloy phase (a possible performance indicator). The conditions for obtaining the maximum amount

of manganese in the alloy are to operate at the highest temperature that allows for stable furnace operation and to limit the amount of input manganese to normal or low amounts. Note again that the use of this response surface is restricted to Furnace 1 and is presented here only to illustrative graphically the results of thermodynamic modelling.

Significance testing (linear regression modelling and analysis of variance) was performed on the thermodynamically modelled data of Furnace 1 to identify the variables affecting production. The table below indicates the adjustable variables (in the leftmost column) and the actions necessary to optimise a target or a specific performance indicator. Only the adjustment actions for the main contributing variables are indicated. It is only sensible to adjust the significant variables within their corresponding high or low limits. Contribution coefficients of interacting variables were also significant in certain instances, but were not considered to maintain simplicity.

**Table 3 Actions required to optimise target variables from a thermodynamic point of view (process dynamics not considered) (Data removed as per confidentiality agreement)**

SIGNIFICANT VARIABLES			TARGETS									
Variable	High	Low	To decrease Slag / metal ratio		To decrease Slag basicity		To maximise Mn <sub>m</sub> / Mn <sub>s</sub> ratio		To decrease % solids in slag			
			Action	Coefficient	Action	Coefficient	Action	Coefficient	Action	Coefficient		
Temperature, °C	1550	1300	MINIMISE	7.32	MINIMISE	0.05	MINIMISE	-8.74	MINIMISE	7.32		
% Mn fed	Confidential	Confidential	MINIMISE	8.78	MINIMISE	0.11	MINIMISE	-9.81	MINIMISE	8.78		
% Fe fed							MAXIMISE	5.70	MAXIMISE	-3.94		
% SiO <sub>2</sub> fed							MINIMISE	-6.00	MAXIMISE	-5.76		
% Al <sub>2</sub> O <sub>3</sub> fed					MAXIMISE	-5.76	MAXIMISE	-0.22				
% MgO fed							MINIMISE	0.13	MAXIMISE	14.44	MAXIMISE	-5.99
% CaO fed					MAXIMISE	-5.99						
% C fed												
% H <sub>2</sub> O fed												
% CH <sub>4</sub> fed												

From this table it can be seen that certain compromises have to be made when selecting suitable setpoints for efficient process operation. Again it should be noted that these results are restricted to Furnace 1. They are presented here for illustrative purposes on how different variables affected the performance of Furnace 1. Significance testing was not repeated for data from Furnace 2, since a genetic optimisation process was employed to automatically analyse the optimum

combinations of variable values that would maximise furnace performance. The following section provides more detail on genetic optimisation.

### **4.3 Modelling methodology quantified**

This section brings together the modelling approach and simulation techniques already discussed, allowing the overall modelling structure to be quantified for a complete hybrid model that would optimise performance setpoints for Furnace 2. A summary of all the primary assumptions are listed and flow diagrams of each subsection of the hybrid model are explained. The last flow diagram illustrated (in section 4.3.3) depicts how the hybrid model can be calibrated and integrated into the existing furnace control strategy. Details pertaining to low-level technicalities (calculations and software programming) of the different subsections of the hybrid model can be found in the appendices of the thesis.

#### **4.3.1 Summary of assumptions**

A summary of the primary assumptions made are listed below:

- The hybrid model to be proposed was designed to receive a fixed number of different feed materials. The proportion of the feed rate of each could vary from zero to the maximum proportion that was recorded over the course of one year's collected data. The inclusion of additional (new) feed materials would require a restructure of the nonlinear modelling step that uses the proportions of specific feed materials as inputs. The hybrid model is further explained in section 4.3.2.
- Since the actual amount of slag was not accurately measured on-site, the approximate daily amount of slag was estimated by the assumption that the total amount of basic components in the feed blend, CaO and MgO, reported exclusively to the slag phase. This assumption was thought reasonable, since assay measurements indicated that only minor amounts of these components reported to the gas and alloy phases.

- Actual data on the temperature of the molten materials in Furnace 2 were unattainable. Approximate equilibrium temperatures were therefore assumed in the thermodynamic modelling performed in FactSage until the equilibrium modelled outputs of alloy and slag were comparable with the actual amounts of alloy tapped and with the approximate amount of slag tapped. A final temperature was therefore determined (through graphical iteration) and this temperature value was subsequently held constant as a modelling parameter. Temperature calibration is explained in section 5.1.2.
- The approximate furnace residence time of Furnace 2 was calculated (in Appendix D) and held constant as a modelling parameter so that input proportions of the feed materials could be appropriately delayed prior to thermodynamic modelling to give accurately timed output results. This is because output results from the thermodynamic models (or FactSage replacement models) are assigned the same timestamps as the input data to these models.
- Outputs from the thermodynamic modelling step would be manipulated to form suitable input variables to dynamic models that would predict furnace performance. The choice of the input variables were based on criteria whereby the variables would logically influence specific performance indicators (outputs from the dynamic models), e.g. a variable can be determined such as slag density, which in turn would affect a performance indicator such as the separability of alloy and slag.
- Neural networks (or multilayer perceptron models) were exclusively selected as the models of choice for all variable prediction. It was assumed that neural networks would effectively characterise the nonlinearities in furnace data. To compensate for a few model outputs that were inaccurately characterised by the thermodynamic neural network models, these outputs were linearly adjusted (manually) to more accurate levels. See Appendix G.1 and Figure 68.

- It was assumed that the magnitude of the value of three KPI (key performance indicator) variables, viz. tonnes of alloy per tonne of feed, Mn recovery and alloy-slag ratio, were sufficient to characterise furnace performance as a whole.
- Subsequent to the prediction of three desired KPI variables (see previous bullet) from three dynamic models, a genetic algorithm technique was employed to optimise these KPI's through the adjustment of specific independent variables. It was assumed that genetic programming is an effective method for evaluating the most appropriate setpoint value for an independent variable from a range of possible values.
- Two of the adjustable variables, viz. CaO-SiO<sub>2</sub> ratio and mass percentage of C in the feed blend, commonly affected two of the three KPI's (Mn recovery and the alloy-slag ratio). The values of both the adjustable variables mentioned were separately manipulated to two different values each so as to optimise the two KPI's. As it is impossible to have two separate values for a single adjustable variable, it was assumed that a best-compromise value can be calculated by determining the arithmetic mean of the two values, e.g.  $\frac{x_1 + x_2}{2}$ . This explanation is better defined in Table 4 of Chapter 5 – refer to the third, fourth and fifth columns of this table for the two adjustable variables mentioned. Use of an arithmetic mean as the most suitable setpoint for an adjustable variable may not necessarily be appropriate, since the relative contribution of a setpoint value may influence two separate KPI's to varying degrees.

### **4.3.2 The proposed hybrid model**

The layout of the hybrid model proposed in Figure 1 of Chapter 1 is repeated in Figure 14 below. The functions performed and variables used are indicated below the high level blocks in the figure. Development of the two sub-models and optimisation step contained are explained in flow diagrams in sections 4.3.2.1 to 4.3.2.3.

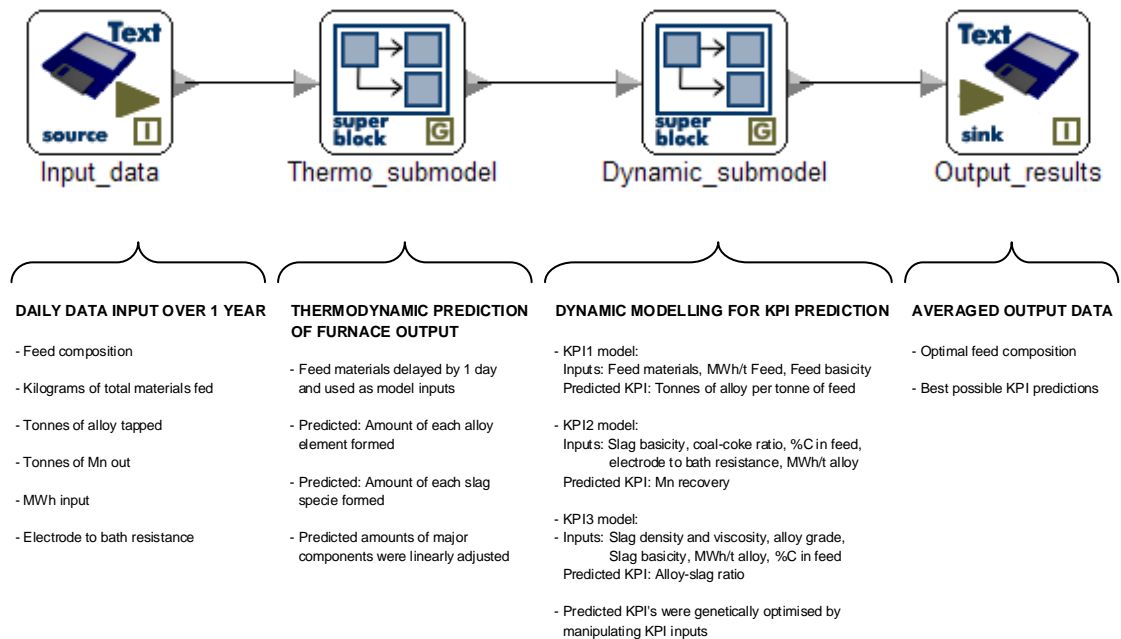


**Figure 14 Conceptual high level layout of the proposed hybrid model (Block diagram illustrated by permission of CSense Systems (Pty) Ltd)**

It is important to first classify the plant data used before the modelling procedure is explained. Plant data were divided into two portions. The first portion contained all data relating to furnace feeds and products. The second portion of the remaining data were the electrical variables that were used to optimally control production, e.g. power supplied and electrode resistance.

The first portion of the data was used to predict probable equilibrium phases using thermodynamic software (FactSage). Two neural network models (collectively displayed in Figure 14 as the thermodynamic sub-model) were trained to replace the role of FactSage and to simulate the lengthy Gibbs minimisation calculations of FactSage in a fraction of the time. These neural networks then predicted, thermodynamically, the most probable compositions and the relative amounts of the equilibrium outputs of alloy and slag. As the actual amount of slag produced was not available from the plant, it was necessary to train the thermodynamic neural network

model on an estimated amount of slag produced by assuming that all the incoming CaO and MgO in the feed blend left the furnace in the slag alone. The uses of CaO and MgO in estimating the amount of slag produced was thought to be relatively accurate, as these two components were highly concentrated in the feed blend and would be expelled almost entirely in the discard slag. The actual amounts and compositions of alloy and slag produced were compared with the model results as a final validation of the thermodynamic sub-model. Prior to the entering of the data into the thermodynamic sub-model, the timestamps of the input data had to be delayed by the approximate furnace residence time so that the modelled furnace output data would be time-aligned with the actual furnace output data. See Appendix D for the calculation of the approximate furnace residence time.

Predictions of three required key performance indicators (KPI's) were modelled with three neural network models (collectively displayed in Figure 14 as the dynamic sub-model) that made use of all the data provided (first and second portions). Outputs from the thermodynamic sub-model would be manipulated to form suitable input variables to the dynamic sub-model. The selection of these input variables were based on criteria whereby they would logically influence the individual KPI outputs, e.g. an input variable can be determined such as slag density, which in turn would affect a performance indicator such as the ease of separation of alloy and slag (or the alloy-slag ratio). In the determination of slag density, a semi-empirical formula was devised (see Appendix C), and equilibrium compositions of the furnace outputs from the thermodynamic sub-model were used to estimate this physical property. The same applied for the determination of the slag viscosity input variable (see Appendix E). All the other dynamic input variables, including the electrical control variables, are listed under the dynamic sub-model in Figure 14.

#### **4.3.2.1 Thermodynamic modelling**

In Figure 14, the first modelling step involved the development and calibration of nonlinear models that characterise the relationship between a blend of known furnace feed materials and the resulting equilibrium outputs of metal and slag exiting Furnace

2, even for varying or alternate blends of the same feed materials. This thermodynamic modelling process is depicted in Figure 15.

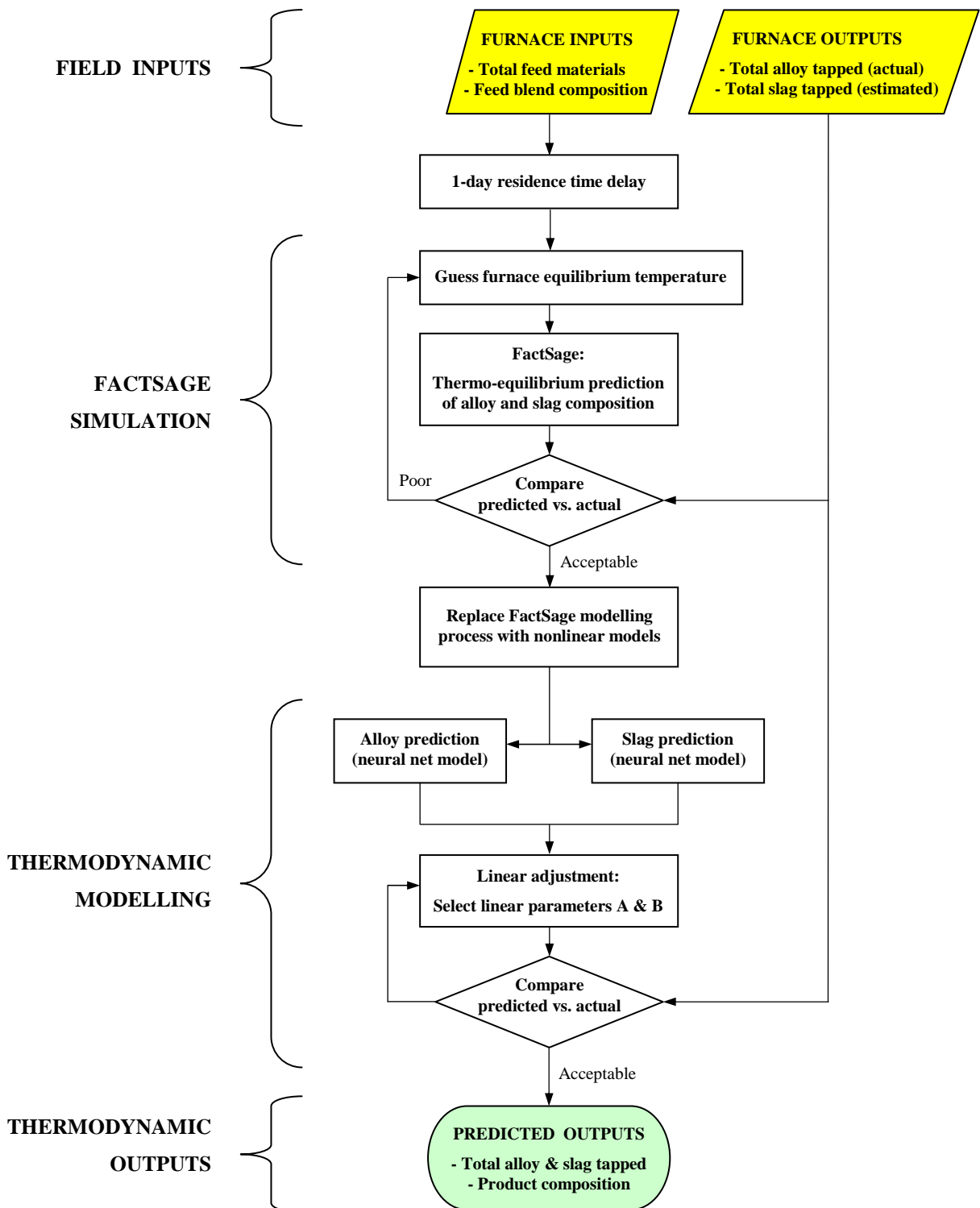


Figure 15 Flowchart of thermodynamic sub-model



### 4.3.2.2 Dynamic modelling

With reference to Figure 14, a second sub-model was developed to combine some of the results of the thermodynamic sub-model with the dynamic influences of controllable electrical variables to predict optimum setpoints for key performance indicators or KPI's. This step is referred to as the dynamic modelling step of the investigation, and the procedure is illustrated in Figure 16.

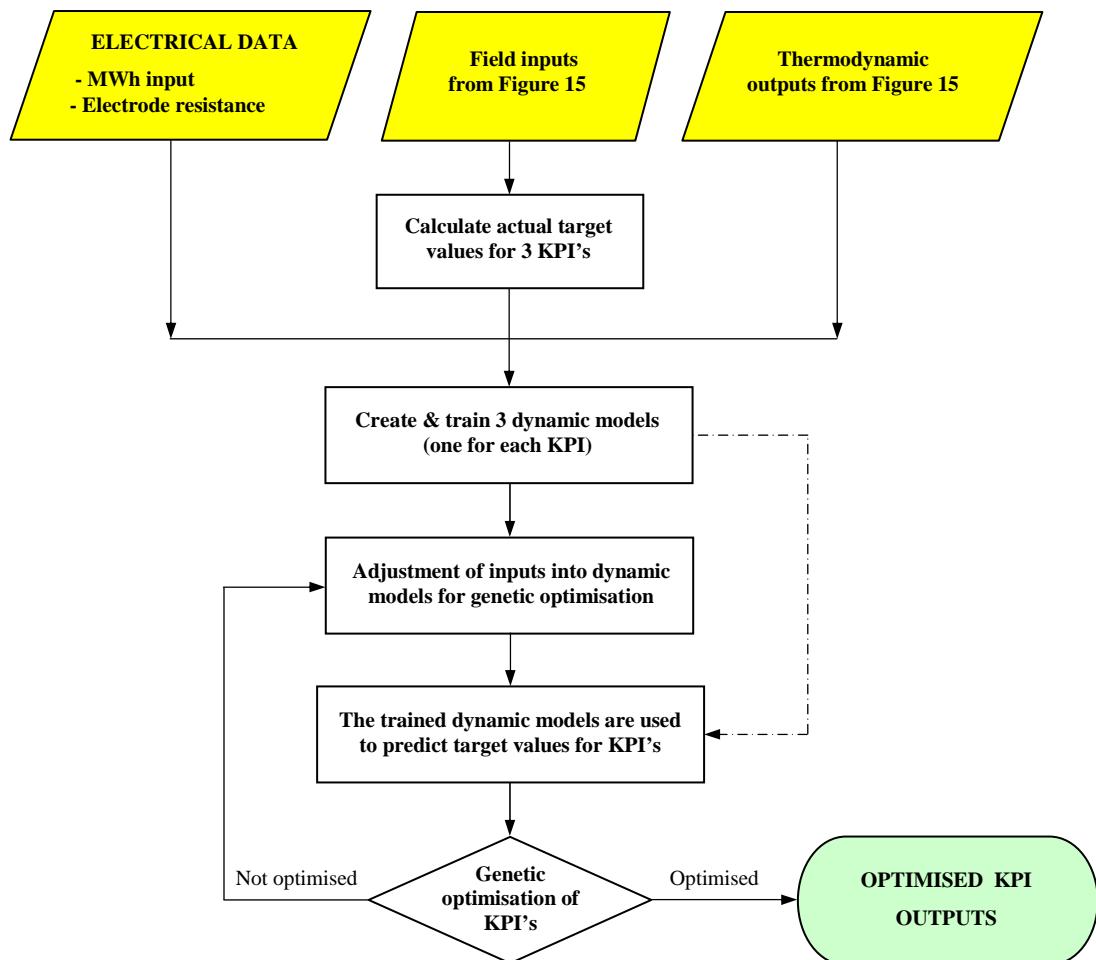


Figure 16 Flowchart of dynamic sub-model

### 4.3.2.3 Optimisation with genetic algorithms

Integrated into the dynamic modelling procedure, as indicated in Figure 14 and Figure 16, is a genetic optimisation algorithm that adjusts to optimum levels the variables that affect selected KPI outputs.

The three performance indicators predicted by the three dynamic models, viz. alloy-feed ratio, Mn recovery and alloy-slag ratio, were optimised using a nonlinear genetic optimisation algorithm from within CSense. A genetic optimisation algorithm is particularly efficient at finding a near-optimal solution in few iterations, because the best-performing variables are continually singled out and manipulated until an optimal solution is achieved. Time is therefore saved through avoiding the evaluation of every possible solution for all combinations of the variable setpoints.

The process of genetic optimisation can be likened to an evolutionary process whereby parent solutions (chromosomes) with the fittest (best) cost function outputs are randomly created and are paired to create children offspring. In this project, the furnace performance indicators are the chromosomes. A fitness function is a rule that ranks the values of these performance indicators from maximum to minimum. In the creation of children outputs, certain variable settings (genes) of two parent chromosomes are crossed-over to produce two child chromosomes bearing the characteristics of the parents. The random gene settings of the child chromosomes are slightly manipulated (mutated) by some random amount to introduce variability to the original gene settings. Children chromosomes may or may not improve the fitness/cost function in a successive generation of chromosomes. The fittest parents and children chromosomes are selected and passed on to the next generation to maintain a constant population count. The creation of successive generations will eventually evolve a set of optimal gene settings which will maximise the chromosome fitness. Optimisation is stopped at this point to give the best solution or is stopped after the creation of a maximum number of 1000 generations to save time on unconverging solutions. Further details are not disclosed for proprietary reasons.

[www.tradingsolutions.com/webhelp/optimization/optimization\\_understanding.html](http://www.tradingsolutions.com/webhelp/optimization/optimization_understanding.html)

[www.codeproject.com/KB/recipes/geneticlibrary.aspx](http://www.codeproject.com/KB/recipes/geneticlibrary.aspx)

It should be noted that the genetic optimisation algorithm is in-built in a nonlinear optimisation block within the CSense Architect. The configuration and usage of this block for optimising a performance indicator within CSense are discussed in Appendix G.3. The flow diagram illustrating the implementation of genetic optimisation in this project is illustrated in Figure 17. Since the code for genetic programming within the CSense software is confidential, further detail on genetic optimisation has been omitted from this thesis.

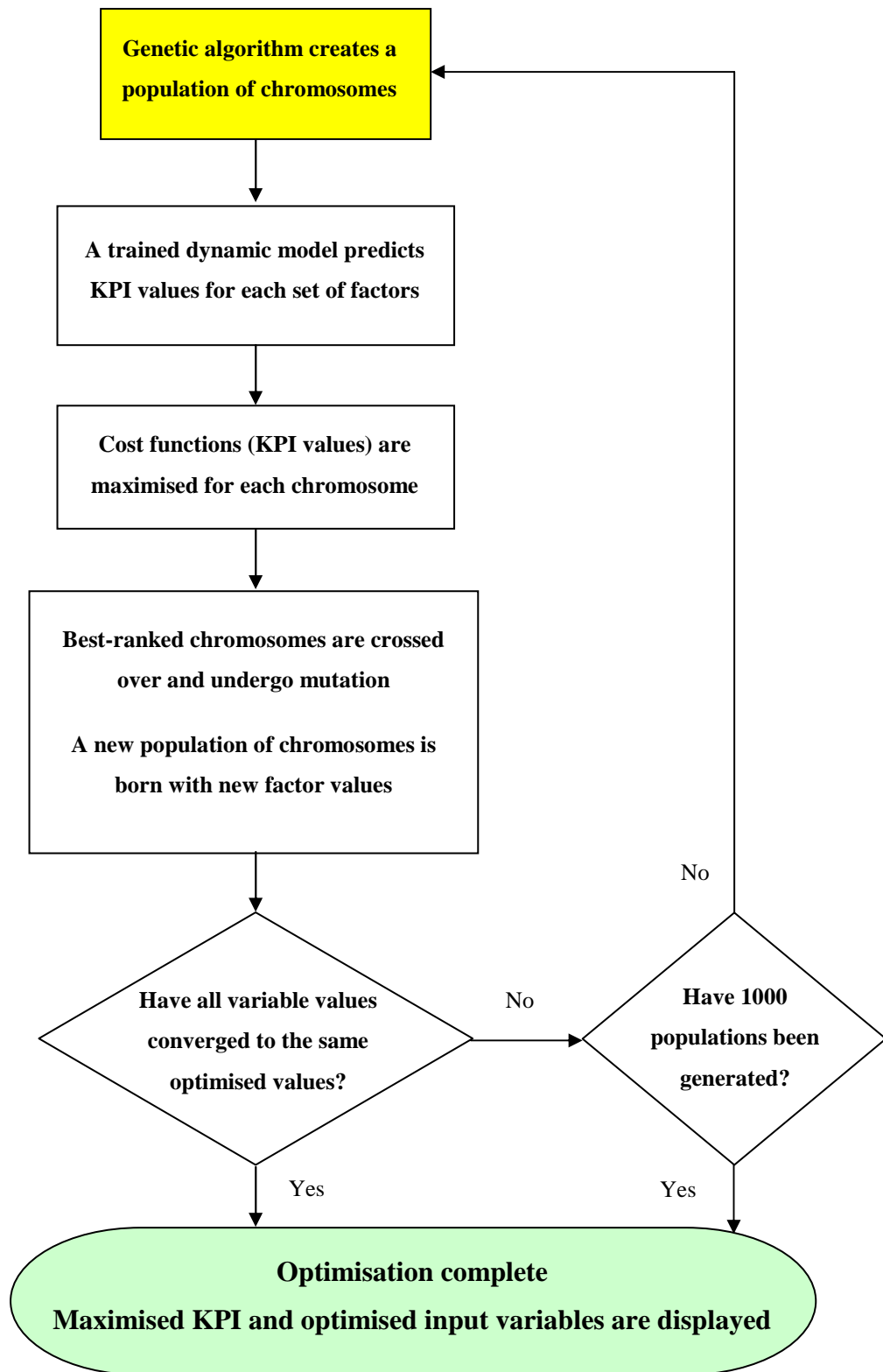


Figure 17 Genetic optimisation of dynamically modelled performance indicators (Lee *et al.*, 2007)

### **4.3.3 Modelling overview**

With a combined modelling approach, furnace performance can be predicted and optimised through the implementation of optimised variable setpoints. The proposed modelling method could fit into the control structure of Furnace 2 in a supervisory capacity in order to complement its normal operation.

Control options could be tested by plant engineers through analysing the response of model targets by the adjustment of field variables to theoretically optimum settings. The complete hybrid model should therefore accompany the diagnostic measures used by plant engineers for improving process performance. This might be an iterative procedure, whereby contributing variables are re-adjusted to obtain optimum performance. If this fails, the predictive model would have to be restructured and the selection of the model variables would need to be reconsidered. The entire modelling process is summarised graphically in Figure 18 (on the following page).

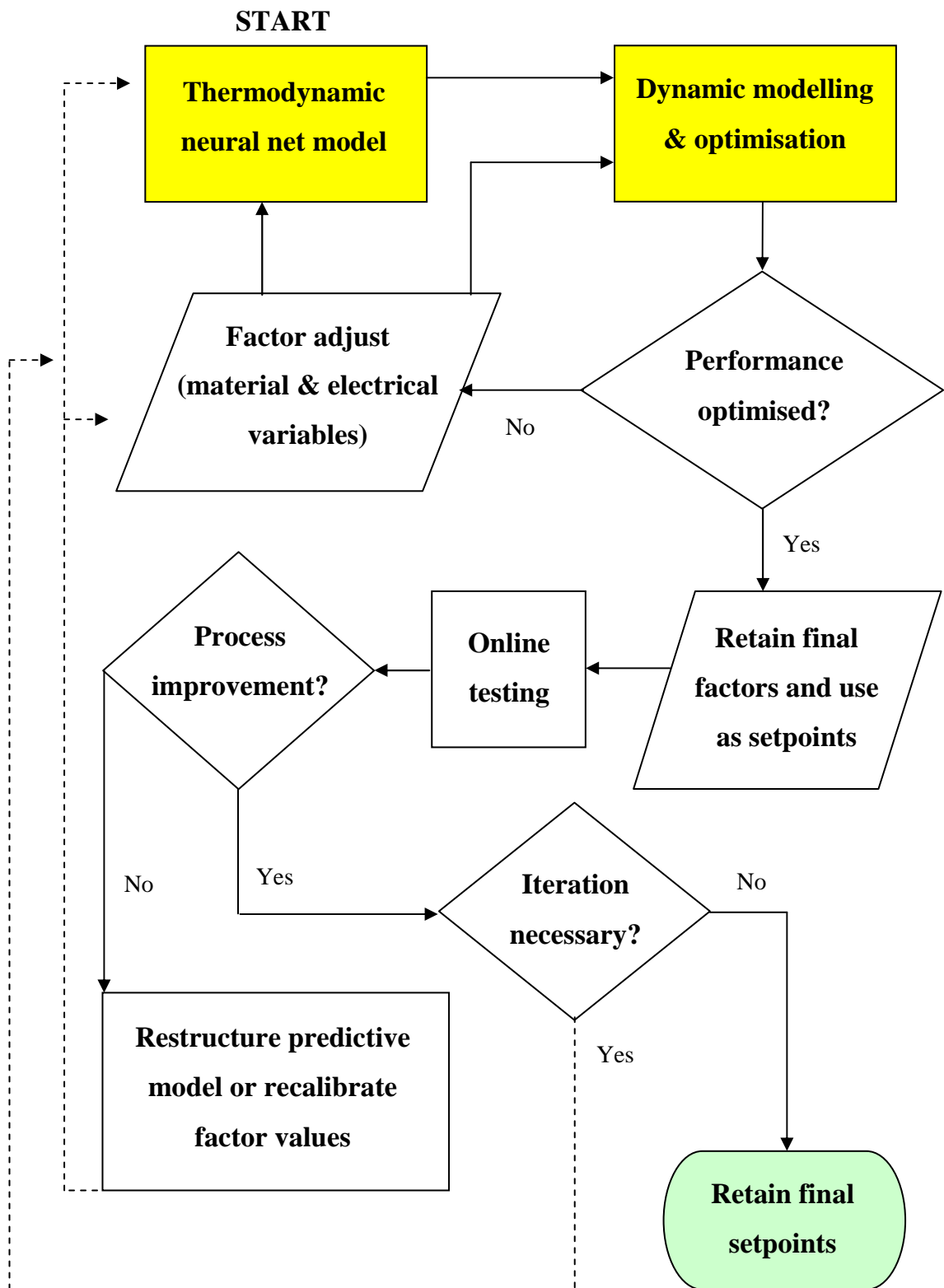


Figure 18 Modelling procedure for production optimisation of a ferromanganese furnace

## CHAPTER 5

# RESULTS AND DISCUSSION

The development of a complete dynamic model for optimising three important furnace performance indicators (alloy-feed ratio, Mn recovery and alloy-slag ratio) was discussed in the consecutive sections of this chapter. First, the performance of the initial thermodynamic model was evaluated. Second, electrical considerations leading to optimised furnace performance were discussed, followed by a performance evaluation of a final dynamic process model that combined outputs from the calibrated thermodynamic model with the dynamic electrical variables of the furnace. Specific setpoints were proposed for the manipulable variables that comprised the final model, so as to maximise the three performance indicators that would lead to improved furnace performance. The three performance indicators were: maximum tonnes of alloy produced per tonne of feed material, maximum Mn-recovery to the product alloy from the feed blend, and the highest alloy-slag ratio possible. The values proposed for the different manipulable variables were set to be within their allowable operational extremes, or at fixed setpoint values, depending on the variable being considered.

### 5.1 Thermodynamic process model

#### 5.1.1 Material flow assumptions

From the proposed model structure that was motivated and described in section 4.3, construction of a thermodynamic model using FactSage and a replacement neural network was the initial modelling step. Before the temperature calibration and performance of the thermodynamic model are explained, the assumptions affecting these are discussed.

According to Reuter and Yang (2000), process modelling can only be commenced after a mass-balance reconciliation exercise wherein average material flowrates are manipulated to force a zero residual accumulation of materials moving through a system, i.e. total materials fed is equated to the total output of product materials. Such an exercise was however not performed on Furnace 2, because not all the product flowrates were accurately measured, or were not measured at all. For instance, the amount of slag produced was not measured over the entirety of the sampling period. Only estimates were occasionally made and were based on the approximate weight of slag that could be contained in a slag ladle. These measurements were highly variable and out-of-range of the estimated amount of slag that supposedly would be produced. A more accurate measure of the amount of slag formed was calculated by assuming that the total amount of CaO and MgO entering with the feed blend, would exit the system only in the slag. This calculation would be possible because the composition of the slag output is known by XRF analysis. Significant loss of the CaO and MgO components to the remaining material output streams (off-gas and alloy tapped) were unexpected.

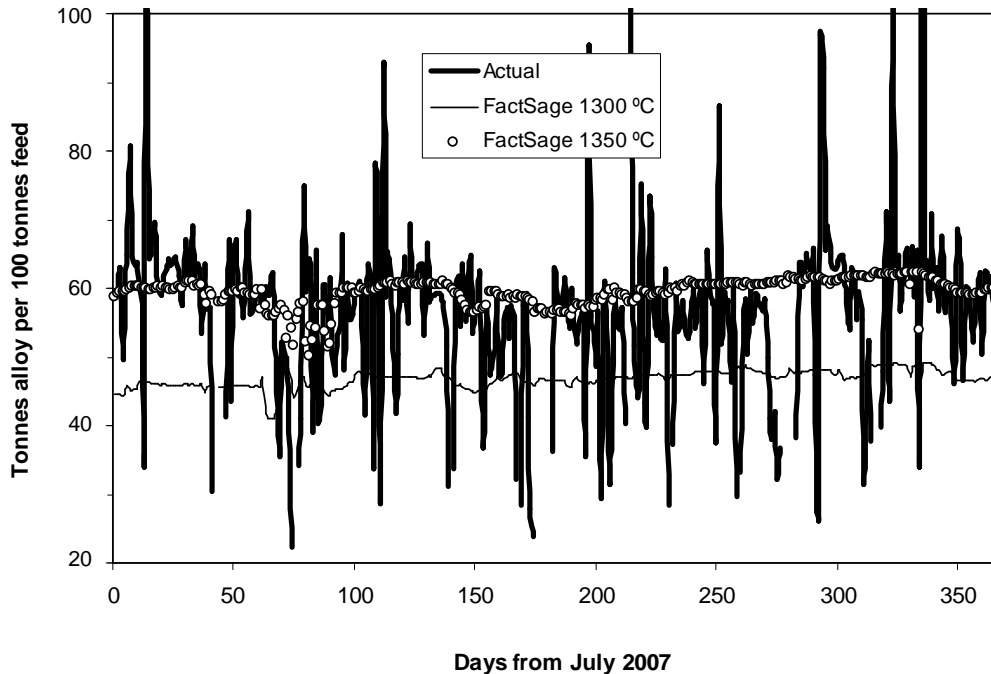
Another material output that was thought not to be accurately measured was the off-gas flowrate. Flow measurements were made in  $\text{Nm}^3/\text{s}$ , and when converted to kilograms of gas produced per day, it was found that the gas flowrate was excessively high with the total sum of the output materials exceeding the total input materials by about 15%. A possible reason for the gas flow being out of range may have been that the measurement instruments for gas-flow were not calibrated correctly.

With the thermodynamic model development for data of Furnace 1, it was observed that FactSage was able to predict reasonably well the flowrates of the condensed material output streams, i.e. alloy and predicted slag steams. The same occurrence was found for the condensed outputs of Furnace 2. In the calculations of FactSage, output material flowrates were automatically calculated so that they balanced with the total amount of input materials. Gas-flow analysis from Furnace 2 was subsequently ignored because of this.

### 5.1.2 Temperature calibration

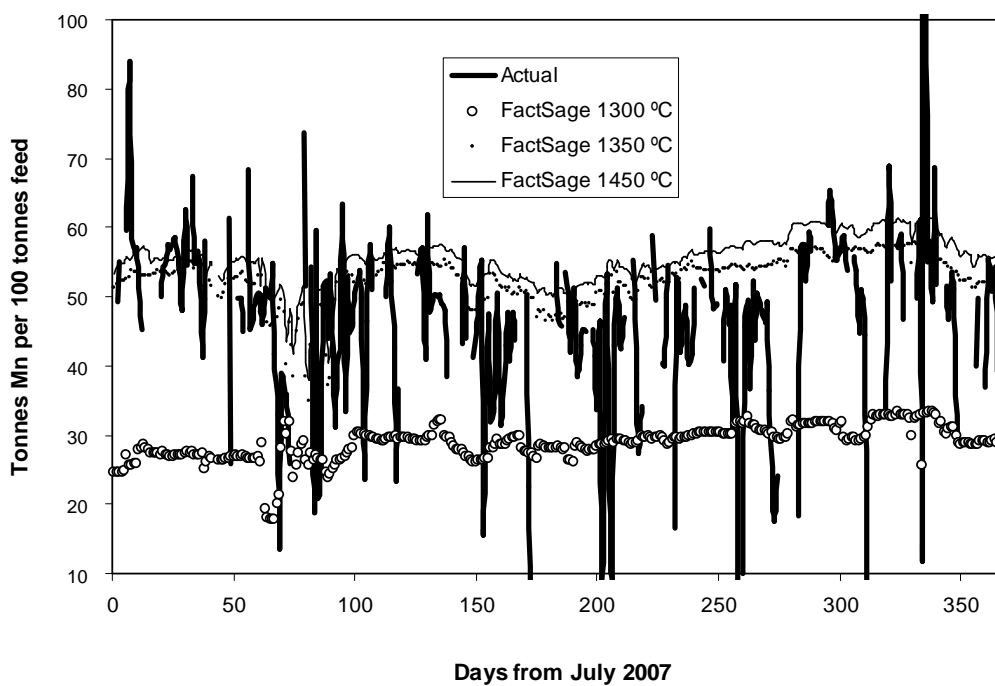
An iterative procedure was employed to calibrate the equilibrium results from FactSage with the actual amounts of alloy and slag tapped. This was achieved by setting a constant reaction temperature in FactSage for each of the 365 factorial runs and evaluating the results. If the results were out of range, then an adjustment to the constant reaction temperature was made and the simulation reiterated. This was continued until good agreement was achieved between equilibrium FactSage results and the actual amounts of alloy and slag tapped.

Figure 19, Figure 20 and Figure 21 show the results of temperature calibration for alloy production. Note that the actual amounts of alloy and Mn produced in Figure 19 and Figure 20 show a high degree of variation, but with the average trend-pattern still visible. In both these figures, FactSage results at 1300 °C were consistently far below the actual production average. Results at 1350 °C appear to be slightly higher than the production average. The equilibrium reaction temperature to be used in FactSage therefore had to lie between 1300 and 1350 °C. Further iteration revealed that the temperature delivering the best comparative result was 1320 °C. This is indicated in Figure 21.



**Figure 19** Effect of temperature on alloy prediction from FactSage  
(Data scaled as per confidentiality agreement)





**Figure 20** Effect of temperature on Mn prediction from FactSage  
(Data scaled as per confidentiality agreement)

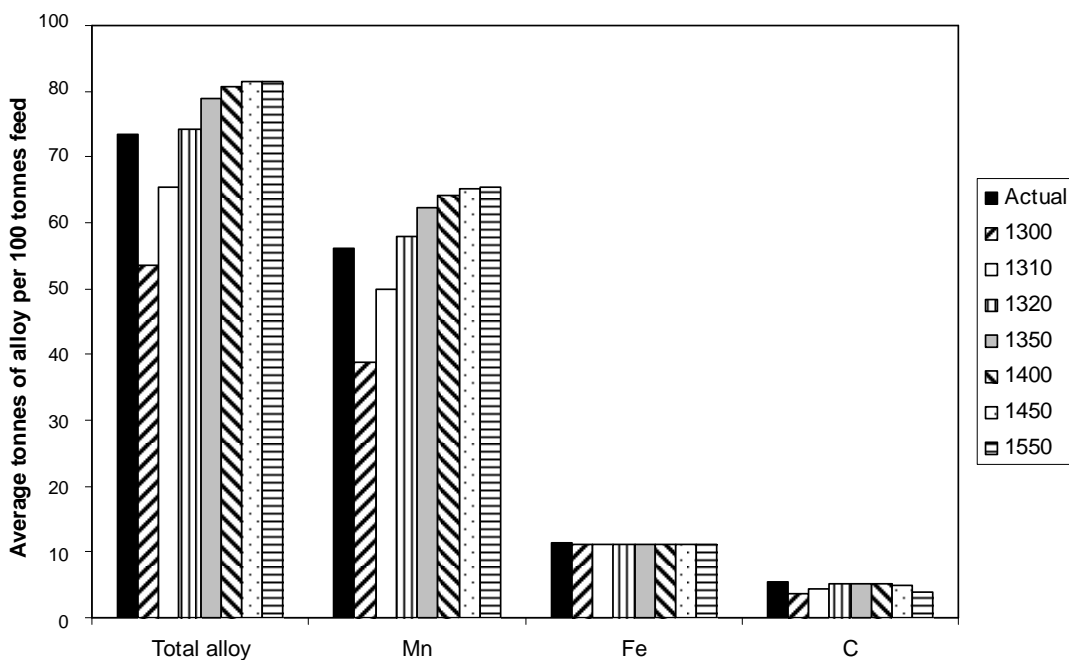


**Figure 21** Best comparative temperature for the average daily alloy production is 1320 °C  
(Data scaled as per confidentiality agreement)

In Figure 21, the average tonnes of alloy predicted per 100 tonnes of feed were calculated over the 365 day period. Good agreement can be observed for all alloy components at 1320 °C.

Figure 22, Figure 23 and Figure 24 show the results of temperature calibration for slag production. The actual amounts of slag and MnO produced in Figure 22 and Figure 23 show less variation than for the actual alloy produced. This is because the actual slag produced was actually estimated using the amounts of CaO and MgO in the more-uniform feed blend. In both these figures, FactSage results at 1300 °C were consistently far above the actual production average. Results at 1350 °C appear to be slightly lower than the production average. The equilibrium reaction temperature to be used in FactSage therefore had to lie between 1300 and 1350 °C again. Further iteration revealed that the temperature delivering the best comparative result was 1320 °C. This is indicated in Figure 24.

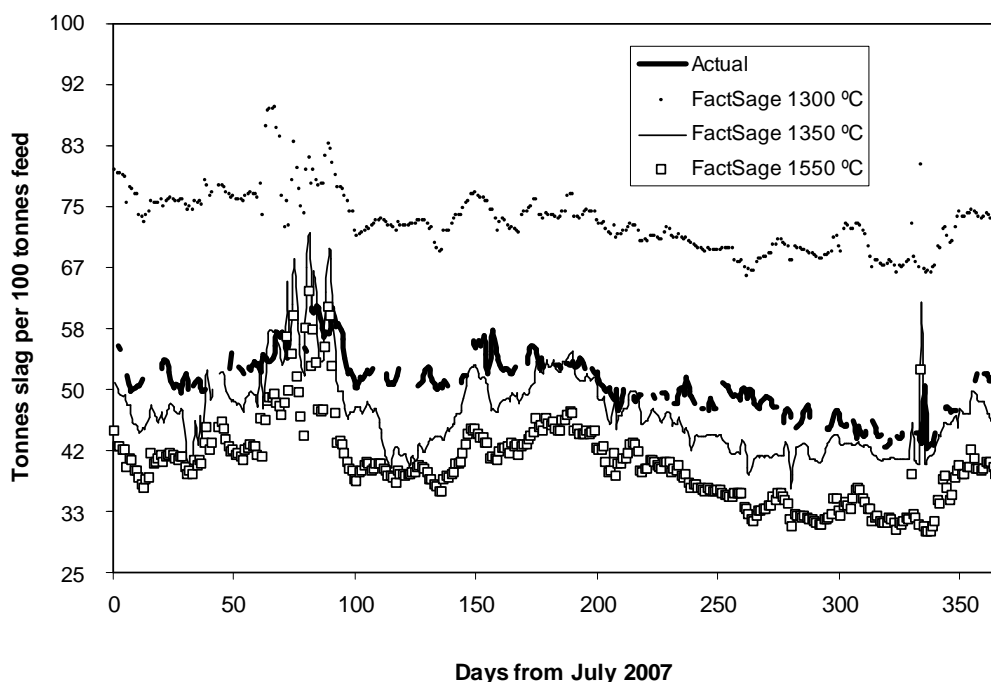


**Figure 22 Effect of temperature on slag prediction in FactSage  
(Data scaled as per confidentiality agreement)**

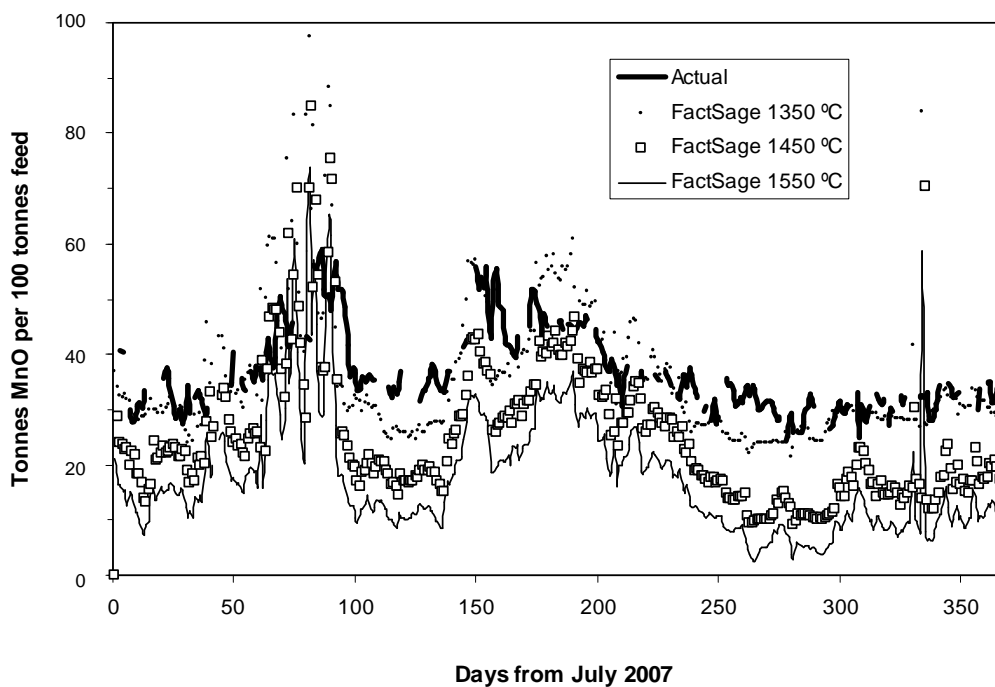


**Figure 23** Effect of temperature on MnO prediction in FactSage  
(Data scaled as per confidentiality agreement)

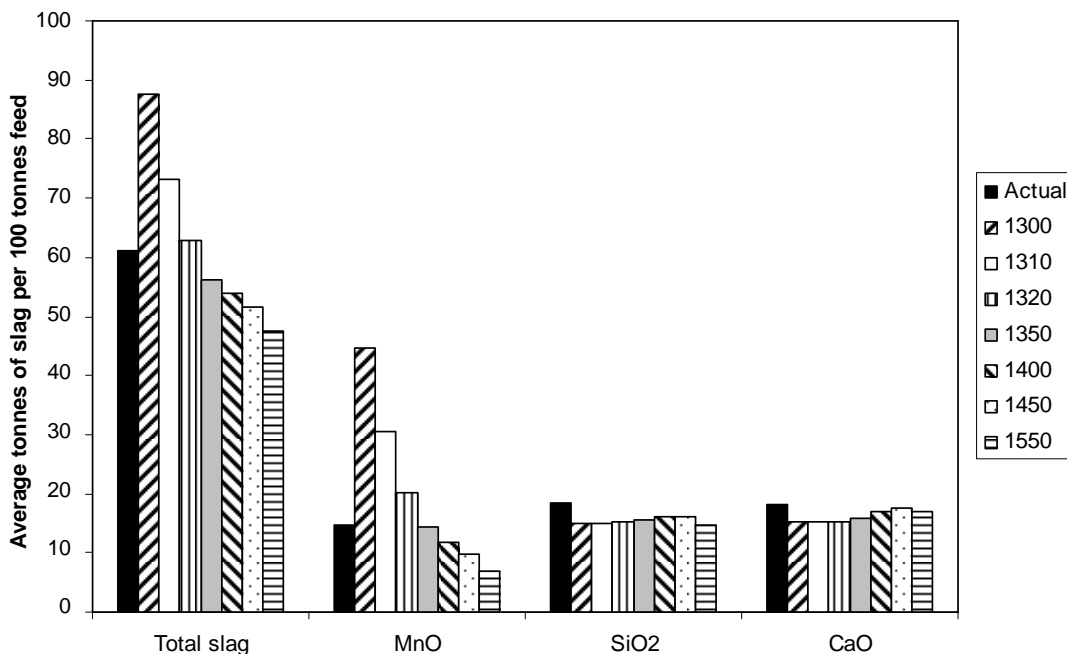


**Figure 24** Best comparative temperature for the average daily slag production is 1320 °C  
(Data scaled as per confidentiality agreement)

In Figure 24, the average tonnes of slag predicted per 100 tonnes of feed were calculated over the 365 day period. Fair agreement can be observed for all slag components at 1320 °C. Inaccuracies between component outputs at different equilibrium temperatures are probably attributable to the exclusion of complex metal silicates. These silicates were found to exist as a minor phase in the results from FactSage.

### 5.1.3 Thermodynamic neural network model

The calibrated temperature of 1320 °C was used for generating results from the 2<sup>13</sup> factorial runs in FactSage. The input and output results were then used to train a neural network model that was capable of predicting the probable equilibrium output for any combination of feed materials. The model was found to work best if feed materials were fed to the furnace in proportions that would produce high-carbon ferromanganese. This means that the model would not perform well if zero reductants are fed to the furnace, because without reductant materials, no product would be formed. Performance of the neural network model for predicting equilibrium amounts of alloy and slag from Furnace 2 are shown in Figure 25 and Figure 26, respectively.

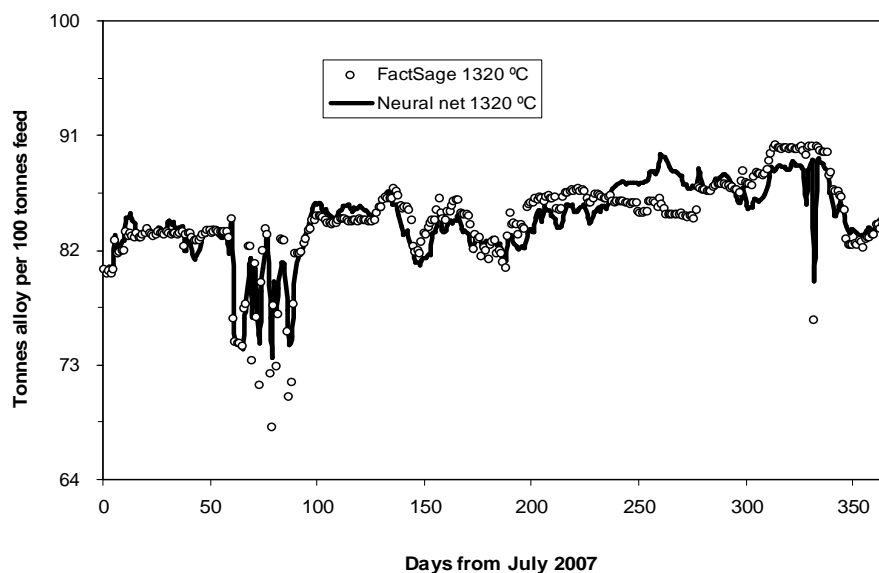


**Figure 25 Thermodynamic modelling results for alloy production  
(Data scaled as per confidentiality agreement)**

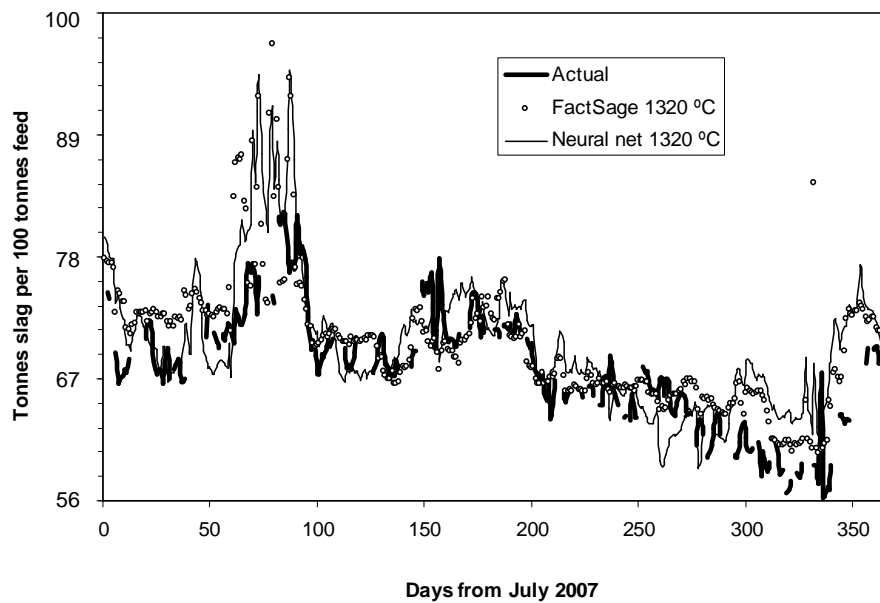


**Figure 26 Thermodynamic modelling results for slag production  
(Data scaled as per confidentiality agreement)**

The model was able to predict the equilibrium amount of alloy with an overall  $R^2$  of 0.91. Equilibrium amounts of slag were predicted with an overall  $R^2$  of 0.99. Observed bias shifts in the output results of the neural network data were adjusted to minimise average bias differences. Only results for the neural network prediction of the total amounts of slag and alloy produced are shown in Figure 25 and Figure 26. Results for each of the alloy and slag components were not illustrated here. Refer to Appendix G.1 for the layout of the complete thermodynamic model, as created in the ‘Architect’ software of CSense Systems Pty (Ltd).

#### **5.1.4 Sensitivity of feed materials on FactSage-modelled outputs**

FactSage predicted outputs were affected differently by the individual feed materials in the feed blend to Furnace 2. The results presented in Figure 27, Figure 28 and Figure 29 indicate the sensitivity of slag, alloy and gas production according to the influence of the different feed material blends as set out in the  $2^{13}$  factorial design. The factorial runs are indicated along the x-axis of the diagrams. The factorial design

was designed so that each of the factorial runs represents a blend of different proportions of feed materials.

In Figure 27, the effects of reductant addition are clearly visible. Between 0 and 2048 runs, no reductant material is added. Only coal is fed from runs 2048 to 4096. Only coke is fed from run 4096 to 6144, and a blend of coal and coke is represented by run 6144 to 8192. Each of these regions of reductant additions are indicated in Figure 27 and variations in the data are also visible in these regions. These same regions of reductant addition are also clearly visible in Figure 28 and Figure 29.

Notice in Figure 27 that addition of reductant brings about a decrease in the output of slag. This is evidence that the furnace reactions occurs when reductant additions are made. It appears that pure coal has a slight advantage over pure coke usage in that the average slag productivity is decreased for coal. From a thermodynamic point of view, average slag production is seen to be significantly less for a blend of coal and coke, i.e. for a higher proportion of reductant feed.

Higher proportions of coal and coke certainly have a significant impact on slag, alloy and gas production as indicated in the figures below. Not only is this sensitivity shown in these diagrams for reductant material, but also for other ore materials. A few repetitive patterns (of variable interaction) in the trends are indicated with the white arrows in Figure 27. A higher noise level in the trends indicates higher sensitivity of the ore materials in that region. Variable interaction is also observed, because production sensitivity is affected more appreciably for additions of ore materials in the presence of pure coal or pure coke than in a blend of these, for instance. The regions in Figure 27, Figure 28 and Figure 29 could also be expanded if so desired to indicate output sensitivity for the materials/variables which alternate from zero to maximum input after only a few factorial runs.

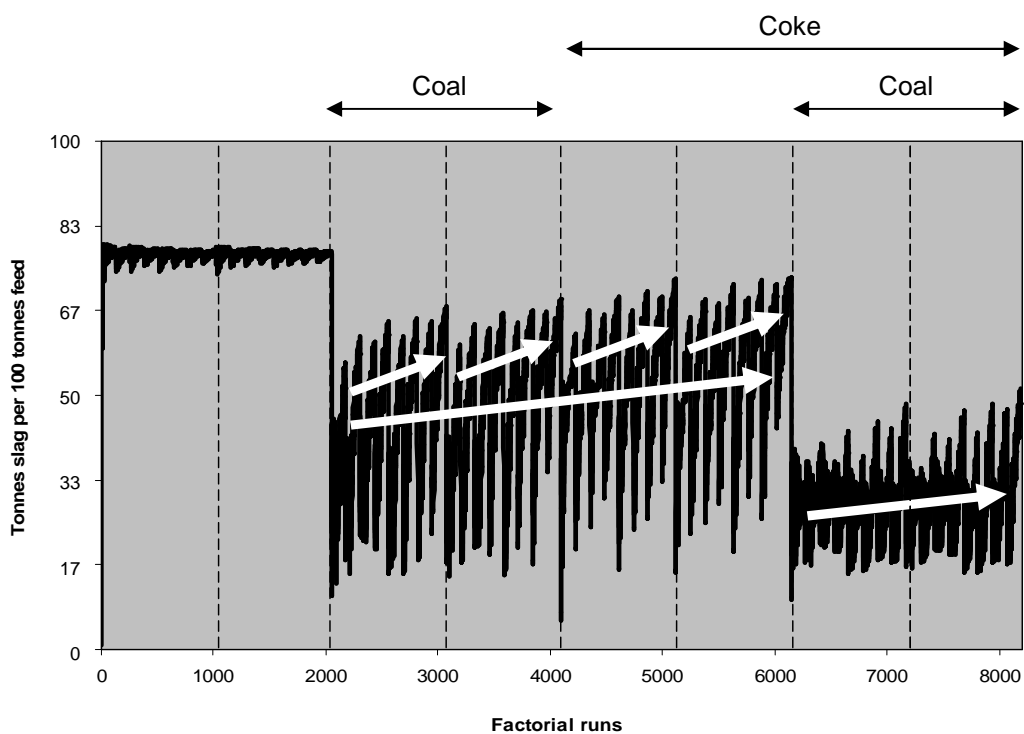


**Figure 27** Effect of FactSage factorial results on slag production. A coal and coke blend is beneficial to the minimisation and stabilisation of slag production  
(Data scaled as per confidentiality agreement)

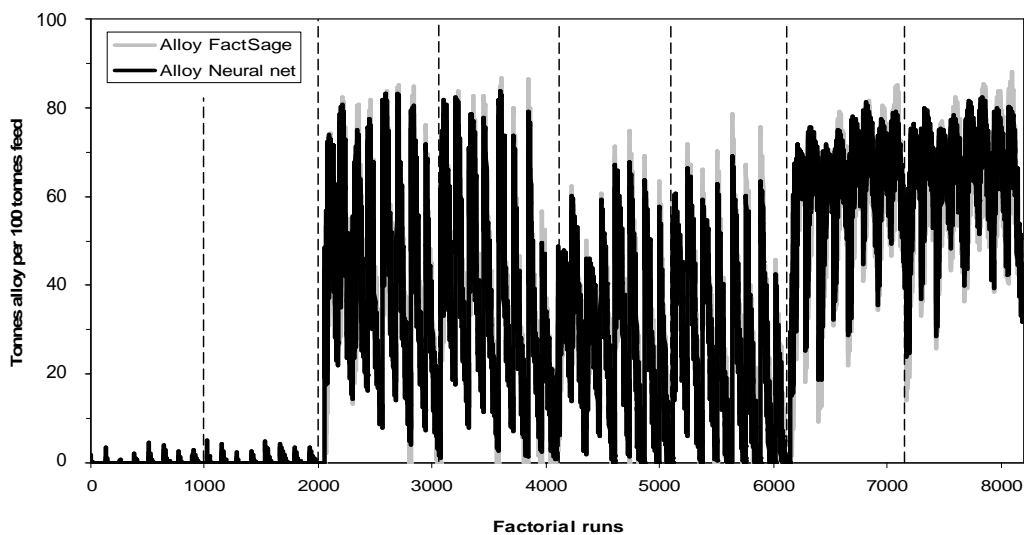


**Figure 28** Effect of FactSage factorial results on alloy production. A coal and coke blend is beneficial to the maximisation and stabilisation of alloy production  
(Data scaled as per confidentiality agreement)

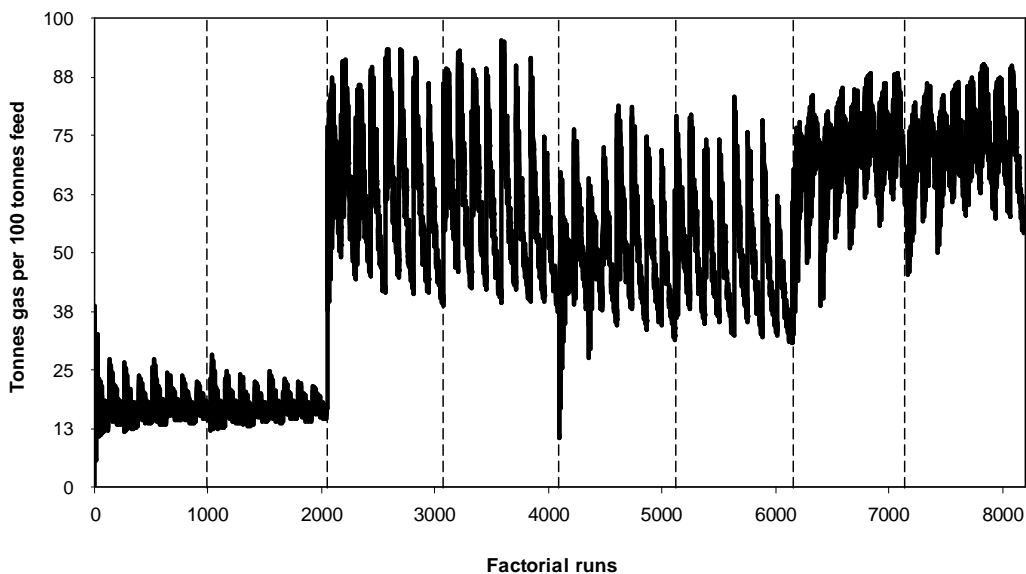


**Figure 29** Effect of FactSage factorial results on gas production. A coal and coke blend is beneficial to the maximisation and stabilisation of gas production  
(Data scaled as per confidentiality agreement)

An analysis of variance (ANOVA) on a fitted linear model for the alloy and slag outputs was attempted with poor success, since the linear model did not match the nonlinear behaviour of the data very well. A well-fitted linear model would have allowed for the accurate pointing out of the significant variables (feed materials) causing variance in production behaviour. Also, a well-fitted linear model would have indicated a measure (gradient or coefficient) by which each specific feed material would affect production. It might have been useful to perform an analysis of variance on a nonlinearly-fitted model. This analysis was not performed, as CSense was able to automatically calculate and display factor effects on production or performance.

## 5.2 Energy considerations

### 5.2.1 Energy balance and power requirements

It certainly is beneficial to maximise the MW input to a furnace so that more materials may be processed. It is also beneficial to reduce the amount of energy used to produce



per tonne of alloy produced, because the material throughput will increase for a given MW value. A minimum energy threshold however exists, since a minimum amount of energy is required per tonne of alloy to fully complete the necessary reactions. In order to classify the minimum energy requirement of the furnace, the reaction chemistry of the component interactions in the furnace needs to be considered. Refer to section 3.3 for these reactions.

It was assumed that the minimum energy requirement for the complete reaction and product forming process should be based on the maximum probable equilibrium temperature of the molten products from the furnace. This allows for a 'worst case' minimum energy input for achieving the highest possible equilibrium temperatures of the product matter. A temperature of 1500 °C was selected as the maximum possible temperature of the molten products. Based on the measured temperatures of the outlet furnace gases, an average flue gas temperature of 400 °C was used in the calculation of the minimum energy requirement for Furnace 2.

The main reaction stage drawing the most endothermic energy is the final reduction of MnO to Mn. The prereduction reactions of the higher oxides of Mn and Fe are all exothermic until the lowest oxidation state of Mn is reached. The final reduction of MnO to Mn is strongly endothermic, using about 40% of the total energy requirement for alloy production.

It was found that the minimum amount of energy lost to cooling water, used for cooling the furnace shell and roof, amounted only to 2% of the minimum energy requirement for alloy production. This is relatively low and it is probable that higher energy losses would occur on-site.

Based on the energy required for alloy production and the associated heat loss to cooling water, it was determined that the actual energy usage can be reduced by 1.8% by tapping more regularly so that less energy is expended to maintain the temperature of the molten furnace contents after completion of the necessary reactions. It was also calculated that this energy adjustment may bring about a 9% increase in the daily production rate of high-carbon

ferromanganese. The specific details pertaining to these calculations are classified and have been omitted from this thesis.

### **5.2.2 Electrical control**

It was assumed that the electrical setpoints employed were already optimum, since they were controlled by an automatic controller, and because the characteristic curves constructed for identifying the electrical operating point of the furnace showed that the system was probably already functioning at optimum electrical settings. Refer to section 3.1 for detail on the characteristic curves.

The main reason why it is difficult to propose new electrical setpoints is that it was difficult to establish from the available data, a correlation between reducing heat loss from the burden (to off-gas and cooling water) and the amount of heating required (to maximise production and to reduce the amount of Mn that is vapourised). Heat transfer from furnace off-gas to the burden might be optimised if a beneficial compromise can be made between the interactions of (1) electrode immersion vs. off-gas temperature and (2) electrode immersion vs. resistance; i.e. a compromise between minimum heat loss (via the release of off-gas) and maximum heat dissipation in the burden. No observable relationship between off-gas temperature and resistance was observed to support the understanding of this compromise.

Accurate information pertaining to the details of the electrode hoist position measurements from Furnace 2 could not be obtained. It was hoped that electrode hoist position measurements would reflect the depth of electrode immersion, which in turn would be related to the electrode-to-bath resistance, according to the resistance-resistivity relationship given in section 3.1. No reasonable correlation was however found between hoist position and resistance. Therefore it remains uncertain if electrode hoist position reflects electrode immersion in Furnace 2. A better understanding is therefore required for details of electrode hoist position measurements, or reliable electrode immersion data should be acquired.

## 5.3 Dynamic process model

### 5.3.1 Results of dynamic modelling

The thermodynamic model explained in section 5.1.3 is useful for predicting equilibrium outputs for alloy and slag from the furnace, but has limitations if it is to be used to model actual furnace behaviour. These limitations are enforced by the dynamics of furnace operation, whereby the fast-changing dynamics of the electrical variables of the process may significantly affect production. Therefore outputs from the thermodynamic model will be combined with other variables in an overall dynamic model that could be used to improve process performance.

The dynamic model used certain material outputs from the thermodynamic model, combined with certain electrical variables to give an estimate of the overall performance of the furnace by means of maximizing three key performance indicators (KPI's). These were: (1) the total tonnes of high-carbon ferromanganese produced per tonne of feed material, (2) the percentage recovery of manganese to the alloy product, and (3) the alloy-to-slag ratio. Maximisation of each of these would contribute to the overall improvement of the process. Each of these KPI's were thought to be affected by a few selected variables:

$$(1) \text{ Alloy/Feed} = f(\text{Feed materials}, \text{Feed basicity}, \frac{\text{MWh}}{t \text{ feed}})$$

$$(2) \% \text{ Mn Recovery} = f(\frac{\text{CaO}}{\text{SiO}_2}, \frac{\text{Coal}}{\text{Coke}}, \frac{\text{MWh}}{t \text{ alloy}}, \%C \text{ in feed}, \text{Resistance})$$

$$(3) \text{ Alloy/Slag} = f(\frac{\text{CaO}}{\text{SiO}_2}, \frac{\text{MWh}}{t \text{ alloy}}, \%C \text{ in feed}, \%Mn \text{ in alloy}, \text{Density}, \text{Viscosity})$$

These KPI's would be dependent on each other, because they are constrained by a mass balance. If the Alloy/Feed ratio (KPI 1) were to increase, then less slag would be produced and consequently the Alloy/Slag ratio (KPI 3) would also increase. The dynamic model was however designed to treat these KPI's separately (not as dependents), so that setpoints may be optimised for the variables that affect the individual KPI's.

Each of the three dynamic models was trained with daily-averaged plant data. For the first KPI, the 'Feed materials' variable includes the ore feeds, reductant materials and silica (13 in

total). Feed basicity was calculated according to the ratio:  $\frac{CaO + MgO}{SiO_2}$ , and the  $\frac{MWh}{t\ feed}$  was calculated from the available  $\frac{MWh}{t\ alloy}$ . The latter calculation was possible because the average daily ratio of alloy to feed materials was known.

For the second KPI, the  $\frac{CaO}{SiO_2}$  ratio is a pseudo basicity of the slag. Predicted outputs of CaO and SiO<sub>2</sub> from the thermodynamic model were used to calculate this ratio. The reason for not determining the normal basicity ratio of the slag according to the ratio,  $\frac{CaO + MgO}{SiO_2}$ , was because the FactSage prediction of the MgO content in the slag was found to be inaccurate. Note that all alloy and slag outputs used in the KPI's above were obtained from the thermodynamic model output instead of the actual furnace data in order to negate the effect of the extreme variation in the actual amounts of products tapped. The  $\frac{Coal}{Coke}$  ratio reflects the effect of these reductant materials on the recovery of manganese from the feed ores to the product alloy. The  $\frac{MWh}{t\ alloy}$  ratio was calculated using the actual daily MWh rating and the alloy output from the thermodynamic model. The concentration of carbon in the feed blend and the electrode-to-bath resistance measurement was also considered. The actual percentage of Mn recovered was calculated as follows:  $\frac{Mn_{product}}{Mn_{feed}} \times 100\%$

For estimation of the third KPI, the variables selected which were different from those of the second KPI were slag density, slag viscosity and the alloy grade (%Mn in the product alloy).

The choices of variables used in the three dynamic models were based on those variables that would contribute a change to the KPI's. At least one electrical variable, such as power input or resistance, was included in each dynamic model to account for their dynamic effects on the system. In the first dynamic model, only variables related to the feed materials were selected as inputs to the model. The trained model had an overall R<sup>2</sup> of 0.86, indicating a good relationship between the variables chosen and the alloy/feed KPI. The model fit is indicated in the bottom-most graph in Figure 30.

## Results and discussion

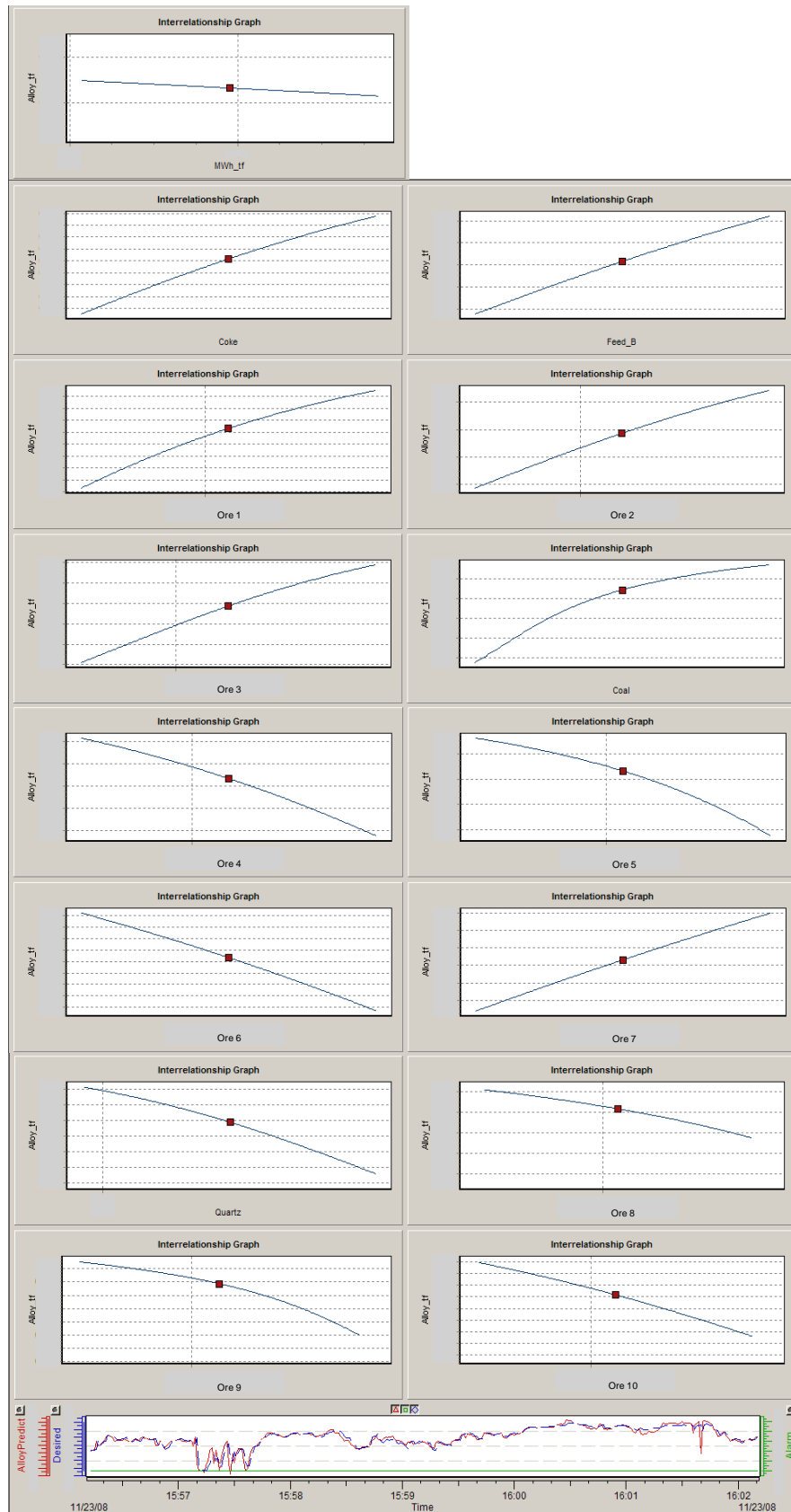


**Figure 30 CSense analysis of all modelled variables affecting the tonnes of alloy per tonne of feed (Permission by CSense Systems (Pty) Ltd) (Data removed as per confidentiality agreement)**

In the bottom-most window of Figure 30, the blue trend represents the actual daily tonnes of alloy produced per tonne of feed. The red trend indicates the model-predicted output. Each of the 365 seconds shown along the timescale of the graph represents one day from 1 July 2007 to 30 June 2008. The remaining windows in Figure 30 illustrate the interrelationships between the variables which affect the target KPI (tonnes of alloy per tonne of feed). Increasing values for each variable are represented along the x-axis in these diagrams. Values along the x and y axes are classified and have not been shown. The operating point at a specific moment in time is displayed by a red square along each trend line. CSense software was used to develop the dynamic KPI model and to perform the variable optimisation. Some of the variables indicated cannot be manipulated directly. These variables are explained later in section 5.3.2.

All variables in Figure 30 are interrelated with the target KPI either positively or negatively, to varying degrees. An increase in the value of a variable that is positively interrelated will bring about an increase in the value of the target KPI. The opposite applies for negatively interrelated variables. Variables which are negatively interrelated should be minimised as much as possible without adversely affecting other variables, so as to prevent weakening of a target variable. An increase in feed basicity, for instance, causes alloy production to be increased. This behaviour of feed basicity and the effects of all the feed materials on alloy production are further discussed in section 5.3.2.

For the second KPI, only variables were selected that would contribute to the migration of Mn from the feed materials to the alloy. Slag basicity was selected as a variable because it affects the slag liquidus temperature which contributes to better or worse alloy-slag separability. The 'Coal/Coke' ratio and the '%C in feed' were chosen as variables because they directly affect the reduction reactions occurring in the heated burden by allowing Mn migration to or from the product alloy. The power supplied per tonne alloy was also considered a key variable in the production of alloy, and the electrode-to-bath resistance would affect current flow and the degree of heating in the burden. The trained model had an overall  $R^2$  of 0.89, indicating a good

relationship between the variables chosen and the Mn recovery KPI. The model fit is indicated in the bottom-most graph in Figure 31. The associated variable interrelations are indicated in the remaining windows.

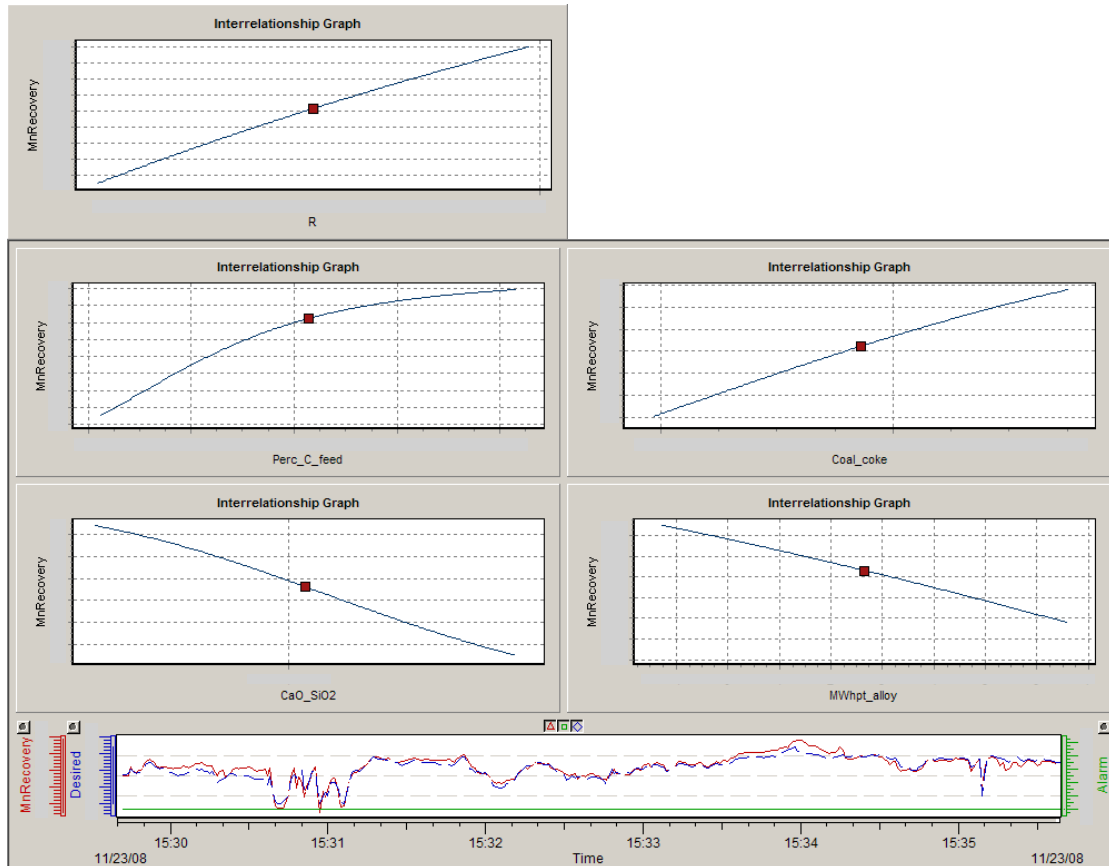


**Figure 31 CSense analysis of all modelled variables affecting the percentage of Mn recovered (Permission by CSense Systems (Pty) Ltd) (Data removed as per confidentiality agreement)**

Some of the variables used for the prediction of the second KPI were again considered for the third KPI, because they also influence the separability of alloy and slag. The product grade (%Mn in alloy) was assumed to be reflective of the alloy/slag ratio. The remaining two variables, slag density and viscosity, are intrinsic to the mineralogy of the product slag. They too were considered to be influential in alloy-slag separation. The trained model had an overall  $R^2$  of 0.85, indicating a good relationship between the variables chosen and the alloy-slag ratio. The model fit is indicated in the bottom-

most graph in Figure 32, and associated variable interrelations are indicated in the remaining windows.

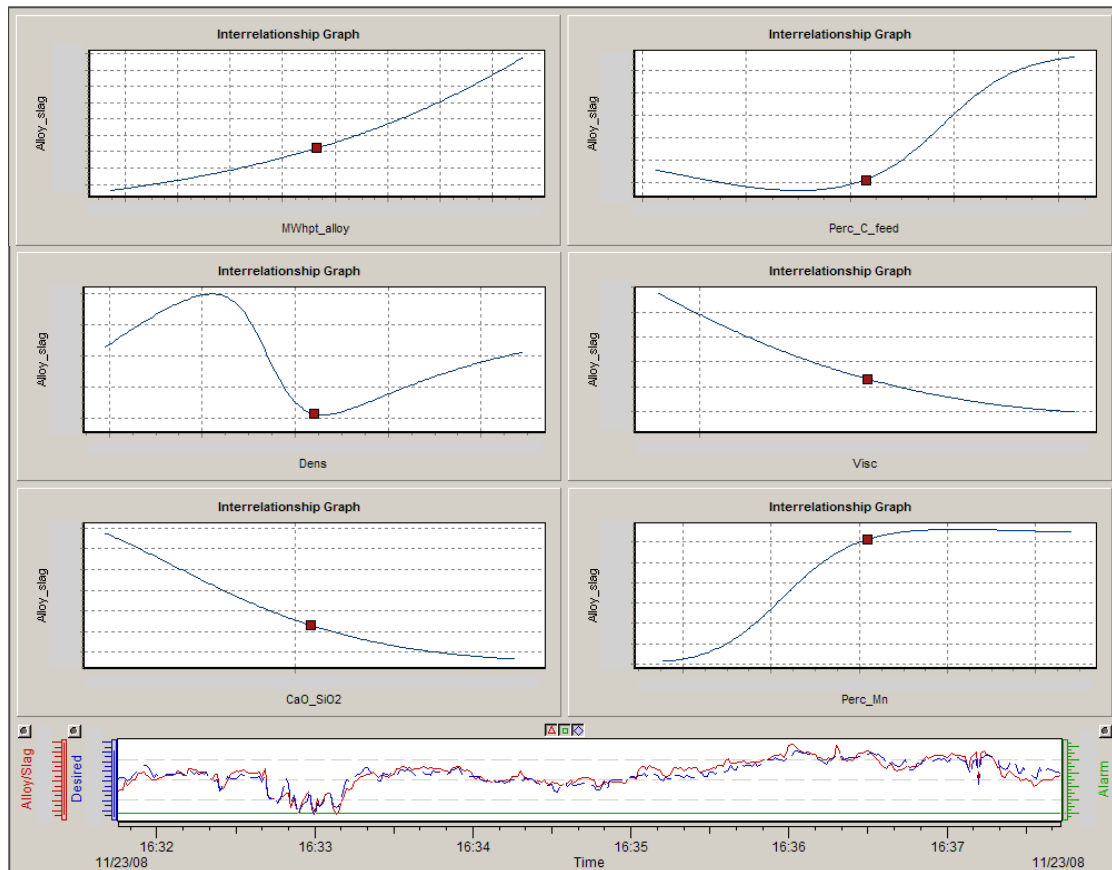


**Figure 32 CSense analysis of all modelled variables affecting the alloy/slag ratio (Permission by CSense Systems (Pty) Ltd) (Data removed as per confidentiality agreement)**

Many of the variable interrelationships for all three dynamic KPI models appear to be nonlinear trend lines. This indicates that the use of neural networks (nonlinear models) was a good choice for characterising the system.

### 5.3.2 Optimisation of the dynamic model

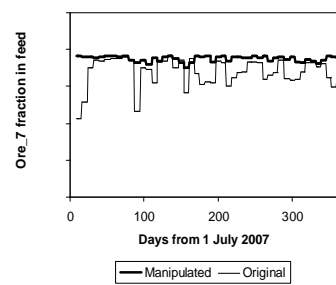
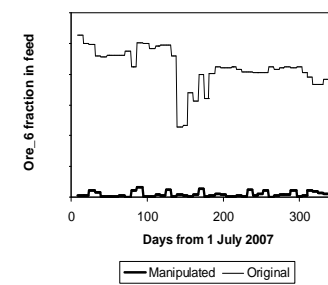
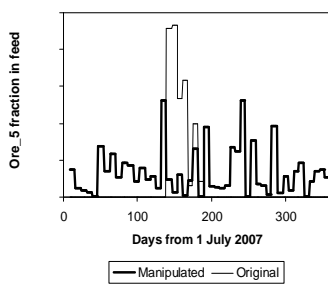
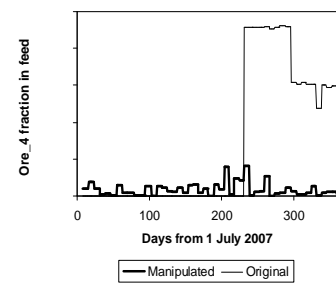
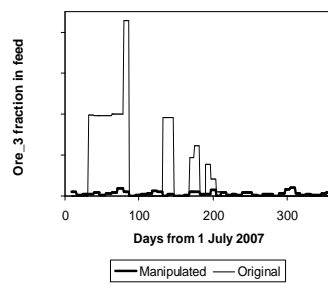
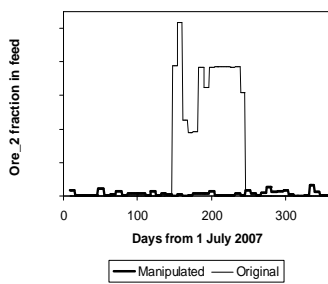
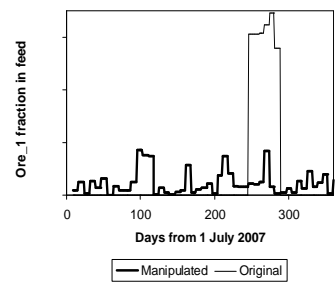
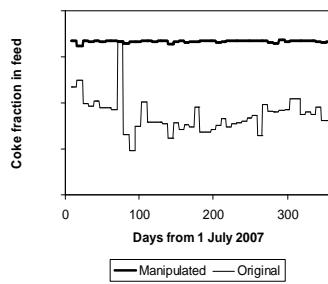
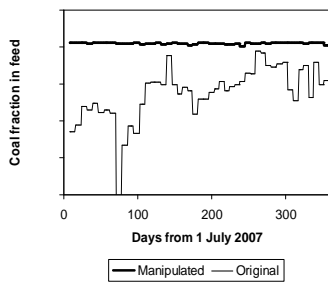
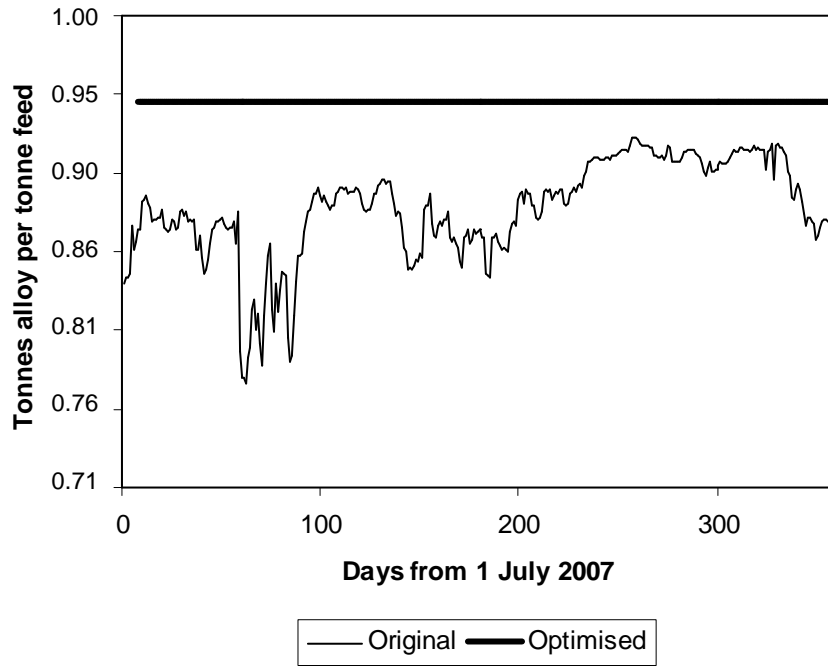
Before the three KPI's were optimised, it was important to understand which of the variables were manipulable. Manipulable variables can be manually/automatically manipulated to bring about a change in a KPI. Manipulable variables would be the



amounts and proportions of feed materials in the feed recipe. Another manipulable variable is the MWh supplied per tonne of alloy. Reduction of the MWh per tonne of alloy by tapping more frequently would increase material throughput. In the second and third dynamic model, the value for MWh per tonne of alloy was held constant at the measured average, since this variable had already been optimised according to the minimum energy requirement determined in section 5.2 of this thesis. Even though the feed basicity and the ‘%C in feed’ are not manipulable, since they are subject to the feed recipe, they were set in the optimisation model to be manipulable in order to observe if their optimum levels were in conflict with the basicity and %C calculated for the optimal feed recipe. Another variable that would be manipulable by electrode movement is the electrode-to-bath resistance. The resistance level was held constant during optimisation at its daily average value, as it was assumed to already be at the optimum setpoint according to section 3.1. Non-manipulable variables included slag density, slag viscosity and the grade of the product alloy. These could not be directly manipulated and were dependent on other variables such as slag composition.

The diagrams presented below compare the optimised KPI’s of the dynamic model with the actual KPI outputs. Setpoints of manipulable variables were adjusted to maximise the KPI’s through a genetic optimisation procedure, whereby each KPI was set as a cost function (or fitness function) in an optimisation step performed in CSense. More information on CSense modelling and optimisation are provided in section 4.3 and in Appendix G. The optimisation was based on the effective contribution of each manipulated variable to a KPI. The optimisation results are graphically displayed in Figure 33, Figure 34 and Figure 35 below. The variables thought to affect each of the three KPI’s appear in the small-scaled graphs in these three figures. Actual and predicted KPI’s are displayed in the large diagrams within these figures. Most of the variables that affect a KPI output were manipulable while others were not. The variables which were not manipulable were either fixed at certain optimum values, or were specified to not be manipulable, e.g. slag density and slag viscosity, so that they continually changed as dependents of other variables. Even though slag density and viscosity were not manipulable, their scale of magnitude gives an indication of the ease by which slag and alloy materials can be separated.

Results and discussion



Results and discussion

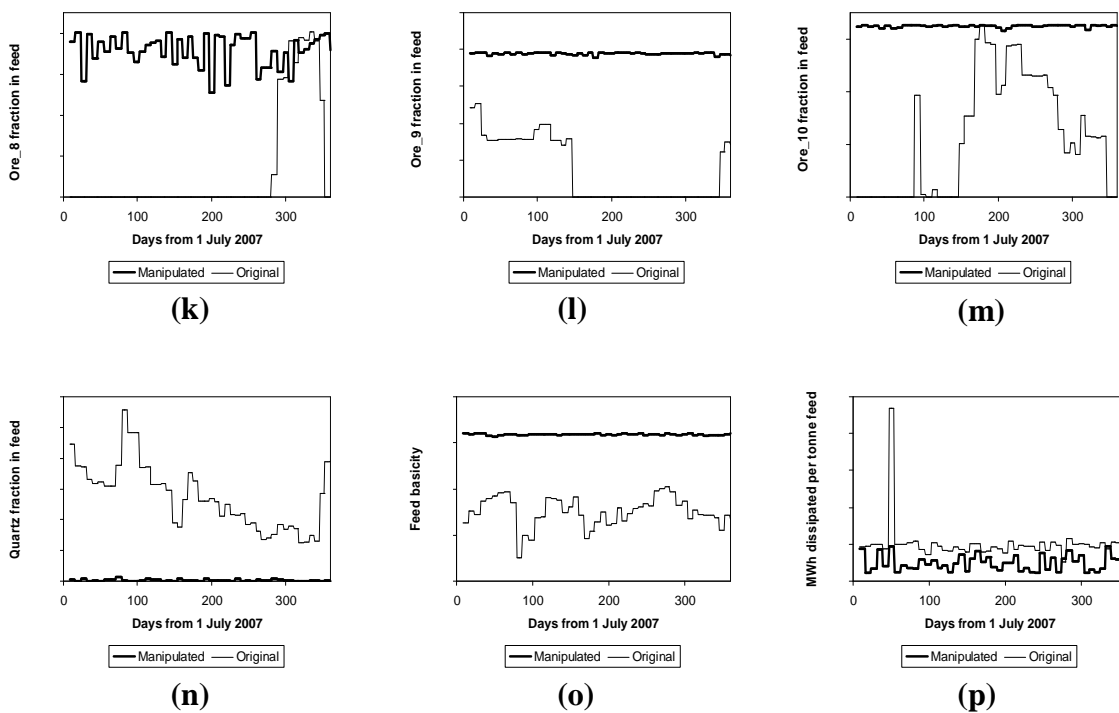
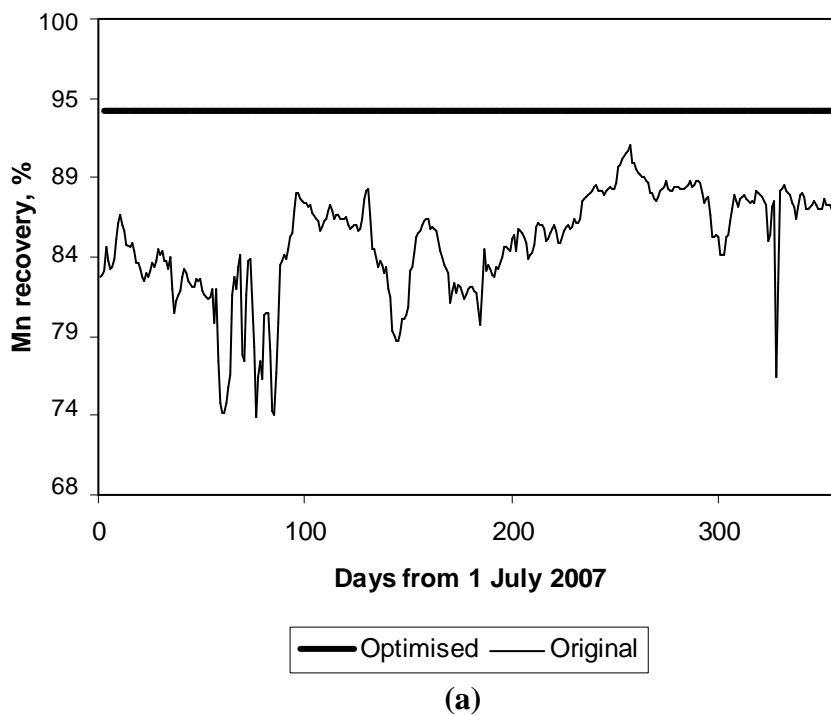


**Figure 33 (a) Performance Indicator 1 – Tonnes alloy per tonne feed**  
**(b) – (p) Variables affecting Performance Indicator 1**  
**(Data scaled/removed as per confidentiality agreement)**



Results and discussion

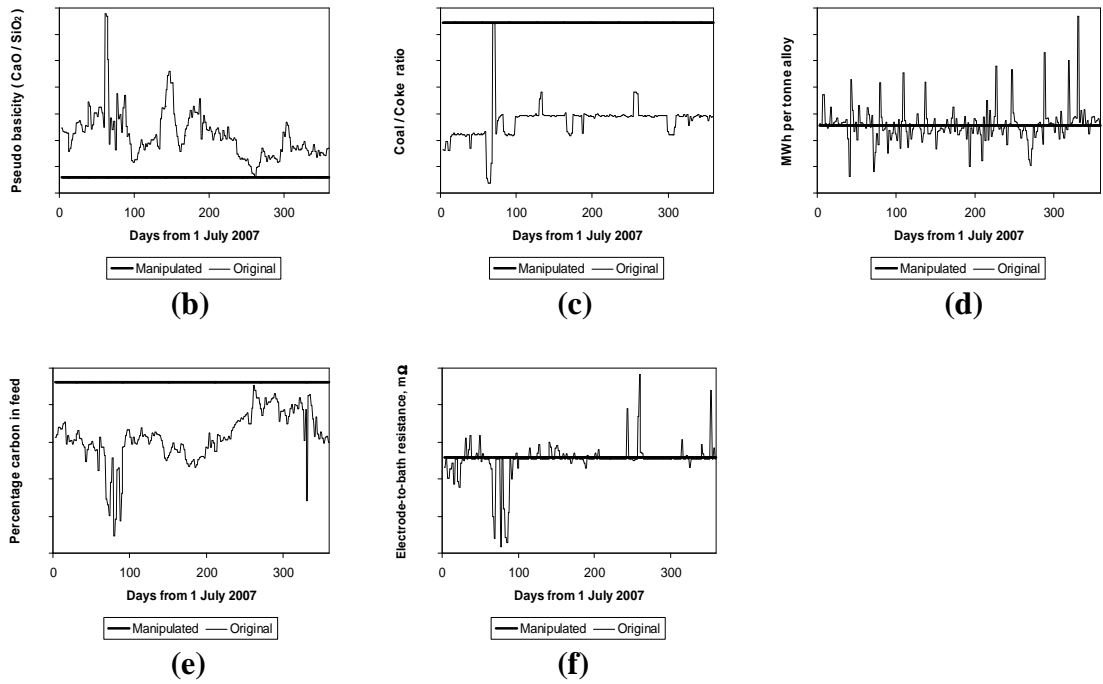
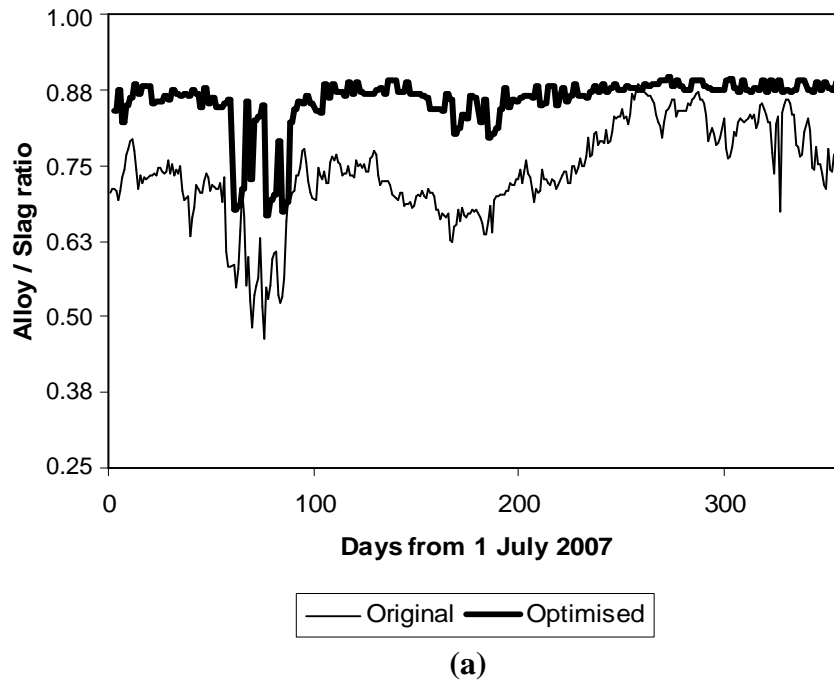


**Figure 34 (a) Performance Indicator 2 – Mn recovery  
(b) – (f) Variables affecting Performance Indicator 2  
(Data scaled/removed as per confidentiality agreement)**



## Results and discussion

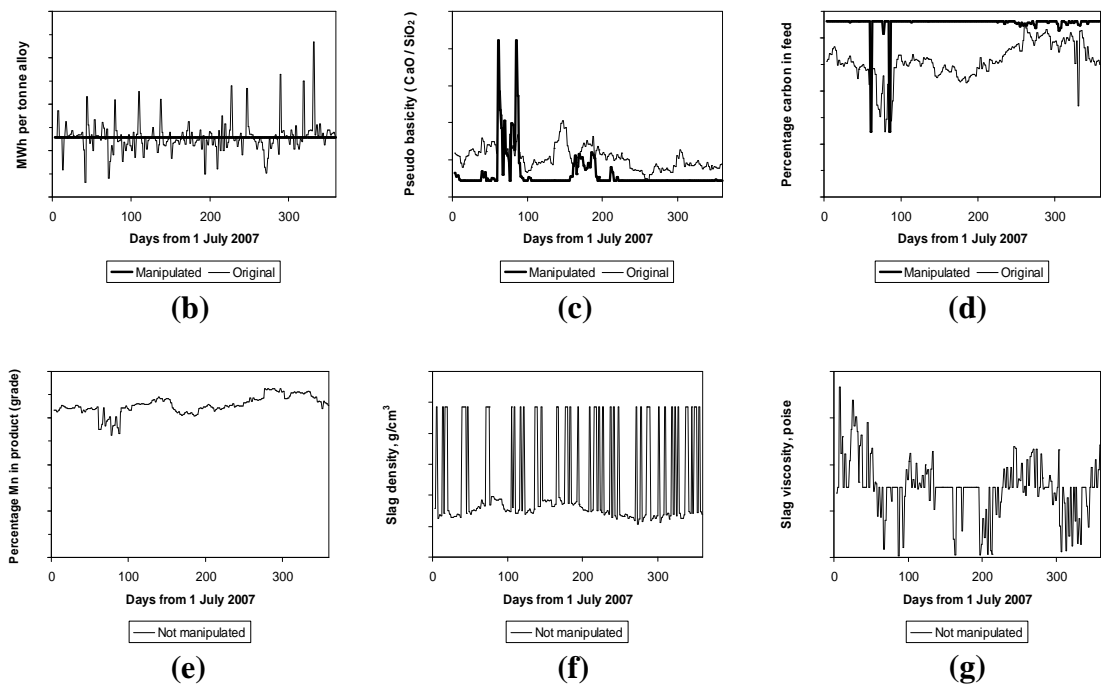


**Figure 35 (a) Performance Indicator 3 – Alloy/Slag ratio  
(b) – (g) Variables affecting Performance Indicator 3, some are non-manipulable  
(Data scaled/removed as per confidentiality agreement)**

With reference to Figure 33(a), it seems that the KPI displayed can be increased by about 7%. Manipulation of the proportions of the feed materials displayed in Figure 33(b) to (n) indicates that certain feed materials are to be fed at their maximum proportions, while others are to be stopped entirely. In Figure 33(o), the feed basicity was increased by about 30%. The corresponding basicity value promotes too high a slag liquidus temperature in the ternary slag phase diagram in section 3.4, and a slag that will be more basic than acidic. The corresponding basicity line would be located nearer to the lower left corner of high basicity than to the upper and more acidic region of desired operation indicated by point X in the ternary phase diagram. The optimised basicity level indicates that a very high slag liquidus temperature will be probable, which will inhibit good slag fluidity and make tapping difficult. It is therefore clear that this optimised basicity level is to be disregarded. Instead, the feed basicity was calculated from the component concentrations of the optimised feed

materials and a basicity value was obtained that would allow the slag to be more acidic than basic. The slag composition will then be closer to the low-liquidus point X in ternary diagram. Note that if the proportion of feed materials cause the basicity value to be too low, then the slag density and viscosity values would be altered undesirably, inhibiting effective slag-alloy separation. Refer to Appendices D and F for details on slag density and viscosity.

In Figure 33(p), the power required per tonne of feed was rightly optimised to slightly lower values (on average), which means that for a given MW power input, a higher throughput of raw materials will be possible. Refer to section 5.2.1 for detail on minimum power requirements.

In Figure 34(a), it can be observed that Mn recovery may be improved by as much as 10%, if the coal/carbon ratio is maximised to the optimum ratio as indicated in Figure 34(c). This is the maximum ratio which occurred from 1 July 2007 to 30 June 2008. It seems that the volatile content of the coal was beneficial for improving and partaking in ore pre-reduction. This maximum amount of coal appears to be anomalous with the result indicated in Figure 34(e), where a maximum carbon input is required for optimised performance. Coke has a fixed carbon content of almost double that of coal, and a compromise therefore exists between maximum inputs of coal and coke. With these optimum results and with the carbon compositions of coal and coke being known, two simultaneous equations were solved to determine the optimum proportions of coal and coke in the feed blend.

Figure 34(b) indicates that low slag basicity improves Mn recovery. This pseudo slag basicity cannot actually be manipulated, but is dependent on the proportions of materials fed to the furnace. The optimum pseudo basicity value does however agree well with the feed basicity calculated for the optimum feed recipe determined in Figure 33.

It has previously been assumed that the electrical variables of the furnace were already set at optimum levels. It was subsequently decided that the measured average

resistance level and measured power usage should be held constant throughout optimisation, hence the straight lines (bold) in Figure 34(d) and (f).

Figure 35(a) indicates an improvement of 18% in the average alloy/slag ratio. As for Figure 34(d), the power usage was again held constant throughout optimisation in Figure 35(b). A minimum pseudo basicity was also found to be beneficial for optimum alloy-slag separation. Again it should be stated that the power usage was held constant throughout optimisation, hence the straight line (bold) in Figure 35(b).

As with Figure 33 and Figure 34, it is notable in Figure 35(d) that alloy-slag separation was optimised at the maximum proportion of carbon in the feed blend. The three non-manipulable variables in Figure 35(e) to (g) are intrinsic to the process and are affected by various variables. In Figure 35(e), the %Mn in the alloy was set to follow the same path as the manipulated %Mn, as large deviations were not expected from the fairly constant %Mn. There may be a chance that the %Mn may be lower than usual if the furnace is tapped more often, i.e. when the power supply is set at the theoretical minimum value. A lower %Mn in the alloy may indicate that the necessary reduction reactions have not been entirely completed. If this happens, then the MWh/t alloy should be raised incrementally until the correct alloy grade is obtained. Slag density and viscosity are also intrinsic to the slag system and were not set to be manipulated. High amounts of variability are observed for slag density and viscosity in Figure 35(f) and (g), because of the variability of the actual proportions of the slag components in the system. Actual proportions instead of modelled proportions of slag components were considered in the determination of slag density and viscosity, since some of the minor slag components were not modelled accurately by FactSage.

Based on the average of the optimised KPI's and manipulated variables over the period of data availability from 1 July 2007 to 30 June 2008, the following table is provided to summarise the most suitable levels of the manipulable variables that would bring about improved performance. New variable setpoints were included in the rightmost column of the table, but have been excluded as per the confidentiality agreement.

**Table 4 Summary of optimised KPI results and associated variable setpoints**  
**(Data removed as per confidentiality agreement)**

VARIABLES AFFECTING KPI's	Units	ORIGINAL SET POINTS	OPTIMUM SET POINTS FOR VARIABLES AFFECTING KPI's			AVERAGE OPTIMUM SP's	BEST SP
			PI 1 - Alloy / Feed	PI 2 - Mn recovery	PI 3 - Alloy / Slag		
Coal	wt %	#	X <sub>1</sub>			X <sub>1</sub>	#
Coke	wt %	#	X <sub>2</sub>			X <sub>2</sub>	#
Quartz	wt %	#	X <sub>3</sub>			X <sub>3</sub>	#
Ore 1	wt %	#	X <sub>4</sub>			X <sub>4</sub>	#
Ore 2	wt %	#	X <sub>5</sub>			X <sub>5</sub>	#
Ore 3	wt %	#	X <sub>6</sub>			X <sub>6</sub>	#
Ore 4	wt %	#	X <sub>7</sub>			X <sub>7</sub>	#
Ore 5	wt %	#	X <sub>8</sub>			X <sub>8</sub>	#
Ore 6	wt %	#	X <sub>9</sub>			X <sub>9</sub>	#
Ore 7	wt %	#	X <sub>10</sub>			X <sub>10</sub>	#
Ore 8	wt %	#	X <sub>11</sub>			X <sub>11</sub>	#
Ore 9	wt %	#	X <sub>12</sub>			X <sub>12</sub>	#
Ore 10	wt %	#	X <sub>13</sub>			X <sub>13</sub>	#
MWh / tonne feed	-	#	X <sub>14</sub>			X <sub>14</sub>	#
Feed basicity	(CaO+MgO)/SiO <sub>2</sub>	#	X <sub>15</sub>			X <sub>15</sub>	#
CaO / SiO <sub>2</sub>	-	#		Y <sub>1</sub>	Z <sub>1</sub>	(Y <sub>1</sub> + Z <sub>1</sub> ) / 2	#
Coal / Coke	-	#		Y <sub>2</sub>		Y <sub>2</sub>	#
Mass % C in feed	%	#		Y <sub>3</sub>	Z <sub>2</sub>	(Y <sub>3</sub> + Z <sub>2</sub> ) / 2	#
Resistance (electrode-to-bath)	mohm	#		Y <sub>4</sub>		Y <sub>4</sub>	#
MWh / tonne alloy	-	#		Y <sub>5</sub>	Z <sub>3</sub>	(Y <sub>5</sub> + Z <sub>3</sub> ) / 2	#
Mass % Mn in product (grade)	%	#			Z <sub>4</sub>	Z <sub>4</sub>	#
Slag density	g/cm <sup>3</sup>	#			Z <sub>5</sub>	Z <sub>5</sub>	#
Slag viscosity	poise	#			Z <sub>6</sub>	Z <sub>6</sub>	#

In this table, optimised setpoints were determined for each of the variables affecting the performance indicators ‘PI 1’ to ‘PI 3’. The greyed out variables are non-manipulable. They are either held constant, such as resistance and MWh/t alloy, or are intrinsic to the system, such as the alloy grade and the density and viscosity of the slag. The average value for each of these optimised setpoints is displayed in the AVERAGE OPTIMUM SP’s column. Red-marked cells indicate which raw material feeds contribute less than 1% to the total materials in the feed blend. Red-marked materials were entirely disregarded in the allocation of final setpoints in the BEST SP column and their flowrates to the process should be stopped entirely. An investigation into why this might occur is discussed later. Contributions of each raw material have been normalised in the rightmost column so that the total sum of the material concentrations add up to 1 (or 100%).

All data in the BEST SP column originate from the setpoints of the previous column, but they are adjusted so that the values of all the interrelated variables agree. The greyed out variables in the last column are directly related KPIs to those (and other) variables marked as green. For instance, the first greyed out variable in the last column is the value for MWh/t feed. It does not have the same value as in the



previous column, because the optimised value was less than the theoretical minimum value. See section 5.2.1. The next greyed cell is the value for the feed basicity. The optimised feed basicity was found to be too high, because the slag liquidus temperature would exceed the furnace equilibrium temperature at this basicity level. The feed basicity value will however depend on the proportions and compositions of each of the best setpoints for each feed material. The same is applicable for the %C in feed. The model predicted correctly that the %C in the feed should be increased for higher proportions of coal and coke in the feed.

As with feed basicity, the slag pseudo basicity will depend on the slag output of the thermodynamic model, which will also be dependent on the proportions of the feed materials. The same applies for the Mn grade of the alloy product, and for the density and viscosity of the product slag. Slag density and viscosity will be affected by the component outputs of the product slag according to the models developed in section 3.5. All manipulable variables were assigned minimum and maximum values based on the minimum and maximum setpoints for each variable over the year for which data was collected.

It should be noted that an increase in the feed basicity brings about process improvement, while a reduction in the pseudo slag basicity is required for optimal performance. Clearly there is disagreement here. Based on the layout of the phase diagram for the oxide components that comprise the slag, it would be best to control the furnace at the lowest possible basicity level, without adversely affecting the best slag density and viscosity levels. It is difficult to estimate the optimum slag viscosity, because the results from the viscosity model may be inaccurate by  $\pm 30\%$ . Slag density values are only inaccurate by  $\pm 7\%$  according to the density models developed. With reference to the density interrelationship graphs in Figure 32, it appears that slag density has an effect on alloy-slag separation (the magnitude of the effect cannot be seen in this figure). The optimised slag density of  $2 \text{ g/cm}^3$  (scaled) may have an advantage over the original slag density of  $3 \text{ g/cm}^3$  (scaled). A lower density value means that the slag contains less of the denser Mn and Fe oxides. Alloy-slag separation may therefore be improved to some extent.

The corrected setpoints (in column BEST SP) produced the best overall performance results for the three KPI's, as can be seen in Table 5 below.

**Table 5 Improvement in KPI outputs after implementation of best variable setpoints**  
(Data removed as per confidentiality agreement)

KPI's	BEST	% IMPROVEMENT
t Alloy per t Feed	#	7
Mn recovery, %	#	10
Alloy/Slag ratio	#	18

From this table, it appears that considerable improvement can be expected if the best optimised setpoints are implemented. The existing setpoints for electrical operation should therefore be maintained while only the power expended per tonne of alloy should be altered (by tapping more regularly) and the proportions of the feed blend modified.

The optimisation results show that certain material feed rates should be discontinued. Further analysis of the feed materials showed that ore materials with the lowest  $\frac{Fe + Mn}{SiO_2}$  ratios corresponded with those which should be discontinued. The discontinuation of certain ore materials may be explained as follows: The requirement for higher amounts of coal and coke in the feed blend (as determined by the optimisation step) will suppress the total amount of ore required in the overall feed blend, and this will then reduce the total concentration of Mn and Fe in the feed blend. Ore materials with the highest Mn and Fe concentrations are therefore required to maintain the correct grade of the high-carbon ferromanganese product. An economic evaluation will indicate whether the discontinuation of certain ore materials measured against the impact of improved furnace performance will be a viable option. An overview of the feed compositions of the different feed materials is illustrated in Figure 36.

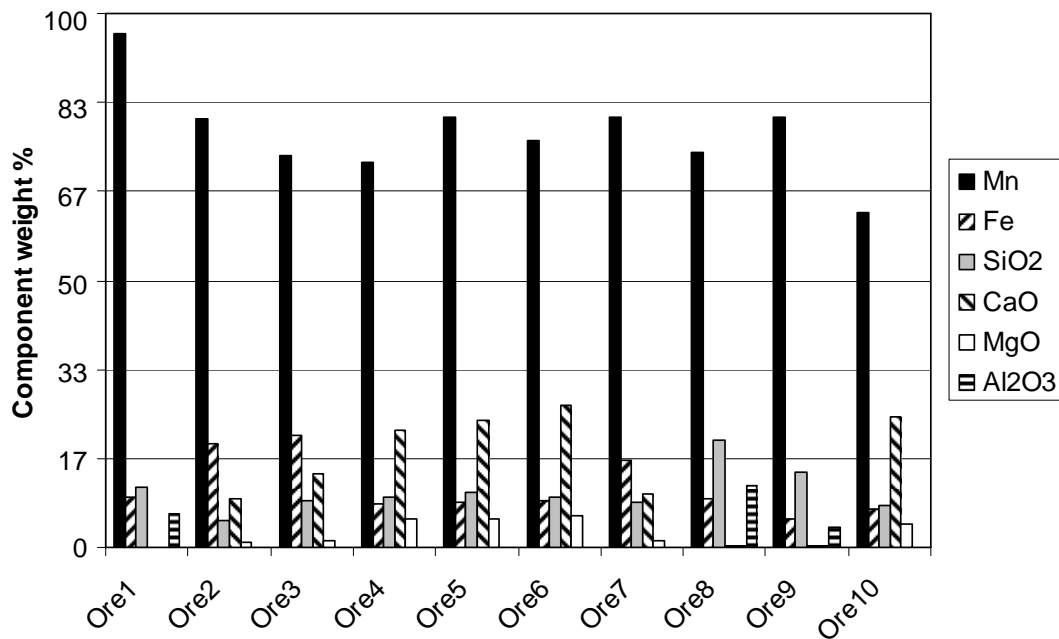


**Figure 36 Composition of ore materials used as inputs to Furnace 2  
(Data scaled as per confidentiality agreement)**

Ore materials with the highest to lowest  $\frac{Fe + Mn}{SiO_2}$  ratio are arranged from left to right along the x-axis. The first five ore materials (Ores 1 to 5) should be continually fed to the furnace to maximise overall performance. Refer to Appendix F for a description of the various raw materials. All the other ore materials impact negatively the tonnes of alloy produced per tonne of feed as their proportions increase in the feed blend. Their usage in the feed blend should therefore be minimised or even discontinued. These results of the optimisation of the feed blend were found to be in accordance with the interrelationship graphs within Figure 30.

## CHAPTER 6

# CONCLUSIONS

It was shown that a hybrid model can be developed for indicating the setpoints of the principal variables that would lead to improved furnace performance in the production of high-carbon ferromanganese. The layout and detail of this hybrid model is proposed in section 4.3.2 of this thesis. Production detail and theoretical concerns pertaining to the processing of high-carbon ferromanganese in submerged-arc furnaces, were discussed (in Chapters 2 and 3) to ascertain which variables are the primal contributors to improved production performance. The modelling intention and the simulation of results are briefly concluded below.

The development of a model that would predict the production output of a furnace ahead of time (using historic data) on a tap-to-tap or day-to-day basis was initially intended. Sampled field data were however not consistently available on a tap-to-tap basis for many of the modelling variables used, but were instead available on a daily basis over the period 1 July 2007 to 30 June 2008. Since the average residence time of the burden movement through the furnace was roughly calculated to be about 1 day, it was found to be inappropriate to construct a day-to-day prediction model, because there would probably be no (or very little) material contained in the furnace from a previous day that would significantly affect the material output on a following day. An alternative approach to the problem was identified in that daily averaged furnace data can be used to (1) construct a model that mirrors or simulates the behaviour of the furnace on a day-to-day basis, and to (2) establish setpoints for variables that would lead to improved production performance. This hybrid design is discussed in Chapter 4.

In the development of the proposed hybrid model, a number of assumptions were made (to facilitate logical and constructive modelling), some of which were simplistic

## *Conclusions*

owing to the complexities and uncertainties of furnace operation. The primary assumptions are summarised in section 4.3.1.

The unique feature of the proposed modelling approach is that a genetic optimisation algorithm was employed to facilitate the iteration of variables across neural network models. This was to obtain optimum variable setpoints (for model inputs) that would contribute to improved measures of furnace performance (model outputs).

Results of model simulation (as summarised in Table 4 of section 5.3.2) indicated that the suggested setpoints (flowrates of feed materials) could raise the amount of alloy produced per tonne of feed by as much as 7%. Also, the percentage of Mn recovered from the feed blend to the alloy product may be improved by 10%, and the alloy:slag ratio may be improved by 18%. It was also determined (through calculation and not by model simulation) that an energy saving of up to 8% can be achieved if an additional alloy (and slag) tap is scheduled for each day without changing the feed recipe or without manipulating the power setpoints. This is analogous to reducing the power usage to the theoretical minimum required. These results may be idealistic, but it nonetheless provides an indication of the expected benefit should the optimum feedrate setpoints be implemented on-site. It should be stated that the accuracy of these results are only as good as the quality of data used and of the assumptions made during model development.

## CHAPTER 7

### RECOMMENDATIONS

All tap-to-tap data should be collected on a consistent tap-to-tap basis to make possible the construction of a useful furnace prediction model.

Principal Component Analysis could be performed on reliable tap data to identify reasons for possible class separation of data.

About one additional tap should be scheduled daily for increasing production (up to 8% improvement), based on the total theoretical minimum amount of energy required per tonne of alloy produced. If this action yields a product of lower than acceptable grade, owing to reactions not running to completion, then the average number of taps per day should be decreased until an acceptable Mn concentration is achieved. A reduction in the product grade may occur if the thermal distribution throughout the furnace burden is poor or if higher than anticipated heat loss occurs. It is not expected that the action of increasing the number of taps should cause the alloy grade to drop, because the minimum theoretical power requirement was calculated to be the worst-case power requirement for heating the molten alloy and slag in the melt to an excessive temperature of 1500 °C instead of to the estimated operating temperature of 1320 °C. This means that a temperature safety margin was included in the determination of the minimum power requirement, and the minimum power requirement affects the number of taps required per day.

Temperature measurement of the furnace materials, perhaps across a range of strategical positions through the furnace burden, would be beneficial for refining the thermodynamic model.

Accurate information explaining the description and details of the electrode hoist positions could not be obtained. It was hoped that electrode hoist position

## *Recommendations*

measurements would reflect the depth of electrode immersion, which in turn would be related to the electrode-to-bath resistance. No correlation was however found between hoist position and resistance. Therefore it remains uncertain if electrode hoist position reflects the level of electrode immersion in the furnace. More reliable data for the measurements of electrode immersion should therefore be acquired.

Heat transfer from produced off-gas to the unreacted burden might be optimised if a beneficial compromise can be made between the interactions of (1) electrode immersion vs. off-gas temperature and of (2) electrode immersion vs. resistance; i.e. a compromise between minimum heat loss (via the release of off-gas) and maximum heat absorption in the burden. No observable relationship between off-gas temperature and resistance was observed to support the understanding of this compromise.

The modelling structure proposed may be subject to further development or improvement owing to the high degree of complexity of the system. Several iteration and calibration steps may be required to accomplish this.

The overall accuracy of the optimised KPI's (key performance indicators) may be improved if a longer time period is specified for every iteration in the optimisation application. This accuracy would be required if the process is to be optimised on a regular basis.

In the proposed hybrid model, the dynamic neural networks may be remodelled with KPI variables that are not interdependent, e.g. the 'coal-coke' ratio and the 'mass percentage of C in feed' variables are interdependent, since a change in the one will affect the other. The 'mass percentage of C in feed' variable, for instance, can therefore be done away with.

Adjustment of the setpoint of a variable affecting more than one KPI should not be done by the calculation of an arithmetic mean for that setpoint value. Rather, the relative contribution of the setpoint values of an adjustable variable on the different KPI outputs should be investigated, enabling the selection of a more sensitive setpoint value.

## REFERENCES

- Barcza, N. A. *Slag-metal equilibrium in the production of low-carbon ferromanganese*. Journal of the South African Institute of Mining and Metallurgy, vol. 79, no. 10, 1979. pp. 269 - 280.
- Barker, I. J.; De Waal, A.; Rennie, M. S. and Klopper, J. *The interaction effect in submerged-arc furnaces*. 49<sup>th</sup> Electric Furnace Conference Proceedings, Iron and Steel Society, 1991. pp. 305 - 310.
- Barker, I. J. and Stewart, A. B. *Inductive reactance, and the operation of large submerged-arc furnaces*. Journal of the South African Institute of Mining and Metallurgy, vol. 80, no. 3, 1980. pp. 123 - 128.
- Benesch, R; Knihnicki, R and Jaworski, M. *Viscosity, density, and surface tension of the calcium oxide + silicon oxide + aluminum oxide + magnesium oxide + manganese(II) oxide blast furnace type slags*. Archiwum Hutnictwa, vol. 29, no. 2, 1984. pp. 277 - 283.
- Channon, W. P. and See, J. B. *The reduction of fluxed and non-fluxed manganese ores by ferromanganese silicide*. Journal of the South African Institute of Mining and Metallurgy, vol. 77, no. 8, 1977. pp. 151 - 162.
- Choudhary, M. and Szekely, J. *Some general characteristics of heat and fluid flow phenomena in electric melting and smelting operations*. Transactions of the Institution of Mining and Metallurgy, Section C: Mineral Processing and Extractive Metallurgy, vol. 90, 1981. pp. 164 - 173.
- De Waal, A.; Barker, I. J.; Rennie, M. S.; Klopper, J. and Groeneveld, B. S. *Electrical factors affecting the economic optimization of submerged-arc furnaces*. Infacon XI: Proceedings of the 6th International Ferroalloys Congress, SAIMM, vol. 1, 1992. pp. 247 - 252.
- Dyason, G. J. and See, J. B. *The movement of the burden in submerged-arc furnaces for the production of high-carbon ferromanganese*. Report - National Institute for Metallurgy (South Africa), no. 1967, 1978. pp. 1 - 35.



## References

- Eksteen, J. J. and Reuter, M. A. *The equilib-ARMAX approach to the dynamic modelling of the melt metallurgy in DC plasma arc smelting operations*. Minerals Engineering, vol. 19, no. 11, 2006. pp. 1174 - 1184.
- Gogiberidze, Yu. M.; Kekelidze, M. A. and Mikiashvili, Sh. M. *Interfacial tension at the boundary between Fe-P alloys and MnO-SiO<sub>2</sub> melts*. Soobshcheniya Akademii Nauk Gruzinskoi SSR, vol. 32, no. 1, 1963. pp. 117 - 124.
- Gray, G. T. *The design and implementation of a microcomputer system for the control of a submerged-arc furnace*. Digital Computer Applications to Process Control, Proceedings of the 6<sup>th</sup> IFAC/IFIP Conference, 1980. pp. 91 - 102.
- Grimsley, W. D.; See, J. B. and King, R. P. *The mechanism and rate of reduction of Mamatwan manganese ore fines by carbon*. Journal of the South African Institute of Mining and Metallurgy, vol. 78, no. 3, 1977. pp. 51 - 62.
- Jiao, Q. and Themelis, N. J. *Correlation of geometric factor for slag resistance electric furnaces*. Metallurgical Transactions B: Process Metallurgy, vol. 22B, no. 2, 1991. pp. 183 - 192.
- Kekelidze, T. M.; Mikiashvili, Sh. M.; Dzhincharadze, T. I. and Khomeriki, R. V. *Density and surface tension of oxide melts of the manganese oxide-calcium oxide-silica and manganese oxide-calcium oxide-silica-alumina systems*. Izvestiya Akademii Nauk Gruzinskoi SSR, Seriya Khimicheskaya, vol. 4, no. 3, 1978. pp. 240 - 244.
- King, P. E. and Nyman, M. D. *Modeling and control of an electric arc furnace using a feedforward artificial neural network*. Journal of Applied Physics, vol. 80, no. 3, 1996. pp. 1872 - 1877.
- Kleyenstüber, A. S. E. *A review of the geology and mining of the Kalahari manganese field*. Journal of the South African Institute of Mining and Metallurgy: Proceedings of the 12th CMMI Congress, 1982. pp. 213 - 220.
- Koursaris, A. and See, J. B. *Reactions in the production of high-carbon ferromanganese from Mamatwan ore*. Journal of the South African Institute of Mining and Metallurgy, vol. 79, no. 6, 1979. pp. 149 - 158.

## References

- Koursaris, A. and See, J. B. *The resistivity of mixtures of Mamatwan manganese ore and reducing agents*. Journal of the South African Institute of Mining and Metallurgy, vol. 80, no. 7, 1980. pp. 229 - 238.
- Lee, H. W.; Teng, Y. J.; Azid, I. A. and Seetharamu, K. N. *Neuro-genetic optimization of micro compact heat exchanger*. International Journal of Numerical Methods for Heat and Fluid Flow, vol. 17, no. 1, 2007. pp. 20 - 33.
- Olsen, S. E.; Tangstad, M. and Lindstad, T. *Production of manganese ferroalloys*. Sintef and Tapir Academic Press, Norway, Trondheim, 2007. pp. 1 - 247.
- Rankin, W. J. and Van Deventer, J. S. J. *The kinetics of the reduction of manganous oxide by graphite*. Journal of the South African Institute of Mining and Metallurgy, vol. 8, no. 7, 1980. pp. 239 - 247.
- Reuter, M. A. and Yang, Y. *Modelling and control of metallurgical reactors*. Delft University of Technology, Department of Applied Earth Sciences, The Netherlands, 2000. pp. 1 - 188.
- Riboud, P. V.; Roux, Y.; Lucas, L. D. and Gaye, H. *Improvement of continuous casting powders*. Fachberichte Huettenpraxis Metallweiterverarbeitung, vol. 19, no. 10, 1981. pp. 859 - 860.
- Samanta, B.; Bandopadhyay, S.; Ganguli, R. and Dutta, S. *A comparative study of the performance of single neural network vs. Adaboost algorithm based combination of multiple neural networks for mineral resource estimation*. Journal of the South African Institute of Mining and Metallurgy, vol. 105, 2005. pp. 237 - 246.
- Segers, L.; Fontana, A. and Winand, R. *Specific density and molar volumes of mixtures of calcium oxide, silicon dioxide and manganese oxide*. Electrochimica Acta, vol. 23, no. 12, 1978. pp. 1275 - 1280.
- Slag Atlas*, Second Edition. Verein Deutscher Eisenhuettenleute, Verlag Stahleisen, Dusseldorf, 1995.
- Smith, M. C. *Manganese Division sampling laboratory: Sampling*. vol. TS 202 WP, 2005. pp. 1 - 17.

## References

- Smith, M. C. *Manganese Division sampling laboratory: Preparations of raw materials, reductants, production samples and final product samples*. vol. TS 203 WP, 2006. pp. 1 - 13.
- Sokolov, V. I.; Popel, S. I. and Esin, O. A. *Density and molar volume of slags*. *Izvestiya Vysshikh Uchebnykh Zavedenii, Chernaya Metallurgiya*, vol. 13, no. 2, 1970. pp. 10 - 15.
- Turkdogan, E. T. and Hancock, R. A. *Equilibrium measurements between carbon-saturated Mn-Fe-Si melts and CaO-Al<sub>2</sub>O<sub>3</sub>-MnO-SiO<sub>2</sub> slags*. National Institute for Metallurgy (South Africa), no. 621, 1958. pp. 573 - 601.
- Urbain, G.; Cambier, F.; Deletter, M. and Anseau, M. R. *Viscosity of silicate melts*. *Transactions and Journal of the British Ceramic Society*, vol. 80, no. 4, 1981. pp. 139 - 141.
- Urquhart, R. C. *The physico-chemical properties of slags associated with the production of high-carbon ferromanganese*. *Canadian Metallurgical Quarterly*, vol. 19, no. 3, 1980. pp. 323 - 327.
- Warren, G. F.; Jochens, P. R. and Howat, D. D. *Liquidus temperatures and activities of manganese (II) oxide in slags associated with the production of high-carbon ferromanganese alloys*. *Proceedings of Infacon 74, the 1<sup>st</sup> International Congress on Ferroalloys*, 1975. pp. 175 - 185.
- Woollacott, L. C. *Viscosities and electrical conductivities of slags associated with the production of high-carbon ferromanganese alloys*. *Proceedings of Infacon 74, the 1<sup>st</sup> International Congress on Ferroalloys*, 1975. pp. 227 - 232.
- Yuan, Z; Sun, M. and Chen, X. *Study of surface tension and density of synthetic slags in the silicon dioxide-ferrous oxide-magnesium oxide-(calcium oxide) system*. *Youse Jinshu*, vol. 40, no. 1, 1988. pp. 58 - 64.

# APPENDICES

## Appendix A *FactSage configuration and factorial design*

### A.1 *Furnace 1*

Prior to any modelling in FactSage, a good understanding of all the possible slag and alloy phase systems are required, because FactSage calculates the relative compositions of slag and alloy phases based on the phase types that are stipulated initially. All possible phases, according to the phase diagrams in Olsen, S. E., *et al.* (2007), were identified for binary phase systems all the way through to the most complex phase systems consisting of five components.

Using the average compositions of slag and alloy for Furnace 1, alloy and slag phases were identified and appear in the FactSage summary in Table 6. The phase systems identified for the molten burden of Furnace 1 were assumed to be equally valid for Furnace 2 or for any furnace producing high-carbon ferromanganese. Slag phases were identified for temperatures varying between 1300 and 1500 °C, and alloy phases were identified for a temperature of about 1400 °C.

It was assumed that all the Mn in the feed sinter and ores was in the oxide form,  $Mn_3O_4$ , because the equilibrium output would be affected by the oxidation state of the Mn in the feed.

An example of the  $3^8$  factorial design with all the input variable combinations for each feed material and the code for setting up the factorial (using 'R' statistical freeware) are given in Table 7 and Table 8. The three feed rate levels, low, medium and high, are represented by the numbers -1, 0 and 1, respectively. The same applies for temperature. These three levels for each input variable and temperature are replaced by the actual high, medium and low values for each variable (see Table 9 and Table 10), as obtained from histogram plots over a specific period of time. See Figure 37 for an example of the histogram plot for Ore 1. Histogram plots for the other variables are not shown.

**Table 6 FactSage configuration for predicting the output composition of high-carbon ferromanganese slag and alloy (Data removed as per confidentiality agreement)**

INPUTS							
Species	Mixtures at 25 °C						
	Ore 1	Ore 2	Ore 3	Coal	Coke	Silica	Fe ore
Mn <sub>3</sub> O <sub>4</sub>	68.88	64.23	75.07				0.15
Fe	5.21	5.57	10.70			95.59	89.05
SiO <sub>2</sub>							
Al <sub>2</sub> O <sub>3</sub>							
P							
MgO							
CaO							
TiO <sub>2</sub>							
H <sub>2</sub> O							
K <sub>2</sub> O							
BaO							
Na <sub>2</sub> O							
Fe <sub>2</sub> O <sub>3</sub>							
S							
C							
CH <sub>4</sub>							
Tot mass %	100	100	100	100	100	100	100
OUTPUTS POSSIBLE							
Pure solids	Gas (ideal)		Solution species		Databases		
C (s)	H <sub>2</sub>		<i>ASlag-liquid</i>		<i>FACT 53</i>		
SiO <sub>2</sub> (all)	O <sub>2</sub>		<i>Aa'Ca<sub>2</sub>SiO<sub>4</sub> slag</i>		<i>FT oxide</i>		
CaSiO <sub>3</sub> (s)	H <sub>2</sub> O		<i>Amonoxide slag</i>		<i>SGTE</i>		
CaSiO <sub>3</sub> (s2)	CO		<i>Liquid (metal)</i>				
Ca <sub>3</sub> MgSi <sub>2</sub> O <sub>8</sub> (s)	CO <sub>2</sub>						
Ca <sub>2</sub> Al <sub>2</sub> SiO <sub>7</sub> (s)	MgO						
Mn (all)	AlO						
Mn <sub>i</sub> C <sub>j</sub> (all)	SiO						
MnAl <sub>2</sub> O <sub>4</sub> (s)	CaO						
Mn <sub>2</sub> Al <sub>4</sub> Si <sub>5</sub> O <sub>18</sub> (s)	Mn						
Mn <sub>3</sub> Al <sub>2</sub> Si <sub>3</sub> O (s)	MnS						
Fe (s)	Fe						
Fe (s2)	FeO						
Fe <sub>3</sub> C (s)							
Fe <sub>3</sub> C (s2)							
FeO (s)							

Table 7 Layout of a 3<sup>8</sup> factorial design

Run	Ore 1	Ore 2	Ore 3	Coal	Coke	Silica	Fe ore	Temp
1	-1	-1	-1	-1	-1	-1	-1	-1
2	0	-1	-1	-1	-1	-1	-1	-1
3	1	-1	-1	-1	-1	-1	-1	-1
4	-1	0	-1	-1	-1	-1	-1	-1
5	0	0	-1	-1	-1	-1	-1	-1
6	1	0	-1	-1	-1	-1	-1	-1
7	-1	1	-1	-1	-1	-1	-1	-1
8	0	1	-1	-1	-1	-1	-1	-1
9	1	1	-1	-1	-1	-1	-1	-1
10	-1	-1	0	-1	-1	-1	-1	-1
11	0	-1	0	-1	-1	-1	-1	-1
12	1	-1	0	-1	-1	-1	-1	-1
↓	↓	↓	↓	↓	↓	↓	↓	↓
6561	1	1	1	1	1	1	1	1

Table 8 R code for a 3<sup>8</sup> factorial grid

```

> A <- rep(c(-1,0,1), 2187)
> B <- rep(rep(c(-1,0,1), each = 3), 729)
> C <- rep(rep(c(-1,0,1), each = 9), 243)
> D <- rep(rep(c(-1,0,1), each = 27), 81)
> E <- rep(rep(c(-1,0,1), each = 81), 27)
> F <- rep(rep(c(-1,0,1), each = 243), 9)
> G <- rep(rep(c(-1,0,1), each = 729), 3)
> H <- rep(c(-1,0,1), each = 2187)
> fact <- cbind(A,B,C,D,E,F,G,H)
> capture.output(fact, file = 'c:/R files/fact.txt')
    
```

Table 9 Example of high, medium and low mass % values for input variables  
(Data removed as per confidentiality agreement)

Variable	Low	Normal	High
Ore 1			
Ore 2			
Ore 3			
Coal	Confidential	Confidential	Confidential
Coke	Confidential	Confidential	Confidential
Silica	Confidential	Confidential	Confidential
Fe ore			
T °C	1300	1450	1550

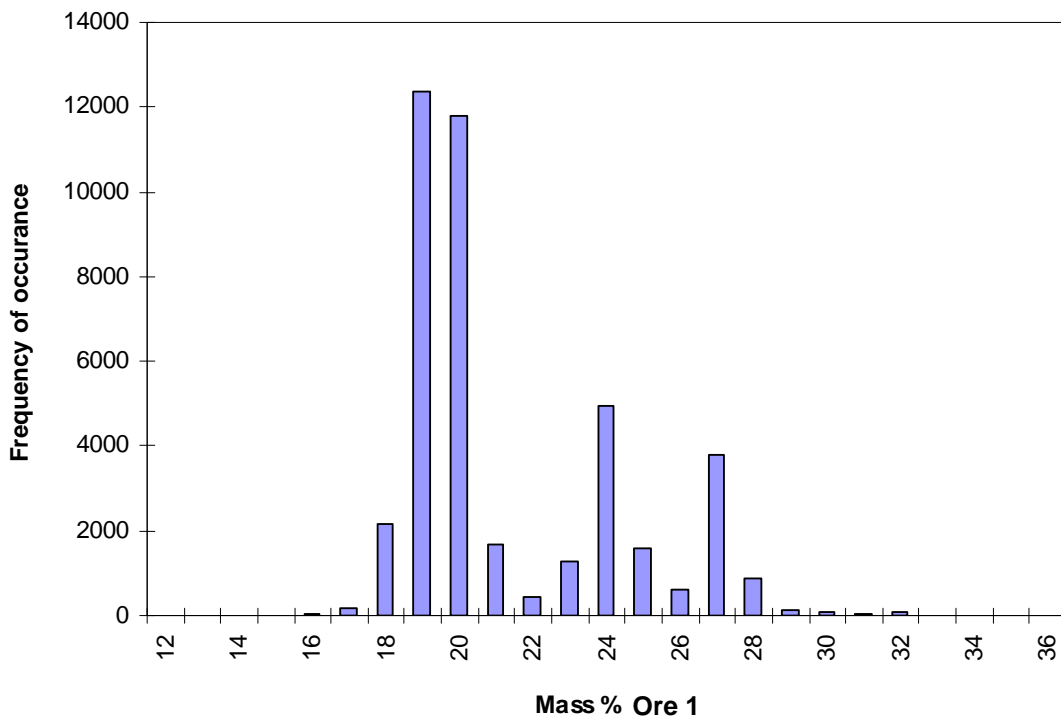


**Figure 37 Frequency distribution for Ore 1 over a period of 2 months**

In Figure 37 above, the high and low mass % of Ore 1 in the feed blend is simply read off where frequency of occurrence of the % of Ore 1 dwindles towards the extremes of the diagram. The occurrence of a percentage of Ore 1 greater than or less than the extreme values will be highly unlikely. A medium value is chosen where the frequency of occurrence is at a maximum, irrespective of the shape of the distribution. The shape of the above histogram appears to be bi-modal, but with the latter assumption, a medium value of 19 mass % Ore 1 is selected. Corresponding high, medium and low values for Figure 37 are indicated in Table 9.

A basis of 100 grams of feed material was set for each of the factorial runs for uniformity of measurement. Adjusting the basis to 100 grams forces the minimum feed rate of a feed material to be higher than is determined when all or many of the other material feed rates are low for a single run. The opposite is true for the maximum feed rate of a material, which appears higher than determined when all or many of the other material feed rates are high for a single run. This adjusted factorial

design was used as input into FactSage. Normalisation of the feed blend to 100 grams per run is shown in Table 10. Pressure is not a specified input variable, but has to be included for input into FactSage. It was set to 1 atm for all the factorial runs.

**Table 10 Adjusting the feed basis to 100 grams for input into FactSage  
(Data removed as per confidentiality agreement)**

(a) Not normalised										
Run	T (°C)	P (atm)	Ore 1	Ore 2	Ore 3	Coal	Coke	Silica	Fe_ore	SUM
1	1300	1								58.8
2	1300	1	Confidential	Confidential	Confidential	Confidential	Confidential	Confidential	Confidential	73.8
3	1300	1	Confidential	Confidential	Confidential	Confidential	Confidential	Confidential	Confidential	88.8
4	1300	1	Confidential	Confidential	Confidential	Confidential	Confidential	Confidential	Confidential	79.8
5	1300	1	Confidential	Confidential	Confidential	Confidential	Confidential	Confidential	Confidential	94.8
6	1300	1	Confidential	Confidential	Confidential	Confidential	Confidential	Confidential	Confidential	109.8

↓

(b) Normalised										
Run	T (°C)	P (atm)	Ore 1	Ore 2	Ore 3	Coal	Coke	Silica	Fe_ore	SUM
1	1300	1								100
2	1300	1	Confidential	Confidential	Confidential	Confidential	Confidential	Confidential	Confidential	100
3	1300	1	Confidential	Confidential	Confidential	Confidential	Confidential	Confidential	Confidential	100
4	1300	1	Confidential	Confidential	Confidential	Confidential	Confidential	Confidential	Confidential	100
5	1300	1	Confidential	Confidential	Confidential	Confidential	Confidential	Confidential	Confidential	100
6	1300	1	Confidential	Confidential	Confidential	Confidential	Confidential	Confidential	Confidential	100

## A.2 Furnace 2

The re-configuration of the FactSage thermochemical modelling for Furnace 2 data remained almost identical as for the Furnace 1 system. These details were therefore not repeated here. Reference can be made to Appendix A.1 for the configuration details of FactSage. It was assumed that all Mn and Fe in the feed sinter and ores was in an oxidic form as stipulated in Appendix E, because the equilibrium output of FactSage would be affected by the oxidation state of all the input components.

An example of the 2<sup>13</sup> factorial design with all the input variable combinations for each feed material and the code for setting up the factorial (using 'R' statistical freeware) are given in Table 11 and Table 12. The two feed rate levels, low and high,



Appendices

are represented by the numbers -1 and 1, respectively. These two levels for each input variable are replaced by the actual low and high values for each variable (see Table 13 and Table 14).

**Table 11 Layout of a 2<sup>13</sup> factorial design**

Run	Quartz	Ore 1	Ore 2	Ore 3	Ore 4	Ore 5	Ore 6	Ore 7	Ore 8	Ore 9	Ore 10	Coal	Coke
1	-1	-1	-1	-1	-1	-1	-1	-1	-1	-1	-1	-1	-1
2	1	-1	-1	-1	-1	-1	-1	-1	-1	-1	-1	-1	-1
3	-1	1	-1	-1	-1	-1	-1	-1	-1	-1	-1	-1	-1
4	1	1	-1	-1	-1	-1	-1	-1	-1	-1	-1	-1	-1
5	-1	-1	1	-1	-1	-1	-1	-1	-1	-1	-1	-1	-1
6	1	-1	1	-1	-1	-1	-1	-1	-1	-1	-1	-1	-1
7	-1	1	1	-1	-1	-1	-1	-1	-1	-1	-1	-1	-1
8	1	1	1	-1	-1	-1	-1	-1	-1	-1	-1	-1	-1
9	-1	-1	-1	1	-1	-1	-1	-1	-1	-1	-1	-1	-1
10	1	-1	-1	1	-1	-1	-1	-1	-1	-1	-1	-1	-1
11	-1	1	-1	1	-1	-1	-1	-1	-1	-1	-1	-1	-1
12	1	1	-1	1	-1	-1	-1	-1	-1	-1	-1	-1	-1
13	-1	-1	1	1	-1	-1	-1	-1	-1	-1	-1	-1	-1
14	1	-1	1	1	-1	-1	-1	-1	-1	-1	-1	-1	-1
15	-1	1	1	1	-1	-1	-1	-1	-1	-1	-1	-1	-1
16	1	1	1	1	-1	-1	-1	-1	-1	-1	-1	-1	-1
↓	↓	↓	↓	↓	↓	↓	↓	↓	↓	↓	↓	↓	↓
8192	1	1	1	1	1	1	1	1	1	1	1	1	1

**Table 12 R code for a 2<sup>13</sup> factorial grid**

```

> A <- rep(rep(c(-1,1), 4096))
> B <- rep(rep(c(-1,1), each = 2), 2048)
> C <- rep(rep(c(-1,1), each = 4), 1024)
> D <- rep(rep(c(-1,1), each = 8), 512)
> E <- rep(rep(c(-1,1), each = 16), 256)
> F <- rep(rep(c(-1,1), each = 32), 128)
> G <- rep(rep(c(-1,1), each = 64), 64)
> H <- rep(rep(c(-1,1), each = 128), 32)
> I <- rep(rep(c(-1,1), each = 256), 16)
> J <- rep(rep(c(-1,1), each = 512), 8)
> K <- rep(rep(c(-1,1), each = 1024), 4)
> L <- rep(rep(c(-1,1), each = 2048), 2)
> M <- rep(rep(c(-1,1), each = 4096))
> fact <- cbind(A,B,C,D,E,F,G,H,I,J,K,L,M)
> capture.output(fact, file = 'c:/R files/fact_2008.txt')

```

**Table 13 Example of high, medium and low mass % values for input variables**  
 (Data removed as per confidentiality agreement)

<b>Variable</b>	<b>High</b>	<b>Normal</b>	<b>Low</b>			
<b>Quartz</b>						
<b>Ore 1</b>						
<b>Ore 2</b>						
<b>Ore 3</b>	Confidential	Confidential	Confidential			
<b>Ore 4</b>						
<b>Ore 5</b>						
<b>Ore 6</b>						
<b>Ore 7</b>						
<b>Ore 8</b>						
<b>Ore 9</b>				19.6	3.8	0.0
<b>Ore 10</b>				13.1	4.6	0.0
<b>Coal</b>						
<b>Coke</b>						

For each run of the 8192 factorial runs ( $2^{13}$ ) for the data from Furnace 2, constituent amounts of each of the thirteen different feed materials were entered into FactSage, using a basis of 100 tonnes of feed material for uniformity of measurement. Adjusting the basis to 100 grams forces the minimum feed rate of a feed material to be higher than is determined when all or many of the other material feed rates are low for a single run. The opposite is true for the maximum feed rate of a material, which appears higher than determined when all or many of the other material feed rates are high for a single run. This adjusted factorial design was used as input into FactSage. Normalisation of the feed blend to 100 grams per run is shown in Table 14. Pressure is not a specified input variable, but has to be included for input into FactSage. It was set to 1 atm for all the factorial runs.

**Table 14 Adjusting the feed basis to 100 grams for input into FactSage  
(Data removed as per confidentiality agreement)**

<b>(a) Not normalised</b>														
Run	Quartz	Ore 1	Ore 2	Ore 3	Ore 4	Ore 5	Ore 6	Ore 7	Ore 8	Ore 9	Ore 10	Coal	Coke	SUM
8185												16.2	10.7	185.5
8186	Confidential	Confidential	Confidential	Confidential	Confidential	Confidential	Confidential	Confidential	Confidential	Confidential	Confidential	16.2	10.7	191.3
8187	Confidential	Confidential	Confidential	Confidential	Confidential	Confidential	Confidential	Confidential	Confidential	Confidential	Confidential	16.2	10.7	193.3
8188	Confidential	Confidential	Confidential	Confidential	Confidential	Confidential	Confidential	Confidential	Confidential	Confidential	Confidential	16.2	10.7	199.1
8189	Confidential	Confidential	Confidential	Confidential	Confidential	Confidential	Confidential	Confidential	Confidential	Confidential	Confidential	16.2	10.7	195.9
8190	Confidential	Confidential	Confidential	Confidential	Confidential	Confidential	Confidential	Confidential	Confidential	Confidential	Confidential	16.2	10.7	201.7
8191	Confidential	Confidential	Confidential	Confidential	Confidential	Confidential	Confidential	Confidential	Confidential	Confidential	Confidential	16.2	10.7	203.7
8192	Confidential	Confidential	Confidential	Confidential	Confidential	Confidential	Confidential	Confidential	Confidential	Confidential	Confidential	16.2	10.7	209.5

↓

<b>(b) Normalised</b>														
Run	Quartz	Ore 1	Ore 2	Ore 3	Ore 4	Ore 5	Ore 6	Ore 7	Ore 8	Ore 9	Ore 10	Coal	Coke	SUM
8185														100.0
8186	Confidential	Confidential	Confidential	Confidential	Confidential	Confidential	Confidential	Confidential	Confidential	Confidential	Confidential	Confidential	Confidential	100.0
8187	Confidential	Confidential	Confidential	Confidential	Confidential	Confidential	Confidential	Confidential	Confidential	Confidential	Confidential	Confidential	Confidential	100.0
8188	Confidential	Confidential	Confidential	Confidential	Confidential	Confidential	Confidential	Confidential	Confidential	Confidential	Confidential	Confidential	Confidential	100.0
8189	Confidential	Confidential	Confidential	Confidential	Confidential	Confidential	Confidential	Confidential	Confidential	Confidential	Confidential	Confidential	Confidential	100.0
8190	Confidential	Confidential	Confidential	Confidential	Confidential	Confidential	Confidential	Confidential	Confidential	Confidential	Confidential	Confidential	Confidential	100.0
8191	Confidential	Confidential	Confidential	Confidential	Confidential	Confidential	Confidential	Confidential	Confidential	Confidential	Confidential	Confidential	Confidential	100.0
8192	Confidential	Confidential	Confidential	Confidential	Confidential	Confidential	Confidential	Confidential	Confidential	Confidential	Confidential	Confidential	Confidential	100.0

## **Appendix B**      *Neural network model development*

The development of a single neural network model including Matlab coding is given below. Snapshots and explanations of neural network modelling in CSense Architect are presented in Appendix F.

The model developed below is for the prediction of the mass of equilibrium elements in high-carbon ferromanganese. The same model can be also be modified slightly for predicting the equilibrium slag species.

Text files containing columns of vectors are uploaded into Matlab:

```
>> load FeedElements.txt;
>> load AlloyElementsOut.txt;
```

The order of the factorial inputs and matching outputs are randomised to ensure that the training, testing and validation data sets represent the entire data set:

```
>> random = rand (6561,1);  
>> combine = [random FeedElements AlloyElementsOut];  
>> sort_combine = sortrows (combine);
```

Input and output vectors are transposed so that they are in a form that is suitable for neural network computation:

```
>> in = transpose (sort_combine (:,2:11));  
>> out = transpose (sort_combine (:,12:14));
```

A principal component analysis is performed to remove redundant vectors that are highly correlated and to reduce the dimension of the input vectors. This technique orthogonalises the input vectors so that they are not correlated with each other. Orthogonalised principal components are then ordered so that those with the largest variation are placed first, and the components that contribute the least variation are eliminated:

```
>> [pn, meanp, stdp, tn, meant, stdt] = prestd (in, out);  
>> [ptrans, transMat] = prepca (pn, 0.02);
```

The first command normalises the input vectors so that they have zero mean and unity variance. The second command eliminates the principal components that contribute less than 2 % to the variation in the data set. The `ptrans` matrix contains the transformed input vectors and the `transMat` matrix contains the principal component transformation matrix that will be used to transform future inputs that are entered into the model into the correct form. Transformed input vectors, `ptrans`, are obtained when normalized input vectors are multiplied by the `transMat` matrix.

Results of the last two commands show that the number of input feed components is reduced by half. This indicates significant redundancy in the data set.

Data is further divided into training, validation and test subsets. Half the data is used for the training set, one fourth for the validation set and another fourth for the test set:

```
>> [R, C] = size (ptrans);  
>> iitst = 2:4:C;  
>> iival = 4:4:C;  
>> iitr = [1:4:C 3:4:C]
```

For `iitst`, the command `2:4:C` means that every 4<sup>th</sup> point is used for the test set, starting at the second point of the vector. All other data will be contained in the validation and training sets.

The network is trained with the training data set, while its performance is measured with the validation data set. Training only stops once a minimum error is reached on the validation data set. This prevents the model from being over-trained. A neural model is only legitimate if the three subsets are statistically similar. Samanta *et al.* (2005)

A two-layer network is selected to approximate the nonlinear behaviour of the data by means of transfer functions. A tan-sigmoid transfer function can be used in the hidden layer, and a linear transfer function in the output layer. A total of three layers will be used to form the structure of the neural network. It was assumed that the use of six nodes in the hidden layer would be adequate, which is roughly half the amount of input variables. A reliable algorithm, the Levenberg-Marquardt 'trainlm', was used for training the neural network. The amount of output nodes are three, one for each main alloy component, Mn, Fe and C.

```
>> net = newff (minmax(ptr), [6 3], ['tansig' 'purelin'], 'trainlm');  
>> [net,tr] = train (net, ptr, ttr, [], [], val, test);
```

The first command establishes the structure and algorithm of the neural network. It also initialises the weights and bias weights. The amount of vector iterations, or

epochs, can also be set to a specific maximum so that overfitting of the model output does not occur. The second command trains the neural net, using the entire data set (training, validation and test vectors).

Linear regression can be used to compare the targets with the corresponding network outputs. The data must first be de-scaled before regression analysis is performed:

```
>> an = sim (net, ptrans);
>> a = poststd (an, meant, stdt);
>> for i = 1:3
>>     figure (i)
>>     [m(i), b(i), r(i)] = postreg (a(i,:), out (i,:));
>> end
```

New data can be simulated with the trained neural network as follows, with `p_new` being the input vector:

```
>> p_new = transpose (newdata);
```

Normalise input data and preprocess with PCA normalisation:

```
>> pnewn = trastd (p_new, meanp , stdp);
>> pnewtrans = trapca (pnewn, transMat);
>> a_newn = sim (net, pnewtrans);
>> a_new = poststd (a_newn, meant, stdt);
```

`a_new` represents the new model outputs. Linear regression can again be reviewed using:

```
>> for i = 1:3
>>     figure (i)
>>     [m(i), b(i), r(i)] = postreg (a_new(i,:), out (i,:));
>> end
```

### Appendix C *Development of a slag density equation*

A density equation was developed through minimisation of the sum of the square of errors; the error being the difference between an actual and predicted density measurement. The interaction effects between the different components of a high-carbon ferromanganese slag system were investigated throughout the systematic development of the density equation. Interaction effects were graphically analysed for the components of the MnO-SiO<sub>2</sub> binary system through to multicomponent systems with components like Al<sub>2</sub>O<sub>3</sub>, FeO, SiO<sub>2</sub>, MnO, MgO and CaO. The minimal influence of temperature on the density of the slag system was also considered in the final model.

In the MnO-SiO<sub>2</sub> slag system, density decreases with increasing concentration of SiO<sub>2</sub>, as in Figure 38 from the experimental results from the Slag Atlas (1995).

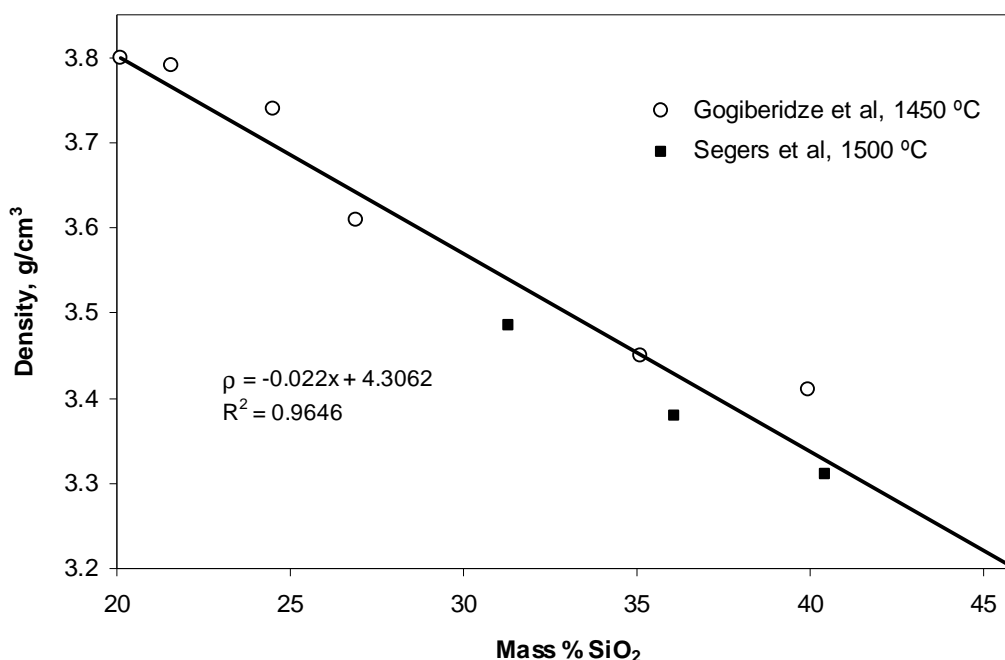
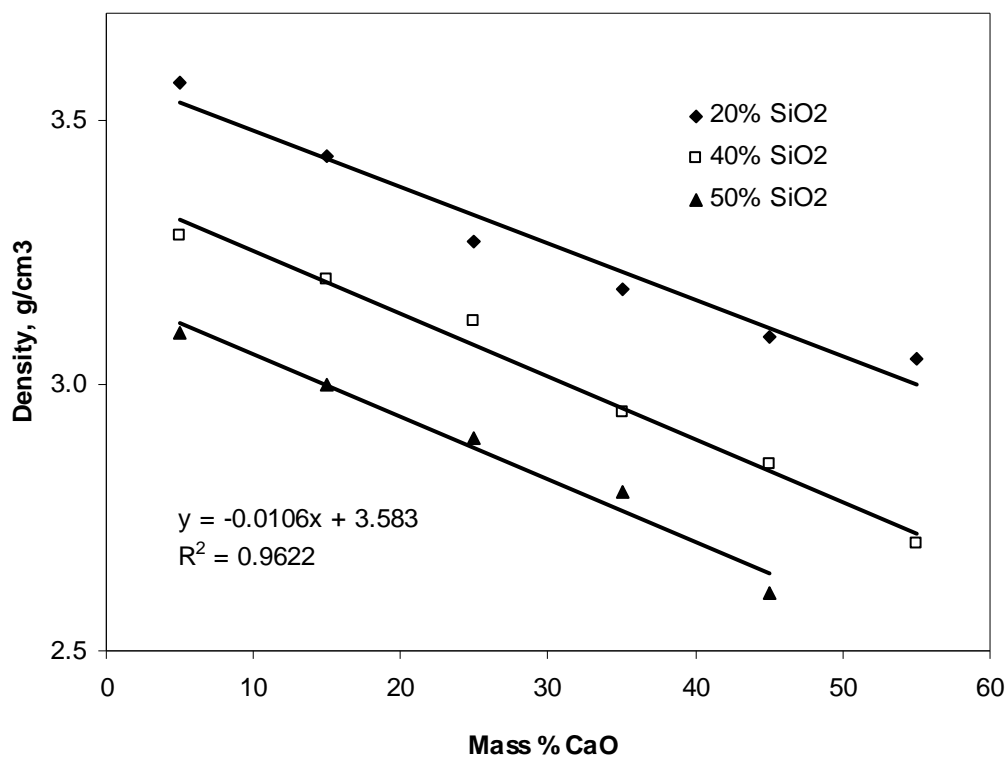


Figure 38 'Effect of SiO<sub>2</sub> concentration on the density of MnO + SiO<sub>2</sub> melts', Slag Atlas (1995)

SiO<sub>2</sub> has the same effect as in Figure 38 for the CaO-MnO-SiO<sub>2</sub> ternary system, but has a less steep gradient of -0.013. Likewise, CaO behaves in the same manner (Figure 39). An increase in MnO concentration, however, has the opposite effect in the same system. See Figure 40.



**Figure 39** Density decreases noticeably with increasing CaO. The same is observed for increasing SiO<sub>2</sub> in the CaO-MnO-SiO<sub>2</sub> system. T = 1500 °C. Measurements cited from Kekelidze *et al.* (1978)



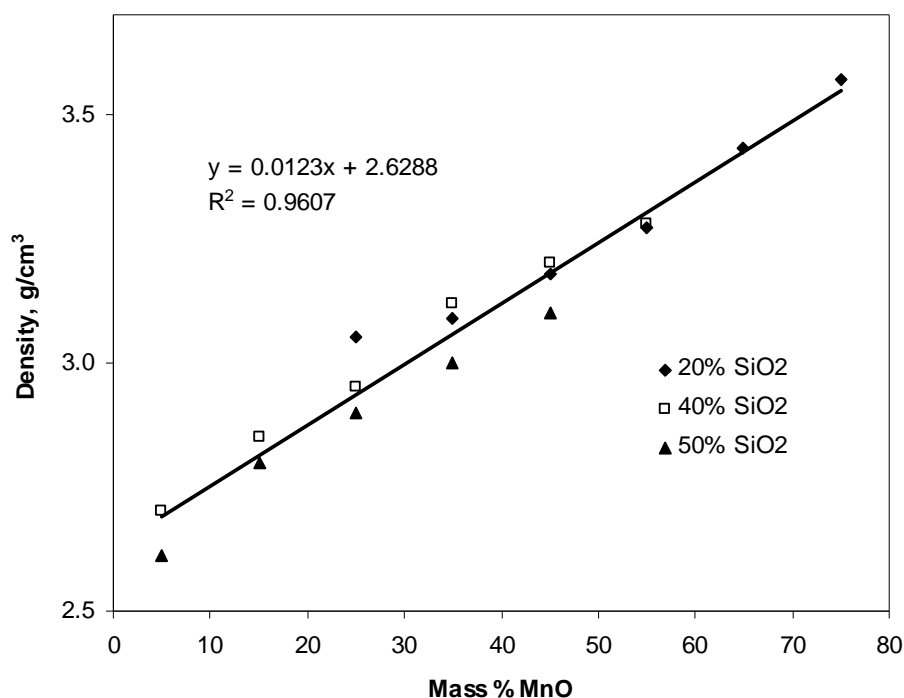


**Figure 40** ‘Density of melts in the system CaO-MnO-SiO<sub>2</sub>, Effects of MnO concentration in slags containing fixed amounts of SiO<sub>2</sub>’, Slag Atlas (1995) T = 1500 °C. Measurements cited from **Kekelidze *et al.* (1978)**

Based on the experimental data supplied in the Slag Atlas (1995) for the ternary system, CaO-MnO-SiO<sub>2</sub>, a well matched equation was developed by adjusting coefficients for each component variable by means of minimising the sum of the square of errors between predicted and actual density measurements:

$$\rho = 3.408 - 0.013(\% SiO_2) + 0.012(\% MnO) - 0.011(\% CaO) \quad [g/cm^3] \quad (8)$$

Equation (8) may be in error by  $\pm 7\%$  and is only applicable within the compositional range for which it was developed:

% SiO<sub>2</sub> : 20 to 50 %

% MnO : 5 to 75 %

% CaO : 5 to 55 %

A similar method to the one used to develop equation (8) was employed to develop a more complex equation that predicts the density of a multicomponent system.

$\text{Al}_2\text{O}_3$  affects the density in MnO melts aggressively for low concentrations of  $\text{Al}_2\text{O}_3$ . This is illustrated in Figure 41, where slag (A) is the most representative of the discard slag of high-carbon ferromanganese production. The decline in density with increasing  $\text{Al}_2\text{O}_3$  concentration was quantified by a straight line drawn for  $\text{Al}_2\text{O}_3$  concentrations less than 5 %. The gradient of this line was used in the final density equation to replicate the effect of  $\text{Al}_2\text{O}_3$  in the system.

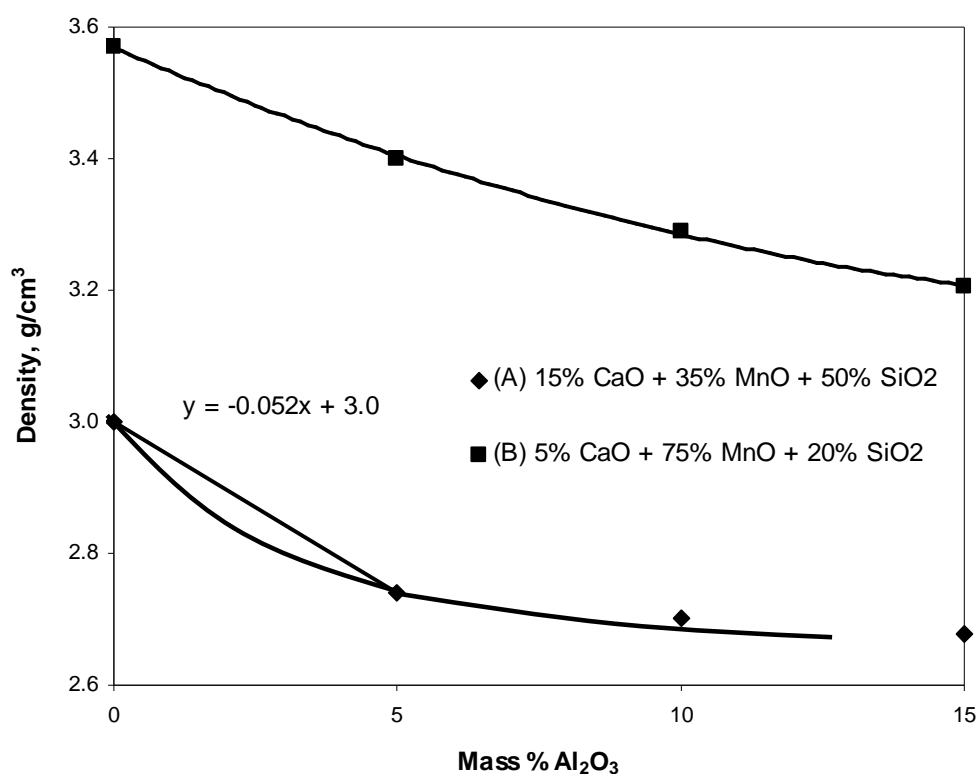


**Figure 41** ‘Effect of  $\text{Al}_2\text{O}_3$  additions on the density of  $\text{CaO} + \text{MnO} + \text{SiO}_2$  melts’, Slag Atlas (1995)  $T = 1500\text{ }^\circ\text{C}$ . Measurements cited from Kekelidze *et al.* (1978)

The effect of MgO on density is presented in Figure 42.

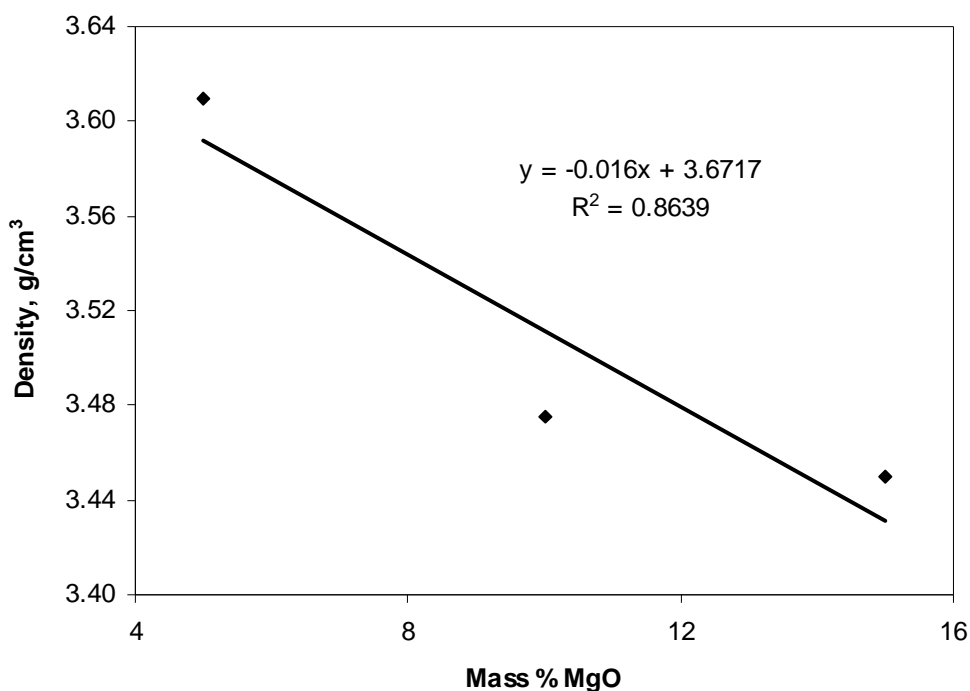


**Figure 42** ‘Effect of MgO concentration on the density of CaO + FeO + MgO + SiO<sub>2</sub> melts which contain SiO<sub>2</sub>’, Slag Atlas (1995) T = 1450 °C. Measurements cited from Yuan *et al.* (1988)

From literature, it is observed that density decreases less aggressively for MgO concentrations greater than 10 %. For practical purposes, the gradient of the regression line passing through all three data points in Figure 42 was assumed to be a reasonable approximation of how density would be affected by low concentrations of MgO.

It was observed in literature that the density-temperature gradient for pure FeO and for Fe<sub>x</sub>O, with a low concentration of Fe<sub>x</sub>O<sub>3</sub>, was very low across the temperature range 1400 to 1550 °C. Also, a maximum density increase or decrease of 2 % may occur across the same temperature range, the gradient depending on the Fe<sub>2</sub>O<sub>3</sub> concentration in Fe<sub>x</sub>O. The presence of Fe<sub>2</sub>O<sub>3</sub> in Fe<sub>x</sub>O causes the density to decrease slightly with a temperature increase, while the density of pure FeO increases slightly

as temperature increases. With this in mind, and with MnO and FeO being chemically similar, it would be reasonable to think that the temperature dependence of the density of MnO or a solution of MnO and FeO would be slight. The density-composition interactions presented in the Slag Atlas (1995), however, indicate that density increases approximately linearly with increasing Fe<sub>x</sub>O concentration for a wide range of multicomponent slags at 1400 °C:

$$\rho = 2.46 + 0.018(\% FeO) \quad [\text{g/cm}^3] \quad (9)$$

This linear approximation was determined to be accurate to within  $\pm 5\%$  of the actual density measurements of multicomponent slags. Even though no MnO was present in the diagram from which equation (9) was derived, it was nonetheless assumed that this equation is also representative of ferromanganese slags on grounds of the atomic similarity between MnO and FeO.

The density values for a multicomponent slag system from the Slag Atlas (1995) that resembled a typical high-carbon ferromanganese slag system most closely was one with the following composition: 4.6% Al<sub>2</sub>O<sub>3</sub> + 18.3% CaO + 35.7% MnO + 9.8% (FeO + Fe<sub>2</sub>O<sub>3</sub>) + 31.7% SiO<sub>2</sub>. The following temperature dependence was observed:

$$\rho = 4.26 - 0.00067T(^{\circ}C) \quad [\text{g/cm}^3] \quad (10)$$

Use of this density-temperature equation rests on the assumption that the iron oxides are representative of the MnO contained in the ferromanganese slag. The density value obtained using equation (10) at the temperature 1400 °C is 3.32 g/cm<sup>3</sup>, which is close the value of 3.4 g/cm<sup>3</sup> at 1400 °C given in Table 8.6 of the Slag Atlas (1995), with the composition: 35.5 % CaO, 19.8 % MnO, 38.4 % SiO<sub>2</sub>, 5.9 % (FeO + Fe<sub>2</sub>O<sub>3</sub>).

The density-composition and density-temperature gradients for each of the slag components above were used to develop a final slag-density prediction equation for a six component slag system. With temperature, the equation has a total of seven

variables. The coefficient values for each variable remain fixed according to the interactional behaviour observed, and a density constant was put in place to be adjusted until the predicted density was as close as possible to the actual density measurements of a specific range of different slag blends. Getting a predicted density value as close as possible to an experimental density was achieved through minimising the sum of the square of density errors for a specific range of different slag blends. Experimental densities for this calculation were sourced from Table 8.6 in the Slag Atlas (1995); some of these data were cited from Sokolov *et al.* (1970). The final density equation has a possible error margin of  $\pm 7\%$  and is given below:

$$\rho = 4.423 - 0.052(\text{wt}\% \text{Al}_2\text{O}_3) + 0.018(\text{wt}\% \text{FeO}) - 0.013(\text{wt}\% \text{SiO}_2) + 0.012(\text{wt}\% \text{MnO}) - 0.016(\text{wt}\% \text{MgO}) - 0.011(\text{wt}\% \text{CaO}) - 0.0007(T, ^\circ\text{C}) [\text{g}/\text{cm}^3] \quad (11)$$

Equation (11) eliminates the need to interpolate on ternary diagrams for obtaining density measurements of multicomponent slag systems. The equation can easily be used as a user defined formula in modelling applications and for calculating densities of most high-carbon ferromanganese slags.

## **Appendix D**      *Furnace mass capacity and burden residence time*

Table 15 illustrates the calculation of the mass capacity of Furnace 2. The calculation was made by first calculating the total burden volume contained in the furnace, based on the physical dimensions of the furnace and the height of stock contained. The volumes of the alloy, slag and penetrating electrodes were calculated and subtracted from the total burden volume to obtain an approximate volume of the solid burden in the upper region of the furnace. The volume of the alloy inventory was based on the probable amount of alloy that can be contained in the hearth of the furnace, and the volume of slag depends on the probable depth of the permanent slag bath. Estimates of the densities of the molten alloy and slag and of the solid burden were subsequently used to calculate the total mass capacity of the furnace.

## Appendices

The average burden residence time was calculated by dividing the total mass capacity of the furnace by the average material throughput. The estimated residence time gives an approximation of the average amount of time that materials could be withheld from being tapped. Long residence times would indicate that the composition of a current melt would greatly influence the chemistry of the materials contained after successive taps in the future. From Table 15, the average furnace residence time was found to be about 0.92 days.

**Table 15 Estimation of the mass capacity of Furnace 2  
(Data removed as per confidentiality agreement)**

<b>FURNACE PARAMETERS</b>	<b>Hearth floor</b>	<b>ORIGIN</b>
Datum level	m	Dyason et al
Inner furnace diameter	m	Dyason et al
Height of assumed stockline	m	Dyason et al
Height of electrode tip	m	Dyason et al
Electrode diameter	m	Dyason et al
<b>LOAD VOLUME</b>		
Approximate load volume	m <sup>3</sup>	Dyason et al
<b>ELECTRODE VOLUME</b>		
Total volume of electrodes (assumed: hemispherical tips)	m <sup>3</sup>	
<b>ALLOY VOLUME</b>		
Assumed alloy density at high temperature	t/m <sup>3</sup>	Dyason et al
Approximate metal inventory in hearth	t	Dyason et al
Total volume of metal inventory contained	m <sup>3</sup>	
<b>SLAG VOLUME</b>		
Estimated slag density at 1500 °C	t/m <sup>3</sup>	Density prediction model
Depth of permanent slag bath	m	Dyason et al
Volume of slag bath	m <sup>3</sup>	Dyason et al
Total slag inventory contained	t	
<b>SOLID VOLUME</b>		
Remaining volume for solid burden	m <sup>3</sup>	
Density of solid burden at 25 °C	t/m <sup>3</sup>	Weighted average
Volumetric % change at 600 °C	%	Coal-coke-ore blend
Assumed volumetric decrease of total raw burden	%	All components
Volume-adjusted density	t/m <sup>3</sup>	
Approximate mass of solid burden in the furnace	t	
<b>TOTAL FURNACE MASS CAPACITY</b>		
Average mass throughput of raw materials to M10 furnace	t/d	Feed data: June 2007 to June 2008
<b>AVERAGE FURNACE RESIDENCE TIME</b>	<b>0.92 days</b>	

## Appendix E Development of a slag viscosity model

The first model investigated for predicting slag viscosity was Urbain's model (Urbain *et al.*, 1981). Urbain identified three types of oxides to be used in the model. These are glass formers, modifiers and amphoteric. The mole fractions of each are calculated below:

$$X_G \text{ (Glass formers)} = X_{SiO_2} + X_{P_2O_5}$$

$$X_M \text{ (Modifiers)} = X_{CaO} + X_{MgO} + X_{MnO} + X_{FeO} + X_{Na_2O} + X_{K_2O} + 3X_{CaF_2} + 1.5X_{FeO_{1.5}} + 2X_{TiO_2} + 2X_{ZrO_2}$$

$$X_A \text{ (Amphoterics)} = X_{Al_2O_3} + X_{B_2O_3}$$

These values are to be normalised so that their sum is unity. Glass former components are those that are acidic and form polymer chains within the slag. Modifiers consist of basic oxides that depolymerise the slag, and amphoteric components are those that act either as an acid or as a base.

In order to predict slag viscosity  $\eta$ , two model parameters,  $A$  and  $B$  are required for substitution into a variation of the Arrhenius equation called the Weimann Frenkel model:

$$\eta = A \cdot T \cdot \exp\left(1000 \frac{B}{T}\right) \quad [\text{poise}] \quad (12)$$

where  $A$  and  $B$  are model parameters, dependent on slag chemistry, and  $T$  is the slag temperature in degrees Kelvin.  $A$  and  $B$  are calculated as follows:

$$A = \exp(-0.2693 B - 11.6725)$$

$$B = B_0 + B_1 X_G + B_2 X_G^2 + B_3 X_G^3$$

$$B_0 = 13.8 + 39.9355 \alpha - 44.049 \alpha^2$$

$$B_1 = 30.481 - 117.1505 \alpha + 139.9978 \alpha^2$$

$$B_2 = -40.9429 + 234.0486 \alpha - 300.04 \alpha^2$$

$$B_3 = 60.7619 - 153.9276 \alpha + 211.1616 \alpha^2$$

$$\alpha = X_M / (X_M + X_A)$$

A viscosity value of 5.88 poise was calculated for a slag system at 1500 °C with the following composition:  $X_{MnO} = 0.223$ ,  $X_{FeO} = 0.001$ ,  $X_{SiO_2} = 0.313$ ,  $X_{CaO} = 0.338$ ,  $X_{MgO} = 0.104$  and  $X_{Al_2O_3} = 0.020$ . For such a system, the slag viscosity should be less than 1 according to experimental measurements. Urbain's model is clearly unsuitable for predicting slag viscosity for the specified slag system.

A simpler and more robust model for determining the viscosity of a high-carbon ferromanganese slag system is the Riboud model (Riboud *et al.*, 1981). In this model, the different slag components are grouped into five oxides, based on the ability of the oxides to form or break polymeric chains in molten slag:

$$X_{SiO_2}^* = X_{SiO_2} + X_{P_2O_5} + X_{TiO_5} + X_{ZrO_2}$$

$$X_{CaO}^* = X_{CaO} + X_{MgO} + X_{FeO} + X_{B_2O_3}$$

$$X_{Al_2O_3}^* = X_{Al_2O_3}$$

$$X_{CaF_2}^* = X_{CaF_2}$$

$$X_{Na_2O}^* = X_{Na_2O} + X_{K_2O}$$

The last two groupings  $X_{CaF_2}$  and  $X_{Na_2O}$  were excluded from the model, as the concentrations of these components are assumed negligible in high-carbon ferromanganese slags. A modification of the Weimann Frenkel equation was used to calculate slag viscosities that are comparable (to some extent) with experimental viscosity measurements:

$$\eta = k \cdot A \cdot T \cdot \exp\left(1000 \frac{B}{T}\right) \quad [\text{poise}] \quad (13)$$

In equation (13),  $k$  is a scaling factor with the value 0.73 and is included to suppress the viscosity of the system. The value of  $k$  was determined through minimising the sum of the squares of the errors between predicted and measured viscosity values for a range of slag compositions.  $A$  and  $B$  are calculated as follows:



$$A = \exp(-17.51 + 1.73 X_{CaO}^* - 33.76 X_{Al_2O_3}^*)$$

$$B = 31.140 - 23.896 X_{CaO}^* + 68.833 X_{Al_2O_3}^*$$

This model is referred to as the modified model of Riboud and it was found to have a possible error margin of  $\pm 30\%$  for viscosity values that are predicted above 1 poise. Predicted data were validated with experimental data from a MnO-SiO<sub>2</sub>-CaO ternary diagram in Olsen *et al.* (2007). Viscosity values of less than 1 poise were predicted for high-carbon ferromanganese slags with SiO<sub>2</sub> concentrations less than 40 wt%. Viscosity values less than 1 poise were not predicted with much accuracy and it is suggested to use a linear equation relating viscosity to SiO<sub>2</sub> concentration when the modified model of Riboud predicts viscosity values less than 1 poise. Only SiO<sub>2</sub> is considered in this instance, because below 40 wt% SiO<sub>2</sub>, viscosity values seem to remain relatively constant for a given SiO<sub>2</sub> concentration irrespective of the concentrations of MnO and CaO in the system. This observation was made from a MnO-SiO<sub>2</sub>-CaO system without taking into account the effects of the minor slag components MgO, FeO and Al<sub>2</sub>O<sub>3</sub>. The linear equation is given below:

$$\eta = 0.09(\%SiO_2) - 2.62, \text{ for } SiO_2 < 40 \text{ wt\%} \quad [\text{poise}] \quad (14)$$

Figure 43, Figure 44 and Figure 45 show the similarity between the nonlinear spread of experimental viscosity measurements and predicted viscosities from the modified model of Riboud. The profiles of Figure 43 and Figure 44 are expected, since addition of SiO<sub>2</sub> promotes polymerisation while MnO depolymerises the oxidic chains within slag. Figure 45 illustrates that CaO affects viscosity in a varied manner. Figure 46 shows the viscosity-temperature relationship for a typical high-carbon ferromanganese slag. The gradient of the curve will vary depending on the relative concentrations of basic and acidic components in the slag. In general, the more basic the slag, the lower is the viscosity value and the lower is the gradient of the viscosity-temperature profile. From Figure 46 it can be observed that the slag viscosity decreases by about 0.6 poise for a 100 °C increase in temperature. This result is

consistent with data for a five component  $\text{Al}_2\text{O}_3\text{-CaO-MgO-MnO-SiO}_2$  system in the Slag Atlas (1995), cited from Benesch *et al.* (1984).

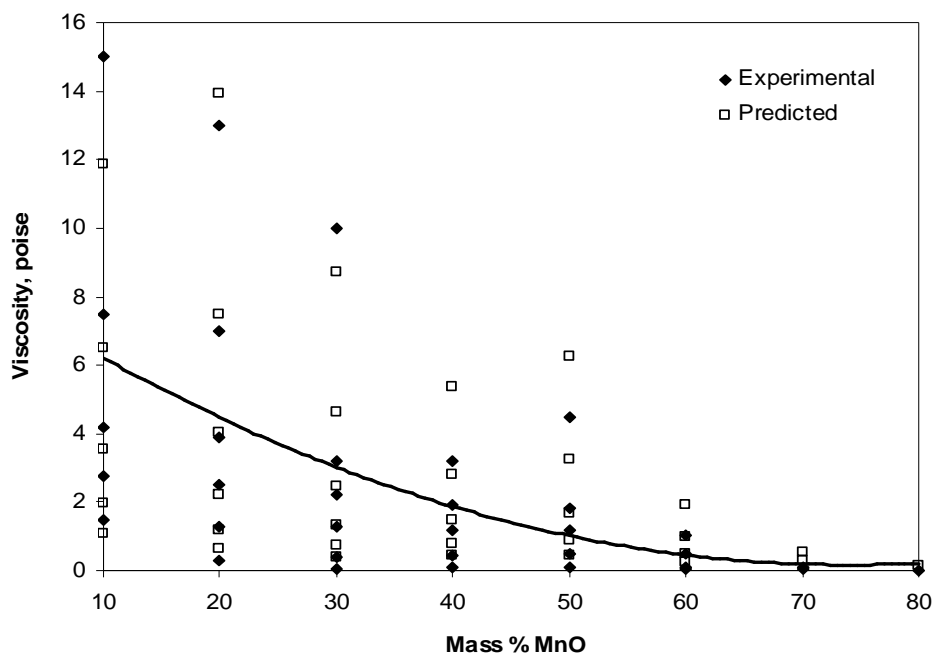


Figure 43 Network breaking effect of MnO on slag viscosity

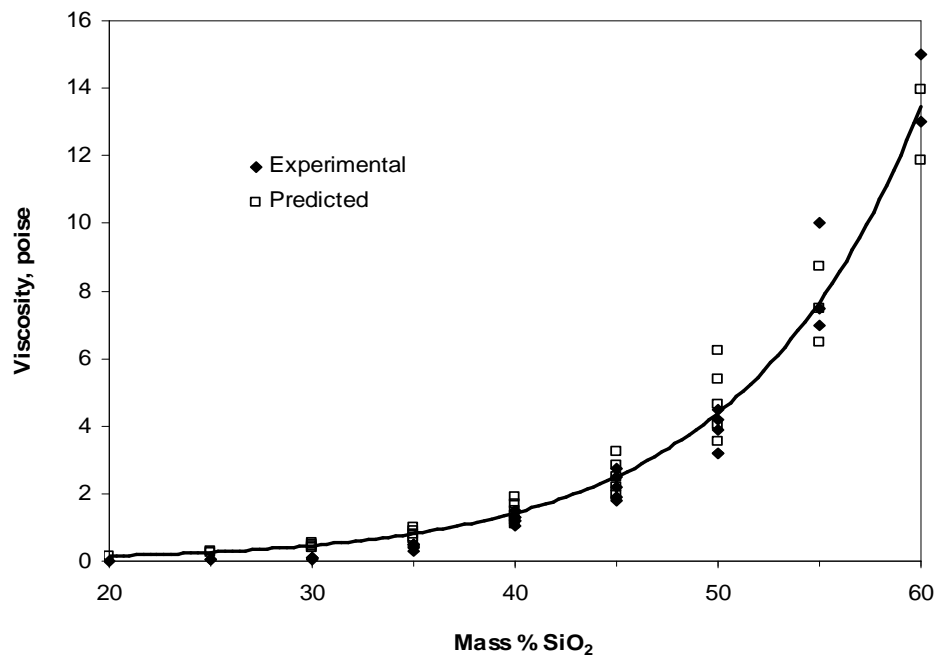


Figure 44 Network forming effect of SiO<sub>2</sub> on slag viscosity

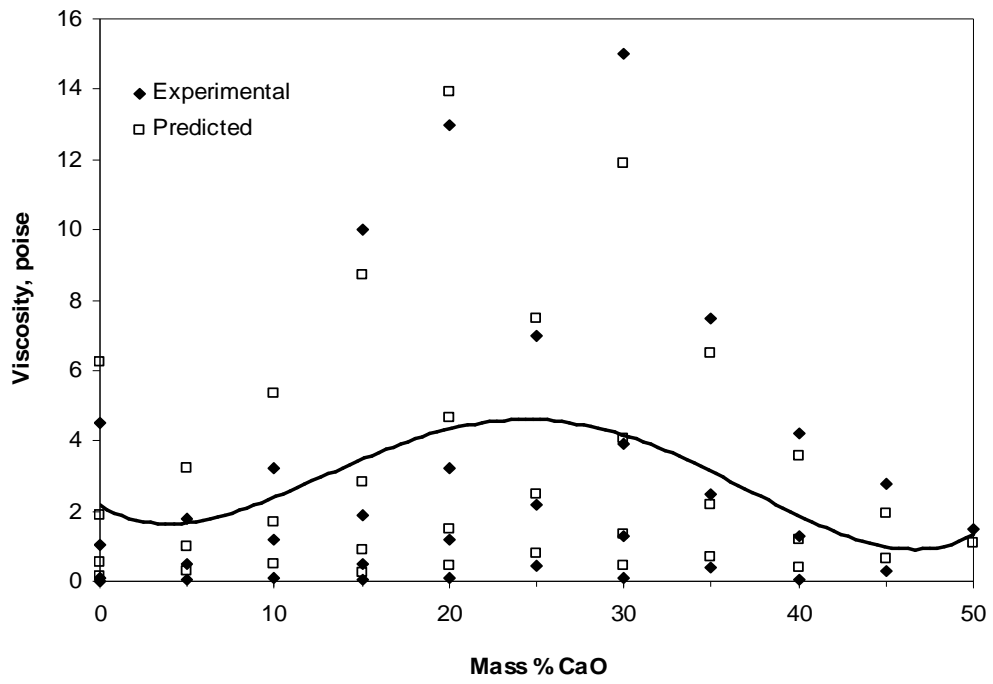


Figure 45 Varied effect of CaO addition on slag viscosity

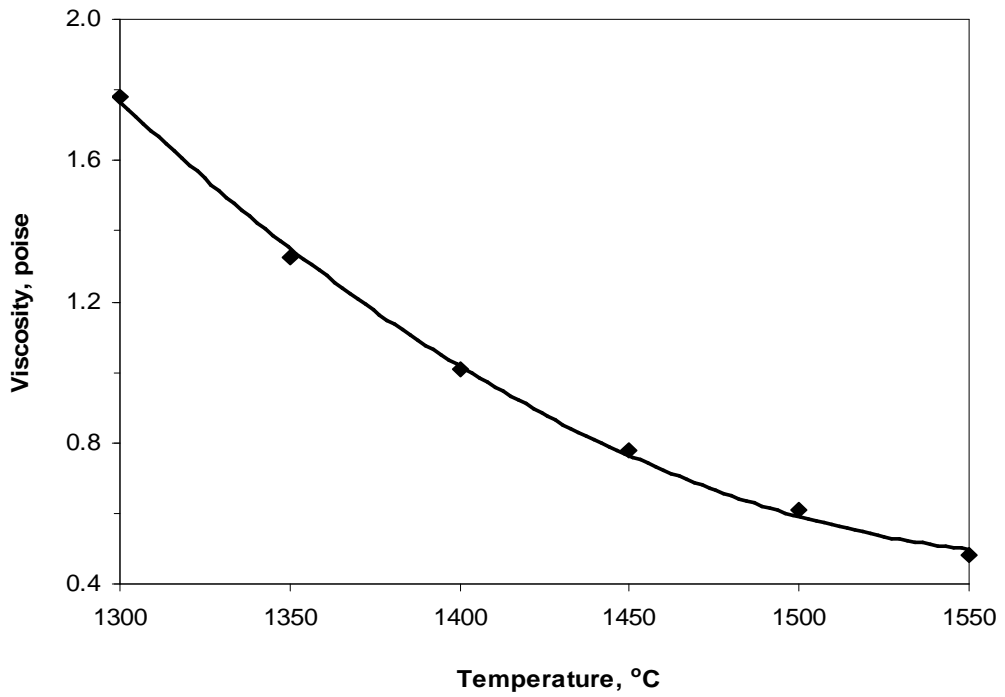


Figure 46 Arrhenius temperature-viscosity profile for typical high-carbon ferromanganese slags

The modified model of Riboud held the same shape as the experimental values given in the ternary diagram of Olsen *et al.* (2007) with the exception that the range of values predicted is excessively high when the concentration of MnO is too high and where the concentration of CaO is too low.

## **Appendix F**      *Feed materials to Furnace 2*

Thirteen feed materials are fed to Furnace 2. Ten of these are different ore materials, rich in manganese oxides, from various manganese mines from the Northern Cape Province in South Africa. Two are reductant materials, containing mainly carbon, for reducing the manganese and iron oxides in the ore materials to manganese metal. The last is quartz, a fluxing agent used for improving the fluidity of the molten burden in order to obtain better alloy-slag separation. Quartz may also be added to increase slag resistivity to allow the electrodes to be penetrated deeper, while maintain a constant electrode-to-bath resistance. Deeper electrodes may prevent excess heat loss from the furnace bed, because hot furnace gases will exchange more heat with the burden over a deeper bed depth. Remelt materials recycled back to the furnace were disregarded, as the combined mass of all remelt materials constituted less than 2% of the total feed blend.

The addition of each material to Furnace 2 from 1 July 2007 to 30 June 2008, is illustrated in Figure 47 to Figure 59 below. The flowrates and compositions of each material have been removed as per the confidentiality agreement. The x-axis indicates the month periods over the time period mentioned above. Only certain materials are continually fed over the entire period, while other are fed intermittently. The unit cost of each ore material, or its availability, may affect when and how frequently it is charged to the furnace. Both reductant materials, coke and coal, were continually fed, because no formation of manganese metal would occur without them. Also, quartz was continually fed, probably to maintain a level of slag acidity for optimum fluidity of the slag. Two ore materials, Ores 6 and 7, were continually charged, probably because they are readily available. It can be noted from the feed profile diagrams for a period of a few days in the 7<sup>th</sup> month of 2007, that no feed materials had been

fed. This may indicate the occurrence of a furnace shutdown for maintenance purposes.

The feed profile in Figure 60 is representative of the total daily amount of all the feed materials combined. Except for some instability in this feed profile from beginning July 2007 to end August 2007, the total daily amount of feed materials remained fairly constant with a moderate level of noise.

In the compositional analyses of the different feed materials in the diagrams below, all the analyses were supplied as metal oxides, except for Mn and Fe. With the acquisition of further information on the most probable oxidic forms of Mn and Fe for each ore-type, the associated mass percentages of the probable Mn and Fe oxides could be calculated from the known concentrations of pure Mn and Fe. This step was necessary because the additional oxygen (of the calculated Mn and Fe oxides) would greatly affect the thermo-chemical calculations performed by FactSage. Obviously the calculated compositions of the oxides of Mn and Fe were used instead of the compositions of pure Mn and Fe in the specification of the FactSage mixtures for each ore material.

Suggestions are made in section 5.3.2, to indicate which of these ore and reductant materials affect alloy production most significantly and to indicate appropriate mass input setpoints of each of these so that that alloy production can be maximised. The average percentage of the total amount of each material consumed over the timescale under investigation is illustrated in Table 16 to indicate which materials were most used. Data has been removed as per the confidentiality agreement.

Appendices

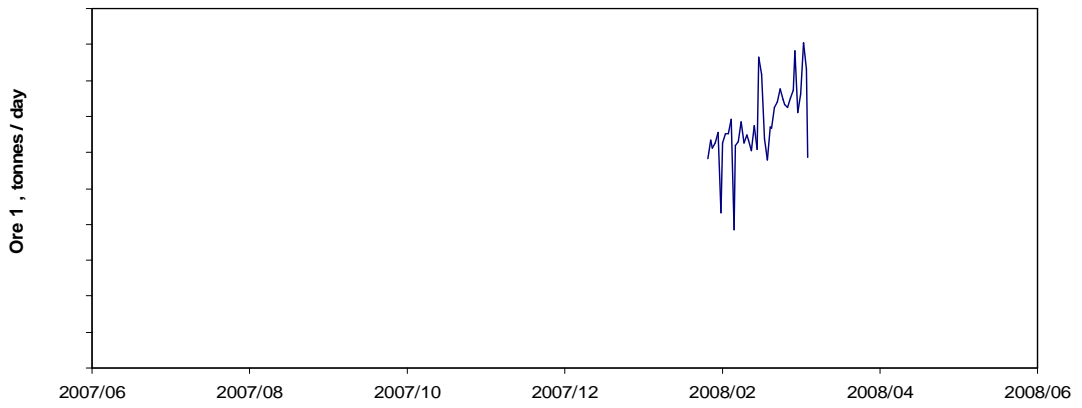


**Figure 47 Feed profile and dry composition of Ore 1 (Data removed)**

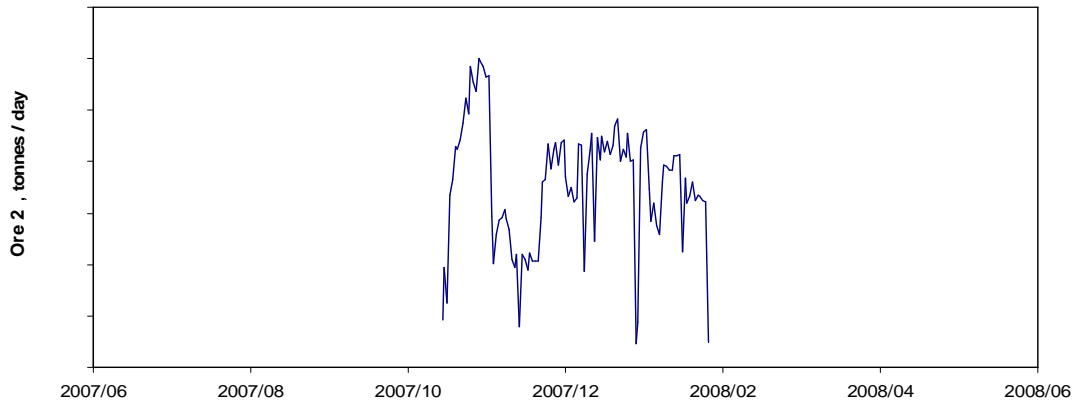


**Figure 48 Feed profile and dry composition of Ore 2 (Data removed)**

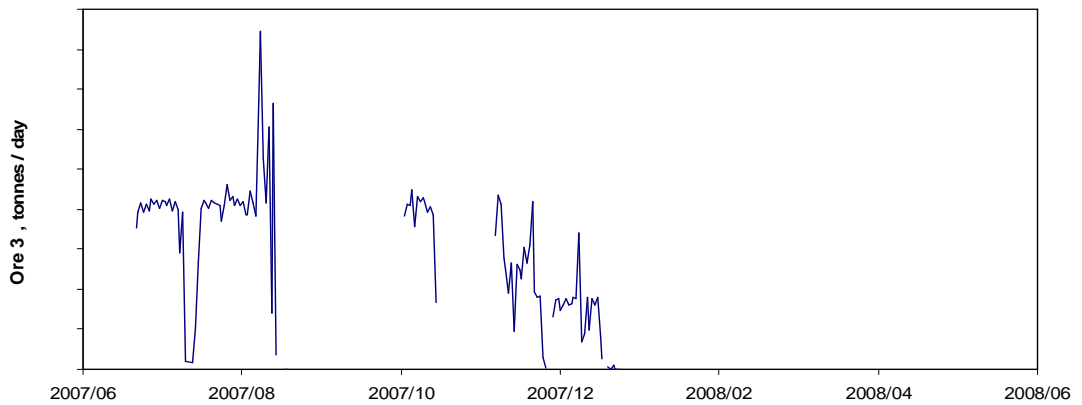


**Figure 49 Feed profile and dry composition of Ore 3 (Data removed)**

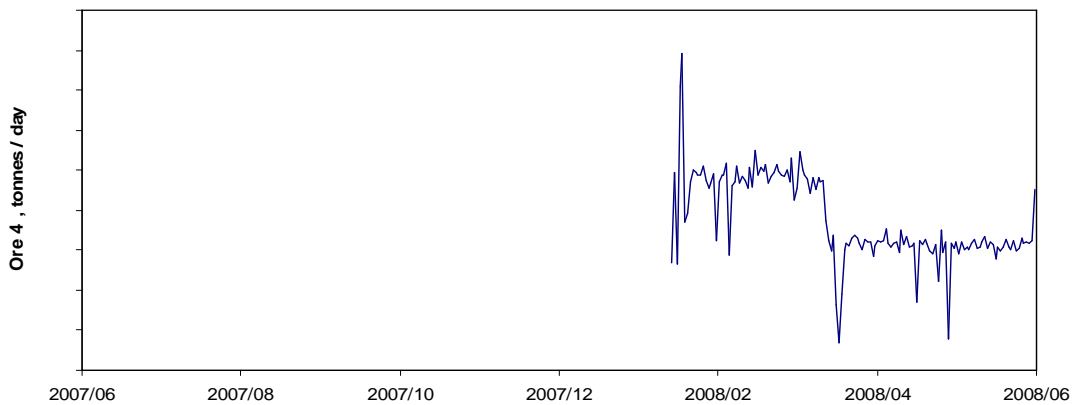


**Figure 50 Feed profile and dry composition of Ore 4 (Data removed)**

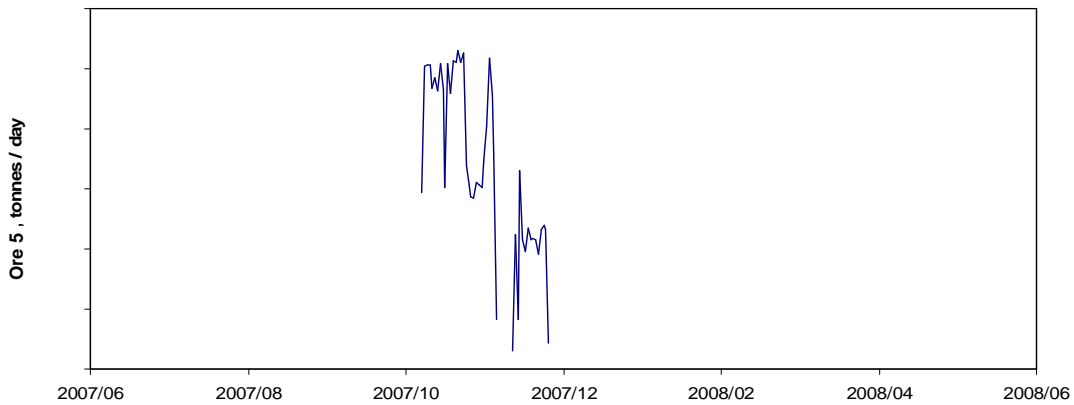


**Figure 51 Feed profile and dry composition of Ore 5 (Data removed)**

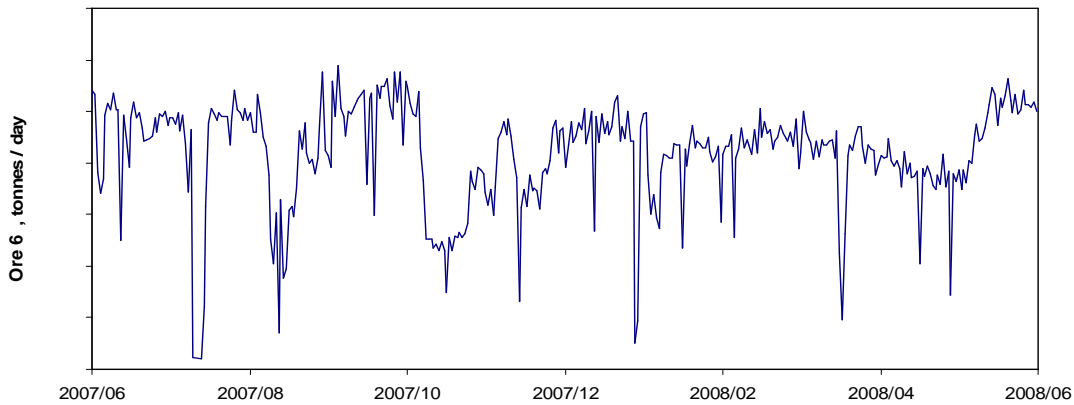


**Figure 52 Feed profile and dry composition of Ore 6 (Data removed)**

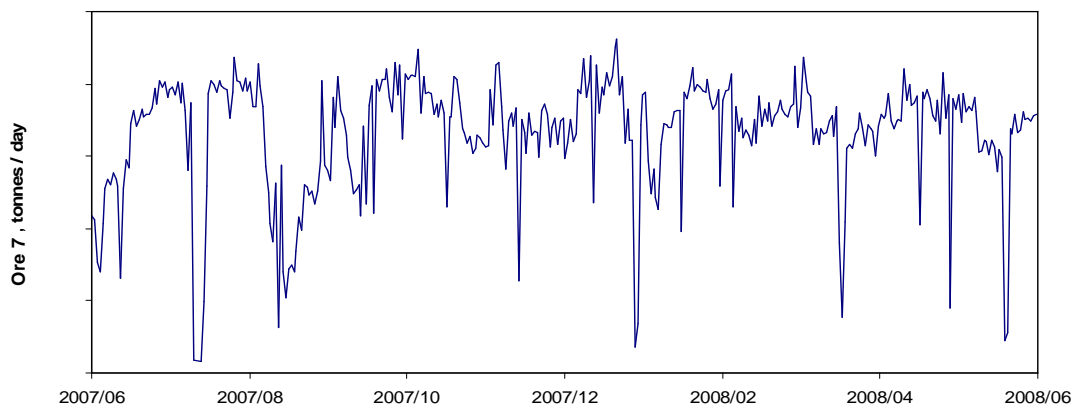


**Figure 53 Feed profile and dry composition of Ore 7 (Data removed)**

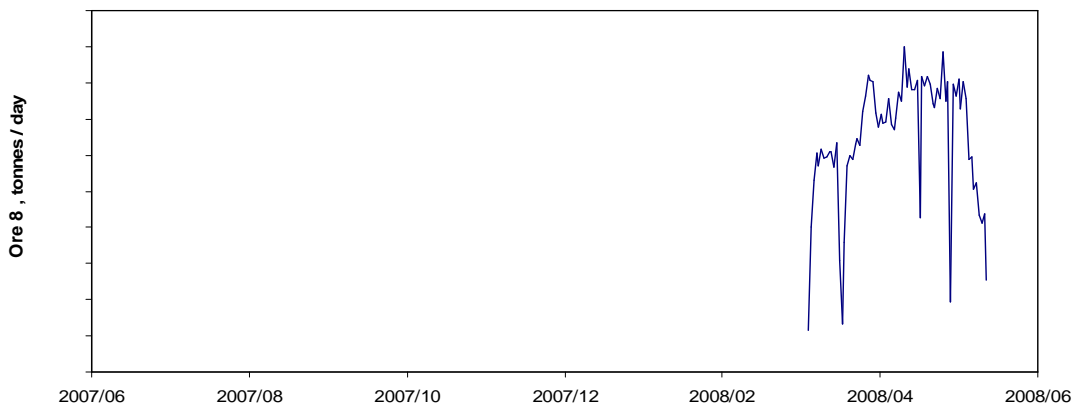


**Figure 54 Feed profile and dry composition of Ore 8 (Data removed)**

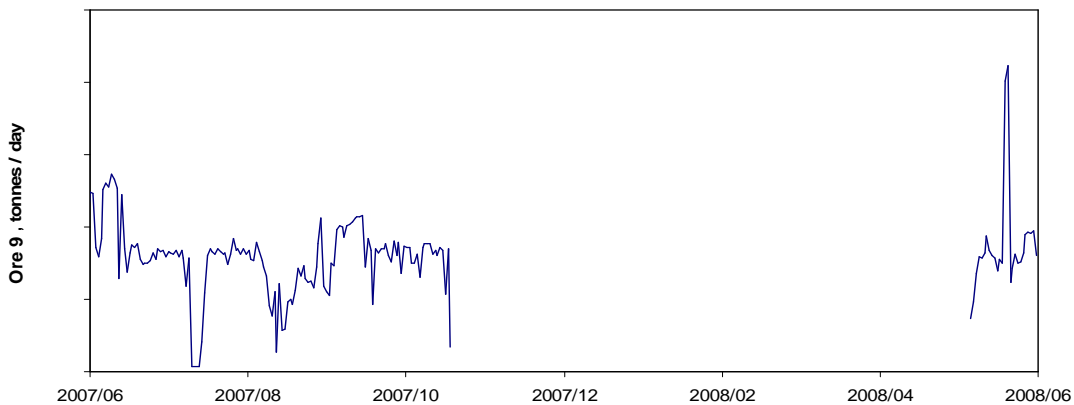


**Figure 55 Feed profile and dry composition of Ore 9 (Data removed)**



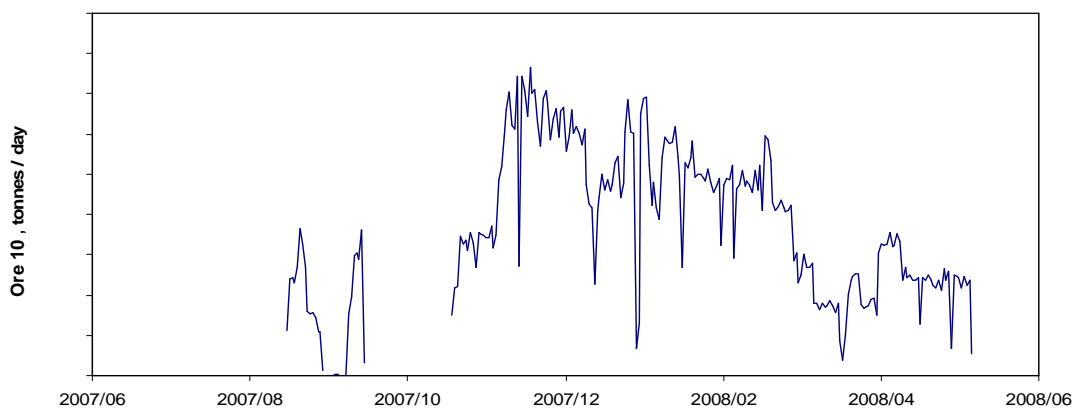


**Figure 56 Feed profile and dry composition of Ore 10 (Data removed)**

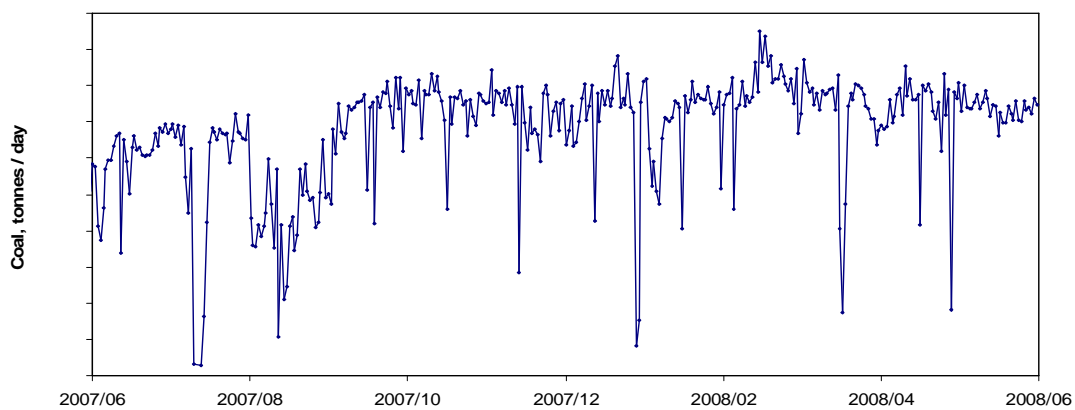


**Figure 57 Feed profile and composition of coal reducing agent (Data removed)**

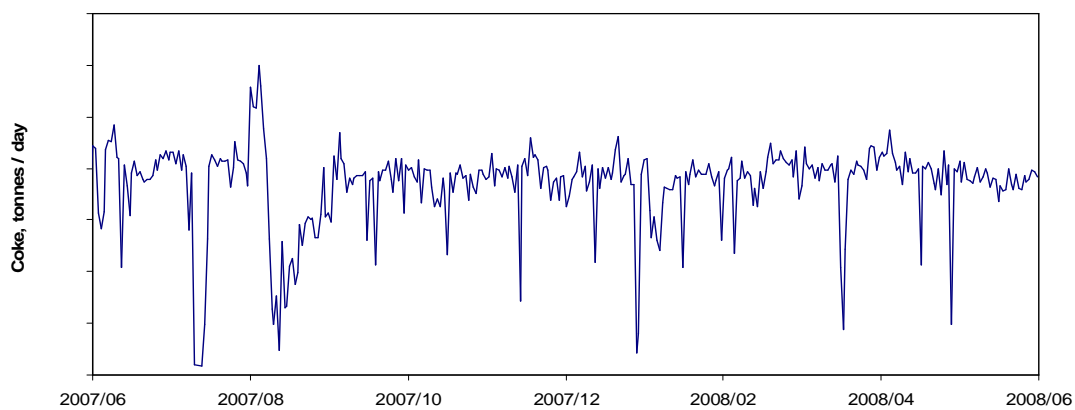


**Figure 58 Feed profile and composition of coke reducing agent (Data removed)**

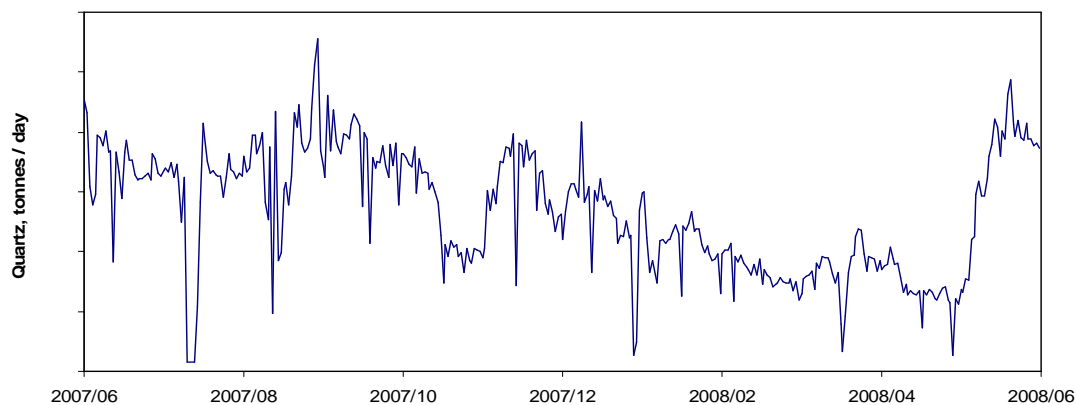


**Figure 59 Feed profile and dry composition of Quartz (Data removed)**

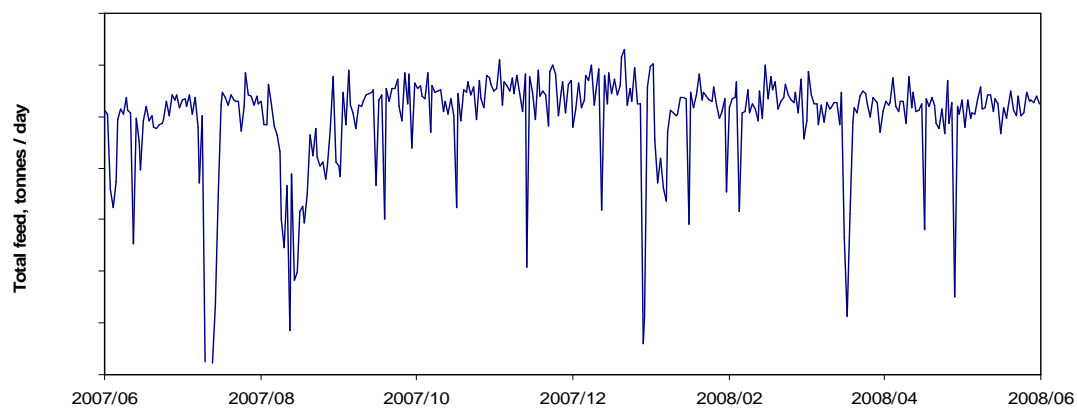


**Figure 60 Feed profile of all materials fed per day (Data removed)**

**Table 16 Average percentage of the total amount of each material consumed  
(Data removed as per confidentiality agreement)**

FEED MATERIAL	Avg % of feed
Quartz	X <sub>1</sub>
Ore 1	X <sub>2</sub>
Ore 2	X <sub>3</sub>
Ore 3	X <sub>4</sub>
Ore 4	X <sub>5</sub>
Ore 5	X <sub>6</sub>
Ore 6	X <sub>7</sub>
Ore 7	X <sub>8</sub>
Ore 8	X <sub>9</sub>
Ore 9	X <sub>10</sub>
Ore 10	X <sub>11</sub>
Coal	X <sub>12</sub>
Coke	X <sub>13</sub>
TOTAL	100

## Appendix G Neural network modelling and optimisation with CSense

### G.1 Thermodynamic modelling

Model training and implementation of the neural network model (or nonlinear model) to process the daily equilibrium output materials from raw material inputs were performed within a 'blueprint' program in the CSense Architect application. See Figure 61. The configuration of each of the numbered blocks contained is discussed.

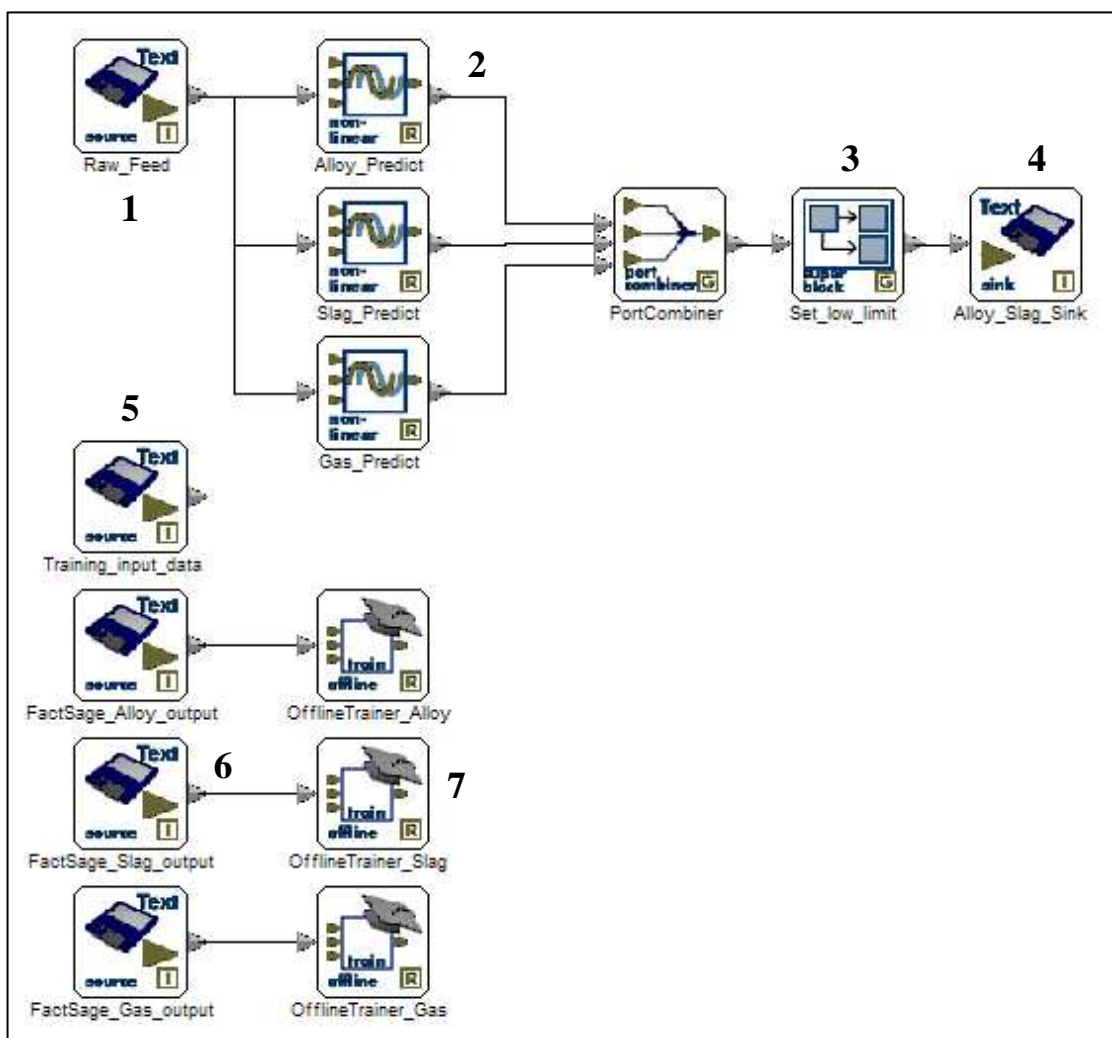


Figure 61 Layout of a thermodynamic model in a CSense blueprint  
(By permission of CSense Systems (Pty) Ltd)

Block1 contains the daily raw material inputs to Furnace 2 over a period of one year. This data is passed to three nonlinear (neural network) modelling blocks, each predicting the approximate equilibrium alloy, slag and gas outputs from the system for the given feed data. An example of the daily material data sourced within block 1 is illustrated in Figure 62, and the statistics of the trained alloy prediction model (block 2) is displayed in Figure 63. Configurations of the other nonlinear models are not illustrated as they are similar to that for alloy prediction.

Day	Material 1	Material 2	Material 3	Material 4	Material 5	Material 6	Material 7	Material 8	Material 9
1	4.44	0.00	0.00	0.00	0.00	0.00	52.89	10.68	0.00
2	4.44	0.00	0.00	0.00	0.00	0.00	52.80	10.59	0.00
3	4.29	0.00	0.00	0.00	0.00	0.00	52.86	10.54	0.00
4	4.28	0.00	0.00	0.00	0.00	0.00	53.09	10.56	0.00
5	4.29	0.00	0.00	0.00	0.00	0.00	52.43	10.82	0.00
6	3.95	0.00	0.00	0.00	0.00	0.00	49.15	13.78	0.00
7	4.00	0.00	0.00	0.00	0.00	0.00	49.95	12.90	0.00
8	3.79	0.00	0.00	0.00	0.00	0.00	50.12	13.00	0.00
9	3.74	0.00	0.00	0.00	0.00	0.00	49.84	12.95	0.00
10	3.73	0.00	0.00	0.00	0.00	0.00	49.94	12.88	0.00
11	3.58	0.00	0.00	0.00	0.00	0.00	49.16	13.10	0.00
12	3.64	0.00	0.00	0.00	0.00	0.00	49.64	12.76	0.00
13	3.60	0.00	0.00	0.00	0.00	0.00	49.35	12.85	0.00
14	3.69	0.00	0.00	0.00	0.00	0.00	49.77	12.91	0.00
15	3.69	0.00	0.00	0.00	0.00	0.00	49.38	16.32	0.00
16	3.66	0.00	0.00	0.00	0.00	0.00	49.40	17.88	0.00
17	3.73	0.00	0.00	0.00	0.00	0.00	49.63	17.57	0.00
18	3.72	0.00	0.00	0.00	0.00	0.00	49.69	17.50	0.00
19	3.59	0.00	0.00	0.00	0.00	0.00	49.70	17.38	0.00
20	3.52	0.00	0.00	0.00	0.00	0.00	49.70	17.49	0.00

Figure 62 Example of the raw material feed data to Furnace 2

(By permission of CSense Systems (Pty) Ltd) (Data removed as per confidentiality agreement)

In the figure above, the first row of data represents the feed proportions of each feed material on the first day of the data set. Only data of some feed materials for the first couple of days are previewed in Figure 62 and the remainder are not visible.

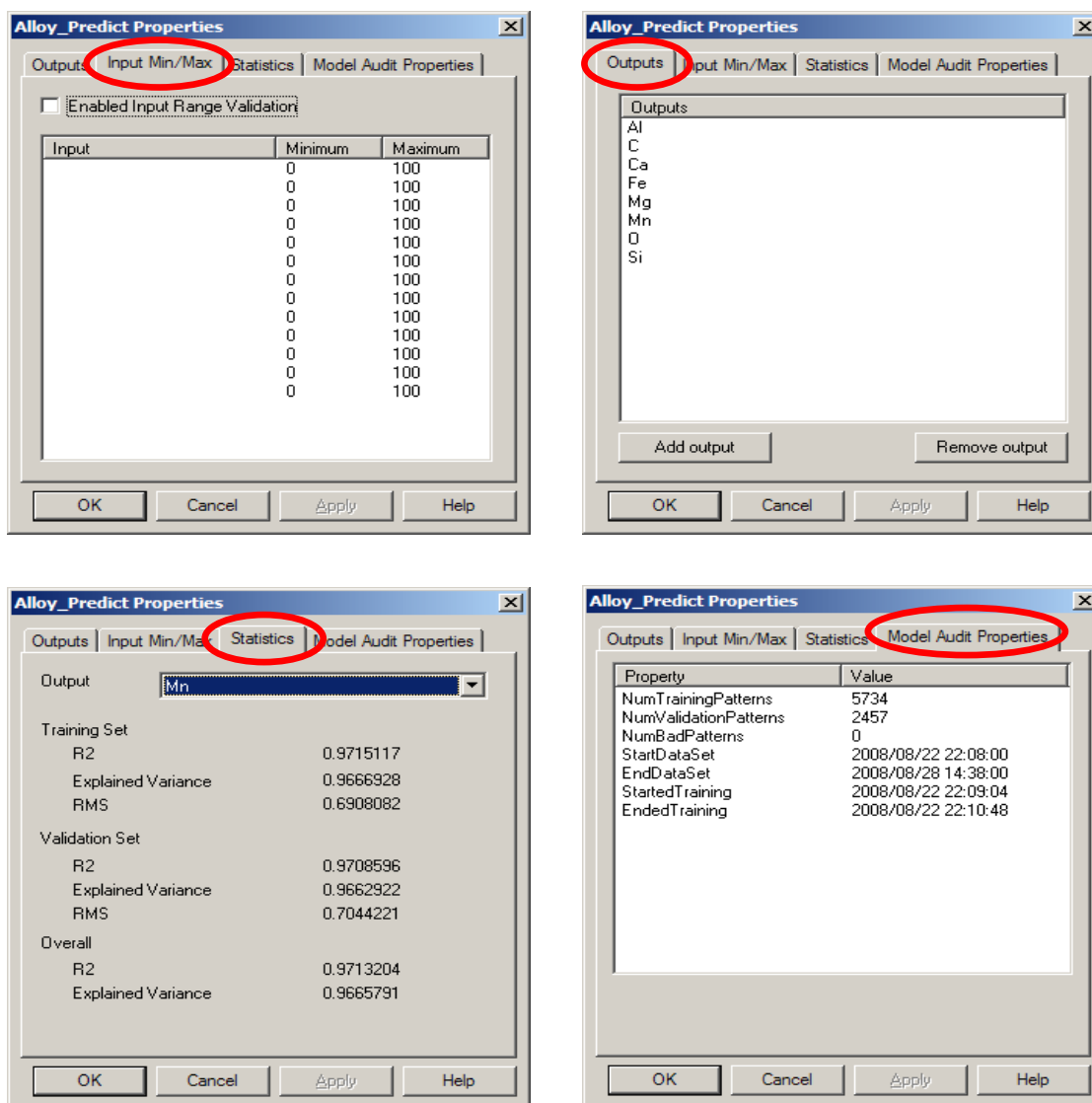


**Figure 63** Statistics of the nonlinear model used for predicting the alloy output of Furnace 2  
 (By permission of CSense Systems (Pty) Ltd) (Data removed as per confidentiality agreement)

The four windows in Figure 63 show the range of allowable compositions of each raw material in the feed blend. Note that any combination of feed materials is allowed (0% to 100% for each). Predicted alloy outputs are shown and the statistics for each alloy component can be listed. Only the model statistics are indicated for Mn. Note that the Mn output is well predicted with an overall  $R^2$  of 0.97. A summary of the amount of data sets trained and validated is also displayed. Note that 30% of the complete dataset is used for validation of the training data set (2457 validation patterns and 5734 training patterns).

Adjustments to the model outputs were performed within block 3 in Figure 61. The contents of block 3 are shown below in Figure 64 and the functions of each the sub-blocks are explained.

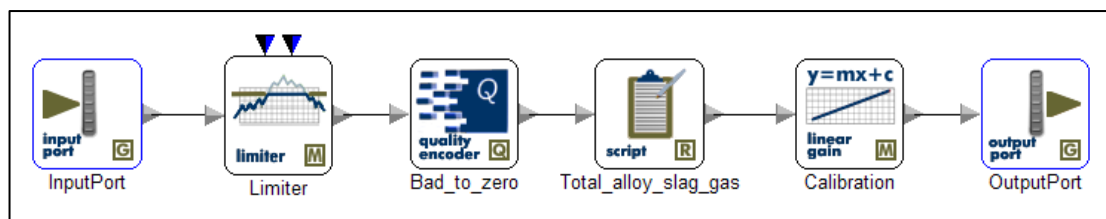


**Figure 64 Adjustment blocks to manipulate modelled outputs**  
(By permission of CSense Systems (Pty) Ltd)

It was found that many of the output components were predicted with insignificantly small mass values below 0.001 tonnes. It was therefore decided that component outputs with values less than this value should be truncated (clipped) to zero. This was performed in the ‘Limiter’ and ‘Bad\_to\_zero’ blocks in Figure 64. Truncation to zero also allowed for easier data cleaning of the output data set. Any value which had been clipped to 0.001 tonnes in the ‘Limiter’ block was assigned with a bad quality, which may have prevented this data from being processed further. To avoid this, the quality encoder block, ‘Bad\_to\_zero’, was used set all data quality to good. The configuration of the ‘Limiter’ and ‘Bad\_to\_zero’ script blocks are displayed in Figure 65 and Figure 66. A script block, ‘Total\_alloy\_slag\_gas’, was employed to calculate the total amounts of slag, alloy and gas from the masses of the components in each of these three phases. See Figure 67. Some component outputs were predicted with reasonable accuracy but may have displayed a slight positive or negative bias shift. A linear gain was applied to components of interest in the ‘Calibration’ block to correct for this shift. This correction is referred to as ‘calibration’ in Chapter 5. Configuration of this block can be seen in Figure 68.

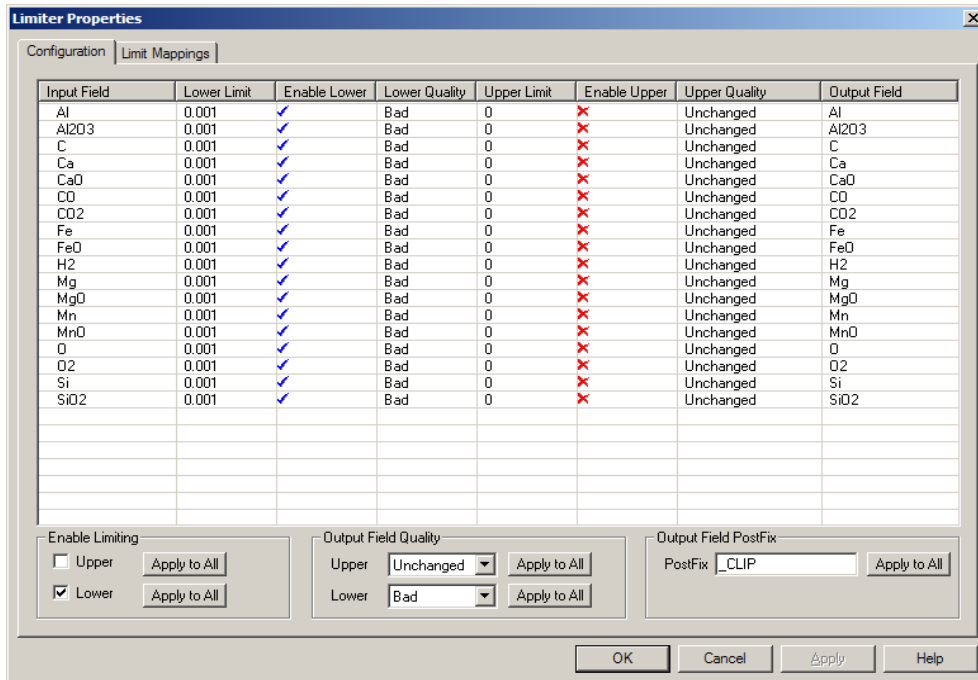


Figure 65 Configuration of the Limiter block to set/clip a low limit of 0.001 tonnes (By permission of CSense Systems (Pty) Ltd)

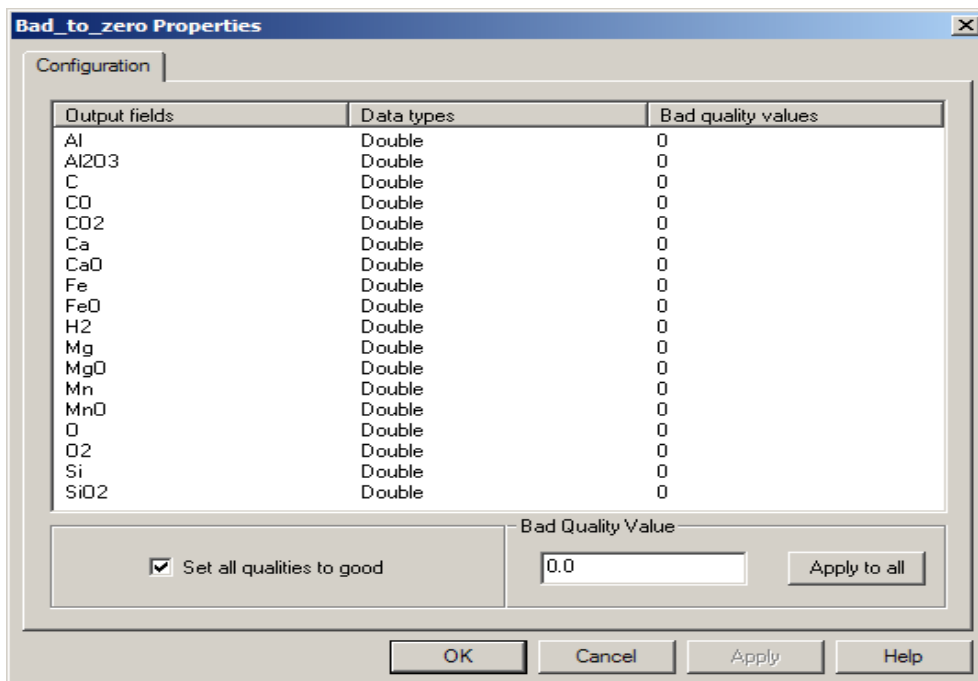
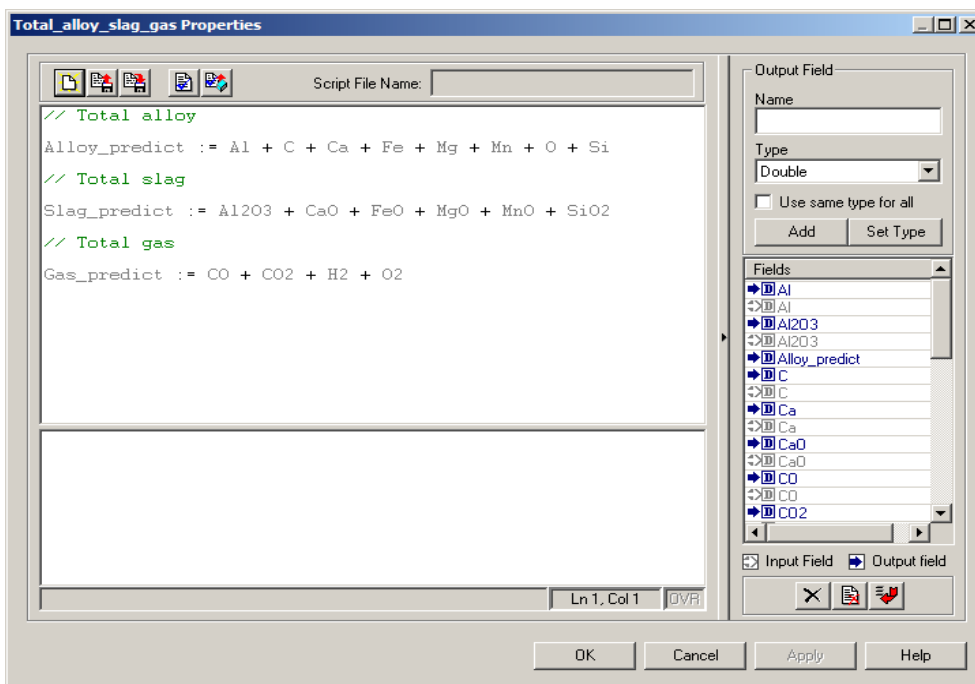
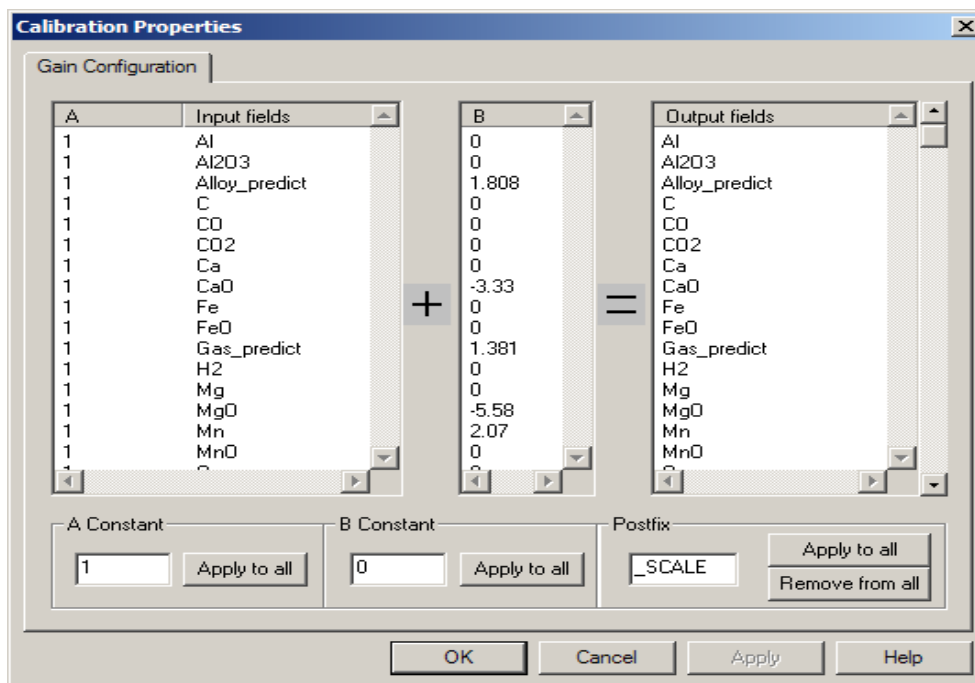


Figure 66 Configuration of the 'Bad\_to\_zero' quality encoder block which assigns good qualities to clipped data (By permission of CSense Systems (Pty) Ltd)



**Figure 67 Calculation of total alloy, slag and gas**  
 (By permission of CSense Systems (Pty) Ltd)



**Figure 68 Assigning linear gain to selected output variables**  
 (By permission of CSense Systems (Pty) Ltd)



Adjusted and calibrated model outputs exit the blueprint through block 4 in Figure 61. The contents of this block are indicated in Figure 69.

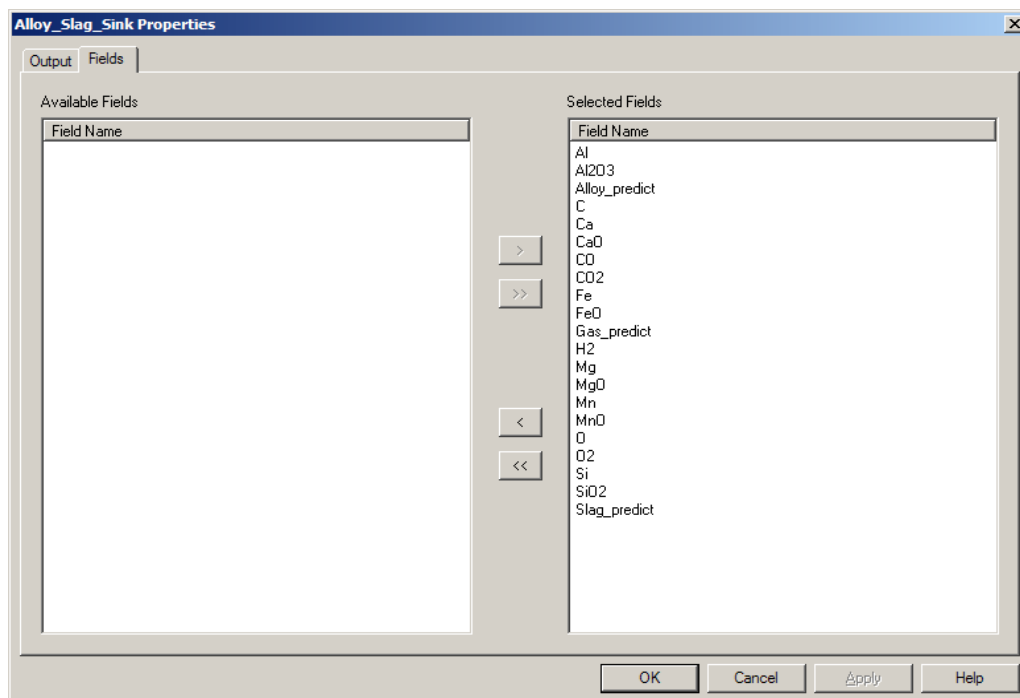


**Figure 69 Adjusted and calibrated variables exiting the thermodynamic model**  
(By permission of CSense Systems (Pty) Ltd)

The statistics of a trained model block has already been illustrated. The training of this block, prior to use, is discussed in this paragraph. Only the method used to train the slag prediction model is discussed, since the alloy and gas prediction models are similar. In Figure 61, blocks 5, 6 and 7 were used to train the slag prediction model, 'Slag\_Predict'. The first step was to temporarily connect the  $2^{13}$  rows of input data for each raw material from block 5 to the 'Slag\_Predict' model block (see Figure 70 for a preview). The FactSage-modelled outputs for each of the  $2^{13}$  runs were sourced within block 6 (see Figure 71 for a preview) and were passed to an offline trainer (block 7). The configuration of the 'Offline\_Trainer\_Slag' block is displayed in Figure 72. The train button is used to initiate model construction and training, and the effects of this action are saved in the 'Slag\_Predict' modelling block. The block can subsequently be used to process outputs for any blend of the incoming feed materials.

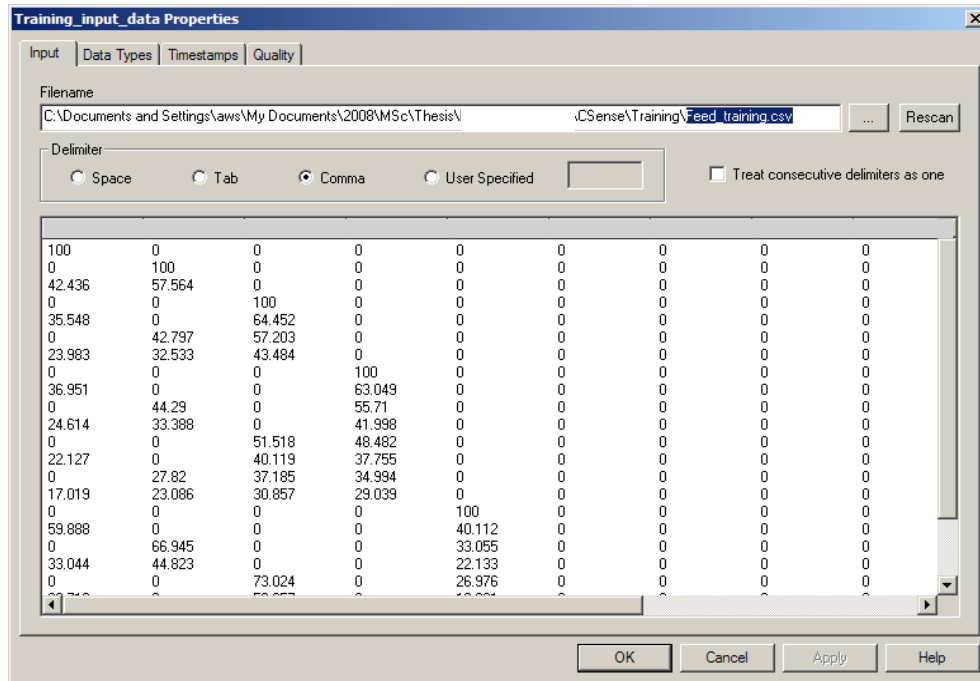


Figure 70 Input alloy data for model training

(By permission of CSense Systems (Pty) Ltd) (Data removed as per confidentiality agreement)

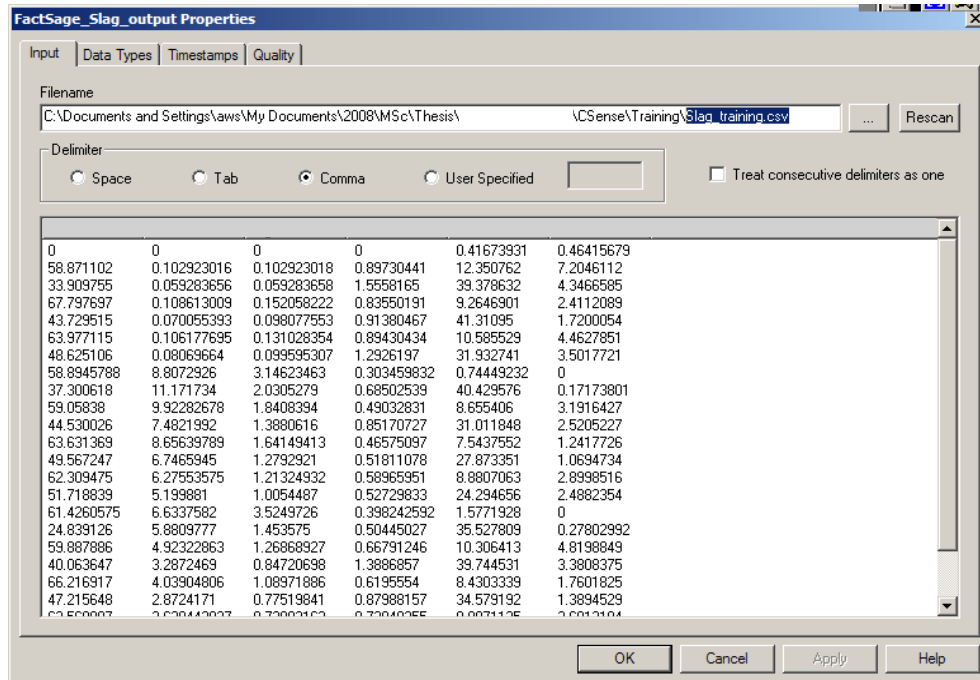
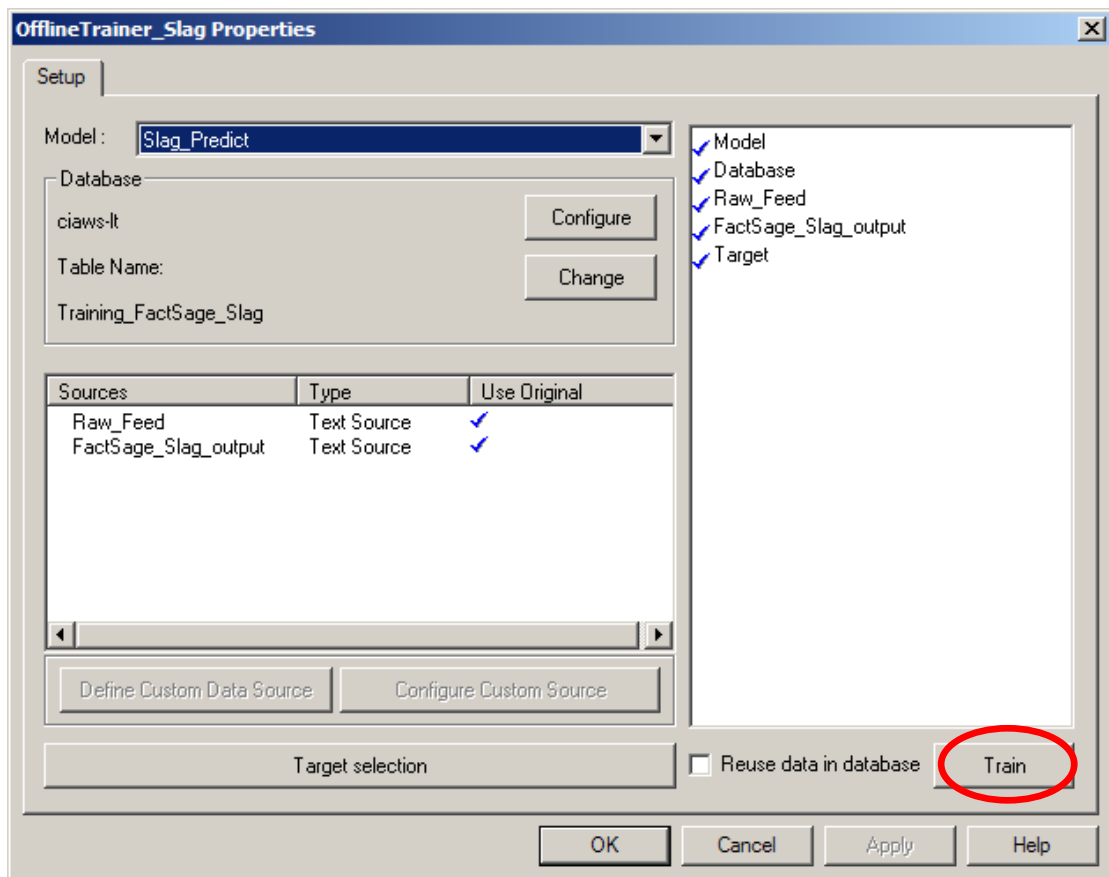


Figure 71 Output alloy data for model training

(By permission of CSense Systems (Pty) Ltd) (Data removed as per confidentiality agreement)



**Figure 72 Model trainer – training input and output data must be specified in this block before training can be commenced (By permission of CSense Systems (Pty) Ltd)**

## G.2 Dynamic modelling

Three dynamic models were created for predicting values for the three KPI outputs from the furnace. Only the dynamic model is discussed for the first KPI (t alloy/t feed), since the method employed for the prediction of the second and third KPI's are the same.

The layout of the dynamic model for predicting and optimising the tonnes of alloy produced per tonne of feed is illustrated in Figure 73. The region below the dotted line contains the blocks that were used to construct the dynamic model and monitor its performance. The area above the dotted line contains the blocks that were used to

optimise the dynamic model and to compare the optimised setpoints with the original setpoints. Only the area below the dotted line will be discussed in this section and the section above it will be discussed in section G3.

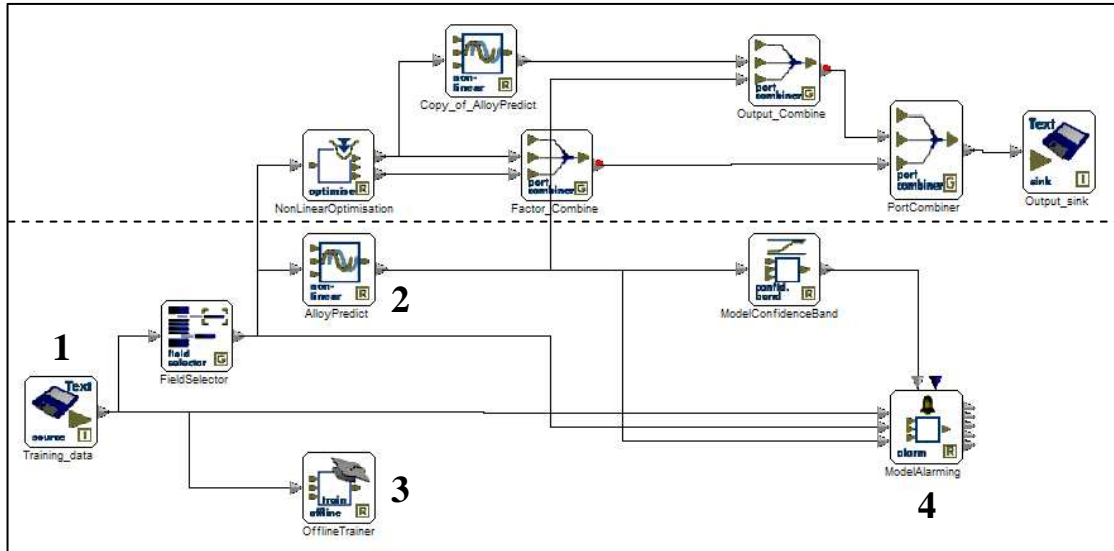


**Figure 73 Modelling layout for KPI prediction and optimisation**  
(By permission of CSense Systems (Pty) Ltd)

The daily average of all the variables and the actual tonnes of alloy produced per tonne of feed were sourced through block 1 and a preview of these variables are displayed in Figure 74. Not all variables are visible in this preview window. In the ‘FieldSelector’ block in Figure 74, the actual t alloy/t feed is withheld, because it is to be predicted using all the other input data. The dynamic model was trained with the daily average data over a period of one year. The statistics of the trained model (block 2) appears within the four windows in Figure 75, and the configuration of the offline trainer (block 3) is displayed in Figure 76. A model alarming block was used (block 4) to view the model-predicted KPI and compare it with the original KPI while the blueprint program was executing. It was configured as indicated in Figure 77 to display the windows in Figure 30, Figure 31 and Figure 32 in chapter 5.3.1. The ‘ModelConfidenceBand’ block was not used, but it can be configured to indicate high and low limits around the KPI variable in order to spot outliers. These limits were ignored in the configuration of block 4, as they were not important for achieving the objectives of the project.

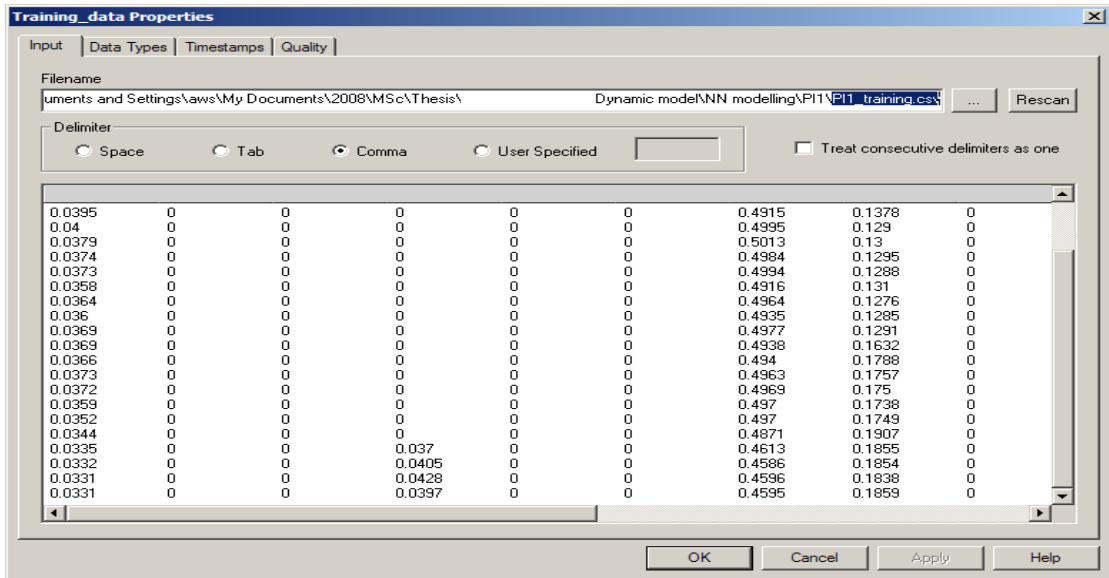


Figure 74 Preview of input variables for modelling and optimisation of KPI 1  
(By permission of CSense Systems (Pty) Ltd) (Data removed as per confidentiality agreement)

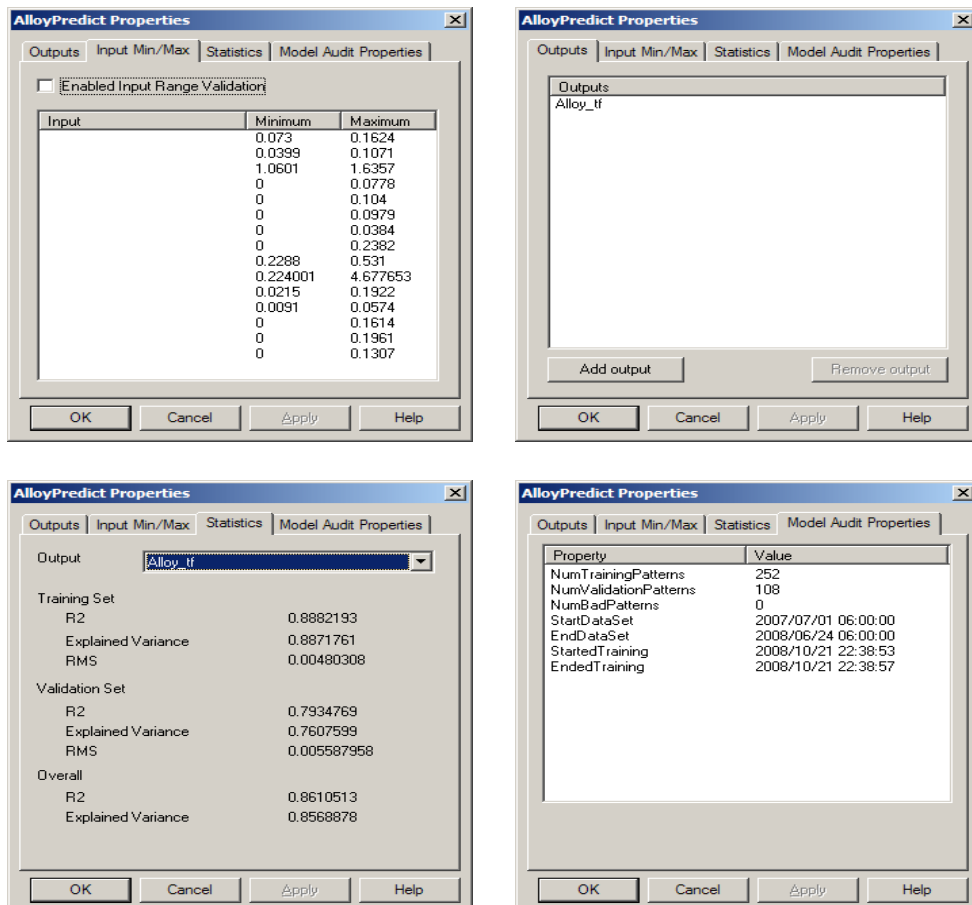
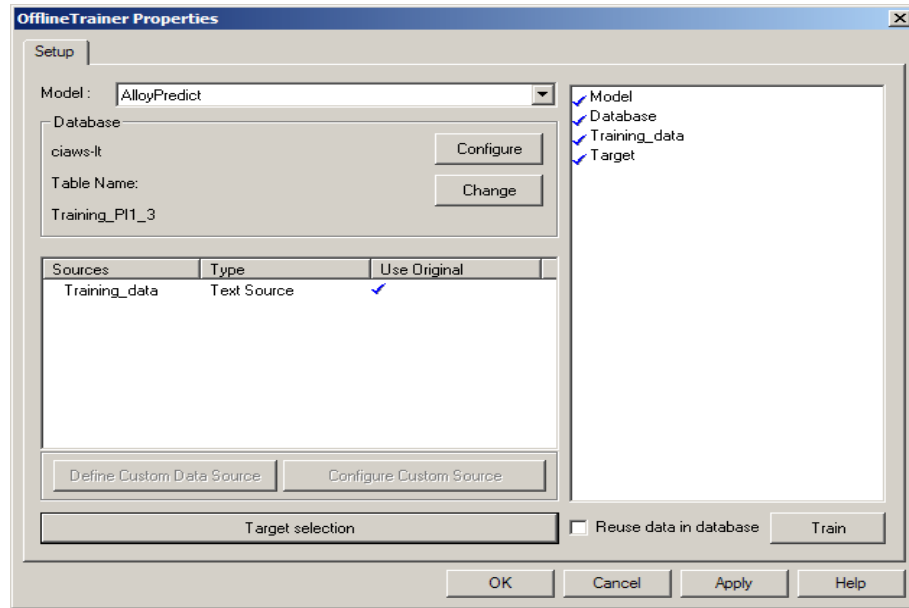
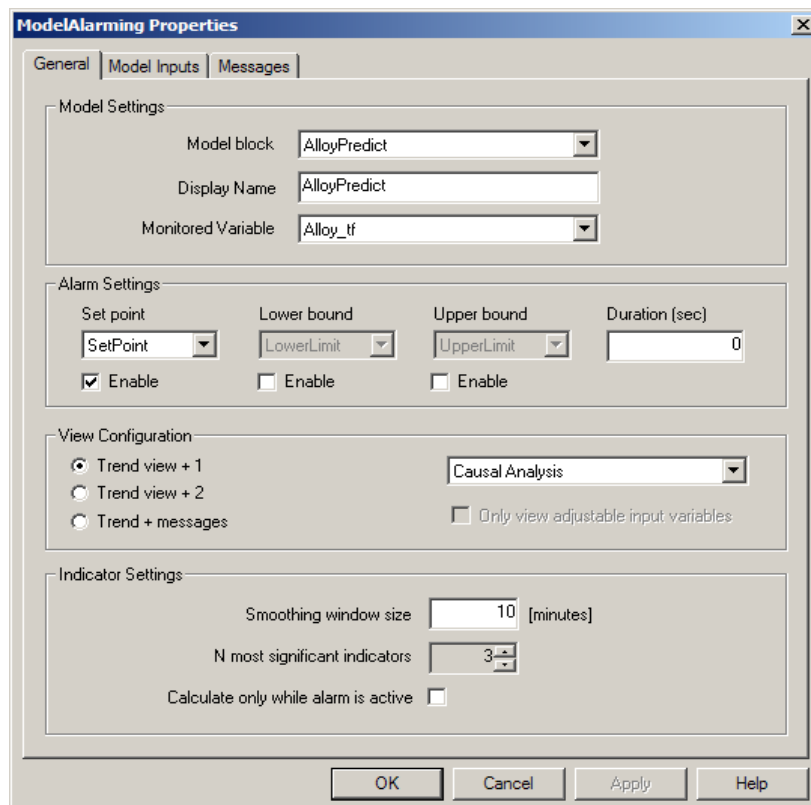


Figure 75 Statistics of the nonlinear model used for predicting t alloy/t feed  
(By permission of CSense Systems (Pty) Ltd) (Data removed as per confidentiality agreement)



**Figure 76 Model trainer – training input and output data must be specified in this block before training can be commenced (By permission of CSense Systems (Pty) Ltd)**



**Figure 77 Configuration of the model alarming block to display trends of predicted and actual KPI values (By permission of CSense Systems (Pty) Ltd)**

### G.3 Optimisation and comparison

In Figure 73 below, the blocks above the dotted line are used to optimise predicted KPI data.

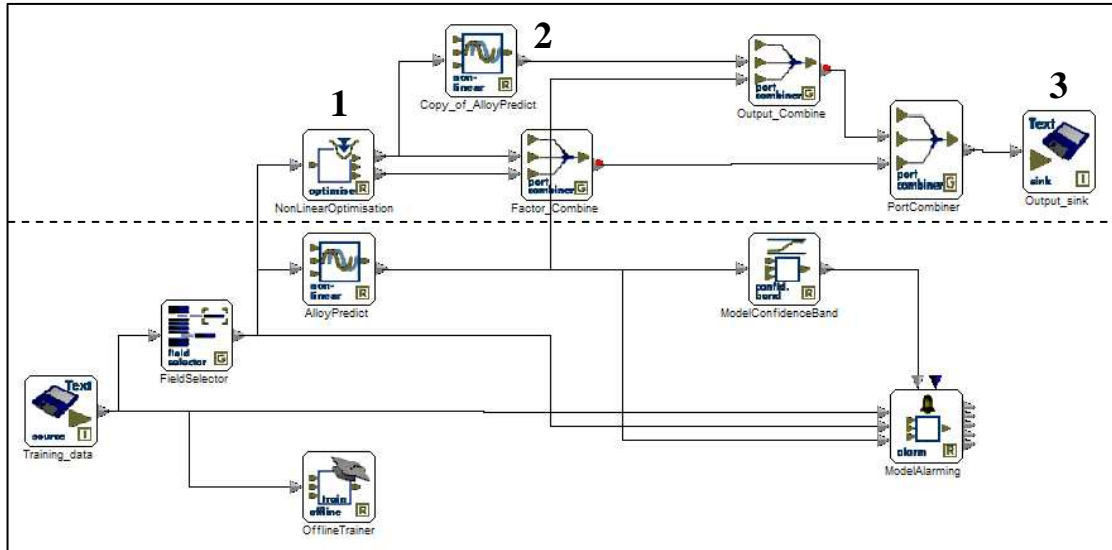


**Figure 73 Modelling layout for KPI prediction and optimisation**  
(By permission of CSense Systems (Pty) Ltd)

In Figure 73, genetic optimisation was performed on all input variables in block 1. This block was configured as shown in Figure 78 and was set to interact with the ‘AlloyPredict’ modelling block according to the genetic algorithm laid out in section 4.3.2.3. Inputs were optimised to maximise the t alloy/t feed ratio as specified by a cost function that was set in Figure 78. The constraints/limits of optimisation of the input variables were also specified in Figure 78, and all input materials were set to trigger the optimisation process when any of the selected field variables changed.

Optimised variables were passed from block 1 to block 2 so that the maximised KPI output could be predicted. Block 2 was identical to the ‘AlloyPredict’ block below the dotted line. All optimised and original input variables and the maximised and original model output variables exiting through block 3 are listed in Figure 79. In this figure, the original variables were appended with the ‘\_2’ name extension. The two red dots attached to the output ports of the two port combiner blocks allowed the original and adjusted variables to be trended during execution of the blueprint program. The comparison of this data is illustrated in Figure 33, Figure 34 and Figure 35 in section 5.3.2.

Optimised variable values were corrected and are listed in the final column of Table 4 in section 5.3.2. These variable values were then processed by the same alloy prediction block as in Figure 73, but in a new blueprint program (see Figure 80) to obtain the best possible alloy output per tonne of feed. The input variables to this new blueprint are displayed in Figure 81. Not all the variables are visible in this diagram.

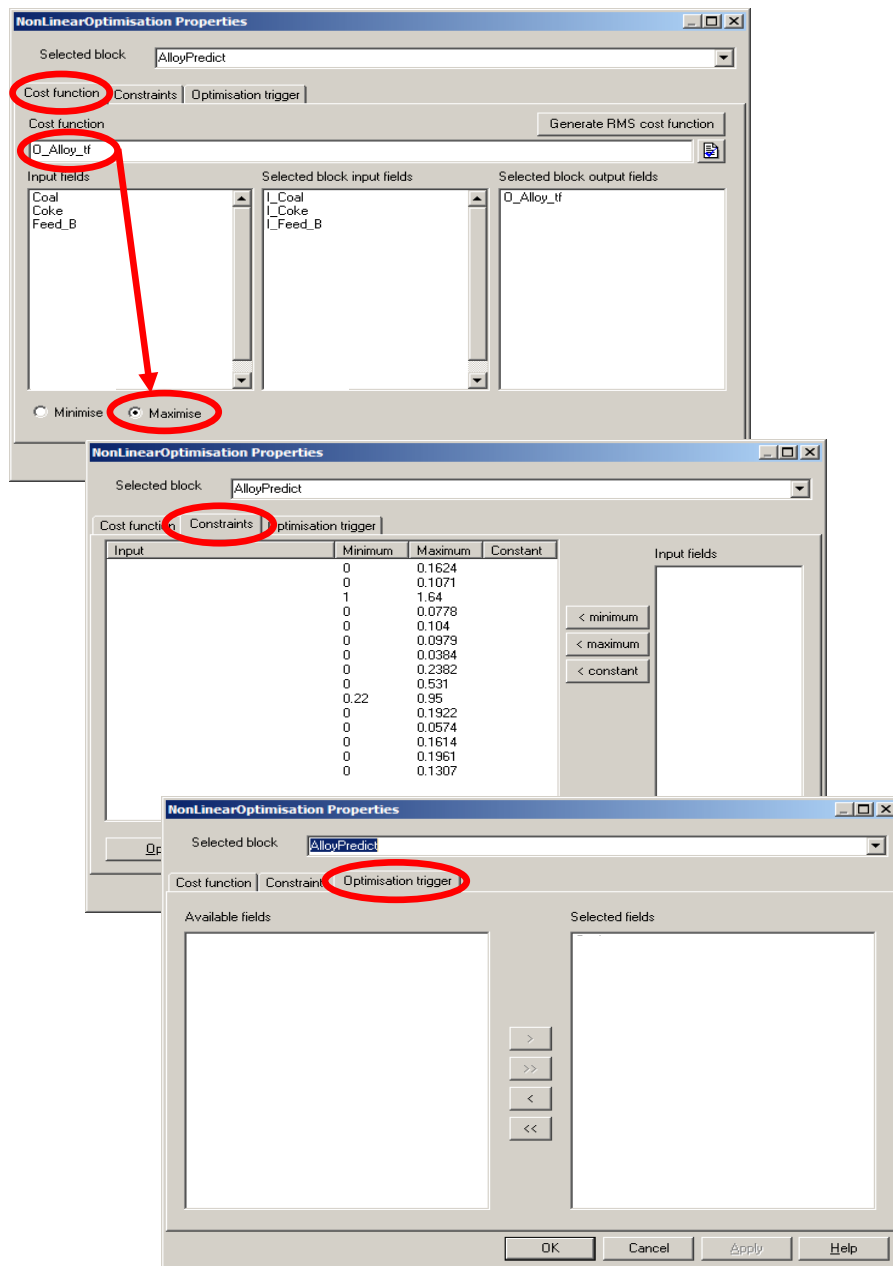


**Figure 78 Configuration of the nonlinear optimisation block for maximising alloy production**  
 (By permission of CSense Systems (Pty) Ltd) (Data removed as per confidentiality agreement)



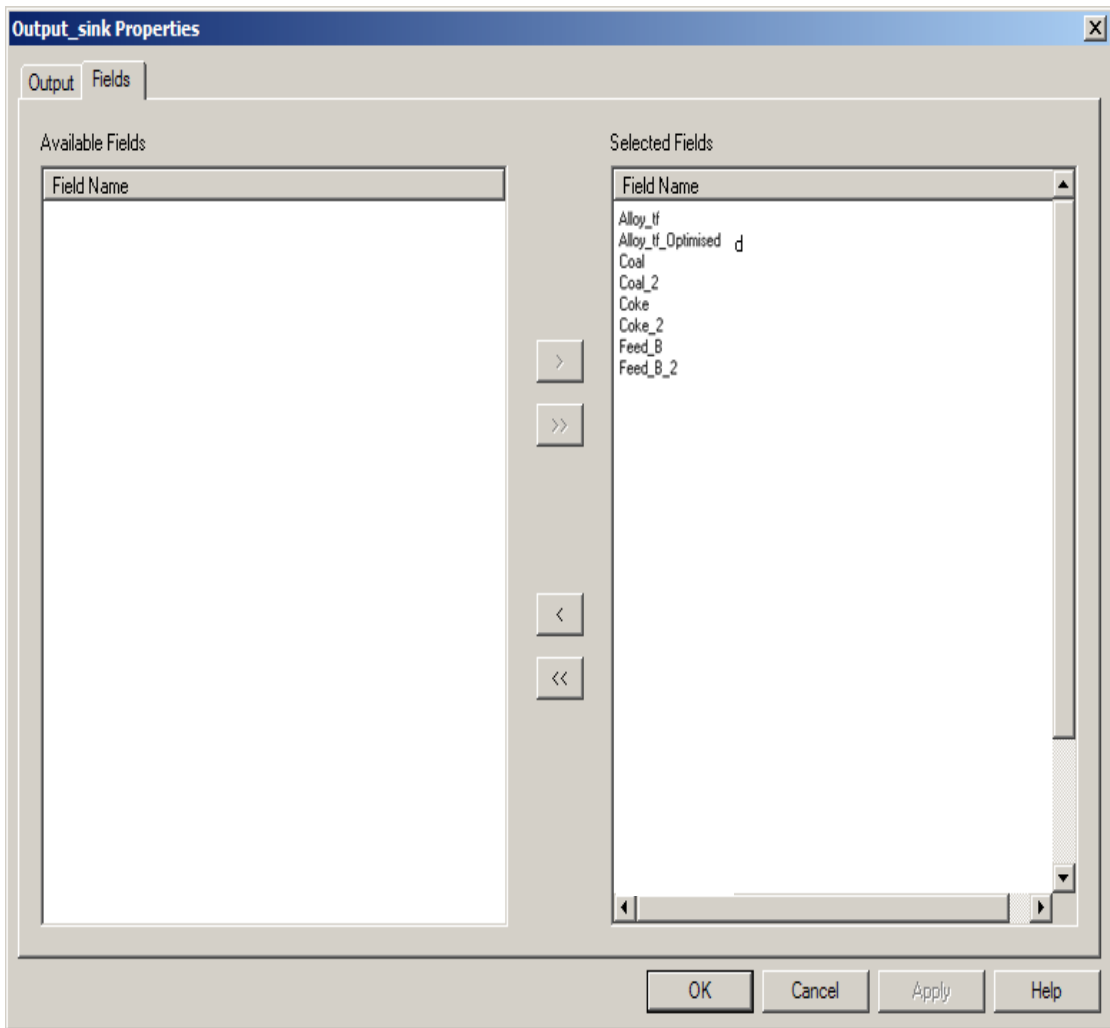


**Figure 79 Optimised and original output variables exiting the dynamic model**  
 (By permission of CSense Systems (Pty) Ltd) (Data removed as per confidentiality agreement)

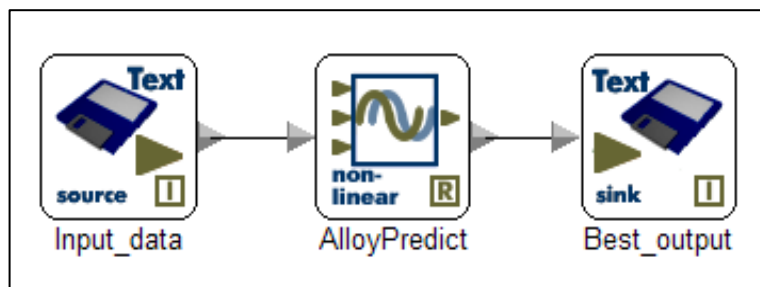


**Figure 80 Final blueprint layout for predicting the best outputs for furnace performance**  
 (By permission of CSense Systems (Pty) Ltd)

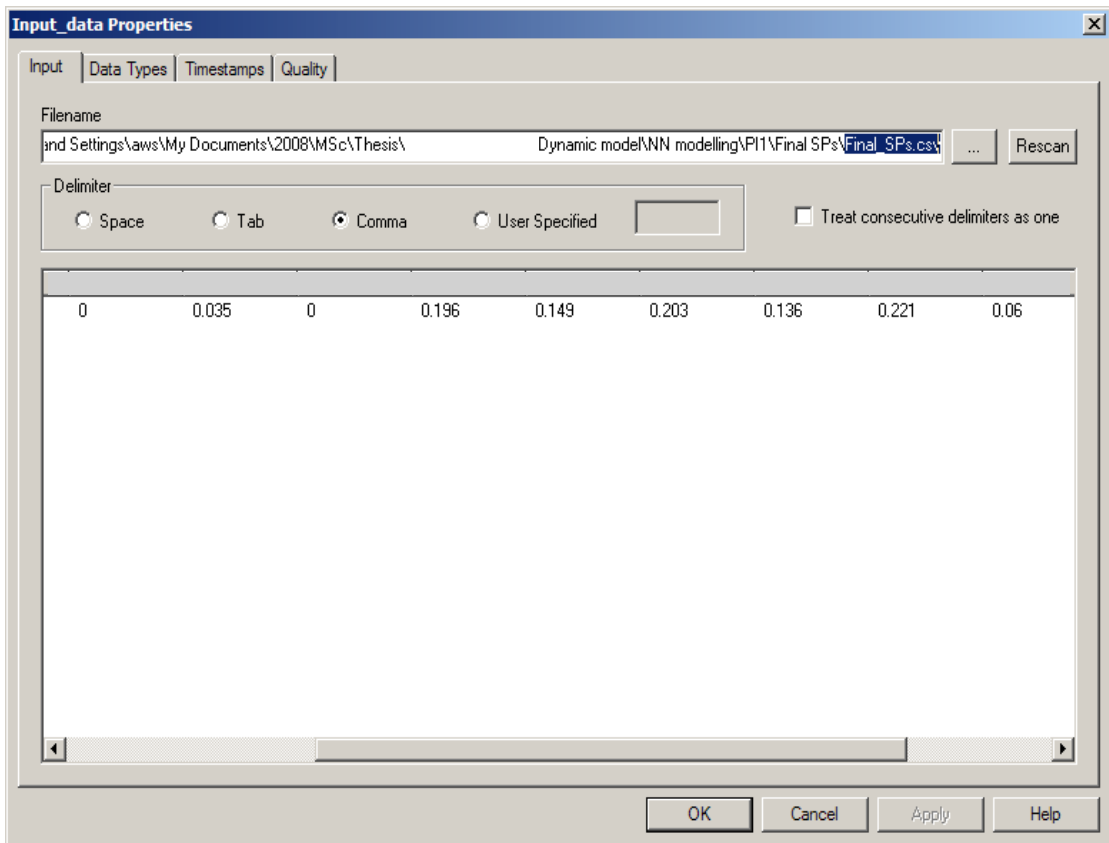


**Figure 81 Best possible setpoint values for predicting the best possible alloy output per tonne of feed (By permission of CSense Systems (Pty) Ltd) (Data removed as per confidentiality agreement)**